UNIVERSITÀ DEGLI STUDI DI PADOVA

DIPARTIMENTO DI INGEGNERIA INDUSTRIALE

CORSO DI LAUREA MAGISTRALE IN INGEGNERIA DEI MATERIALI

Tesi di Laurea Magistrale in

Ingegneria dei Materiali

POLYMER-DERIVED CERAMICS FOR ENERGY STORAGE APPLICATION

Relatore: Prof. Paolo Colombo

Correlatore: Prof. Gurpreet Singh

Laureando: Riccardo Cuccato

ANNO ACCADEMICO 2016-2017

To R.C.

my star,

my perfect silence.

Contents

Introduction

It is widely acknowledged that the global energy consumption is constantly increasing. Nowadays the world main energy source are fossil fuels even though their future exploitation is unsustainable. Two of the major challenges of our time are the research for sustainable energy sources and the development of innovative storage methods. Electrochemical storage devices (Batteries and Capacitors) present the highest efficiency and are the most portable; for these reasons, they are widely used in the modern human society. Among the different kinds of electrochemical storage devices, supercapacitors possess high charge/discharge rate, outstanding cycling stability and the possibility of working in conditions prohibitive for other storage methods. Even though efforts in recent decades to simultaneously improve the energy and power density of capacitors have been extremely efficient, the limiting factor of these device is still their specific capacitance. New materials, suitable for building storage device which meet the requirement of low price, ease of production, high power/energy density and durability; are constantly being studied and developed. The purpose of the present work is to study the usability of three different kind of polymer-derived SiOC fibers for making a self-standing electrode and to understand which are the main processing variables which can be modified in order to tune the material's structure and so the final electrochemical properties.

In the first chapter, short compendium about the evolution of energy and bird's eye view on renewable energy sources are exposed. After that, storage methods, in particular supercapacitors; are presented.

In the second chapter, polymer-derived ceramics, the basis of electrospinning process and the electrochemical characterization techniques are described.

In the third chapter, the experimental procedures followed for the synthesis and characterization of the studied materials are presented.

In the fourth chapter, the results of the morphological, chemical and electrochemical characterization techniques are displayed and discussed.

Finally the conclusion drawn from the tests conducted are summarized with the aim to point the way for future developments of polymer-derived ceramic SiOC fibers for self-standing, binder-free, cost-effective, electrodes.

Chapter 1

Energy and its Storage

Energy in all his forms is fundamental for all the activities of modern human society. The continuous research for new energy resources and innovative storage methods is a crucial topic and one of the major challenges of our time [1]. In this chapter after a short compendium about the evolution of energy and a bird's eye view on renewable energy sources, storage methods are presented. A particular focus on Supercapacitors is adopted.

1.1 Energy through time

The first industrial revolution, happened during the second half of the 18^{th} century, moved the whole word from an economy based primarily on the agriculture and craft to an economy based on the industry. This transformation changed radically and forever the whole society, turning it from an archaic to a more contemporaneous one. For the first time in history mankind start demanding more and more energy, searching raw materials in order to provide it and implementing new technological methods for facing this need. The first energy source used was coal. This mineral, composed substantially by carbon and available in underground deposit all over Europe, gave energy to the first and the second industrial revolution. During the second industrial revolution, also oil start to be used and processed in large quantities. Hydrocarbons like natural gas, oil and its derivatives have gained more and more importance over the years, and in the 2005 about 80% of global energy was based on fossil energy sources [2]. In the last 50 years, also nuclear energy started to be used, as it is shown in figure 1.1.1.

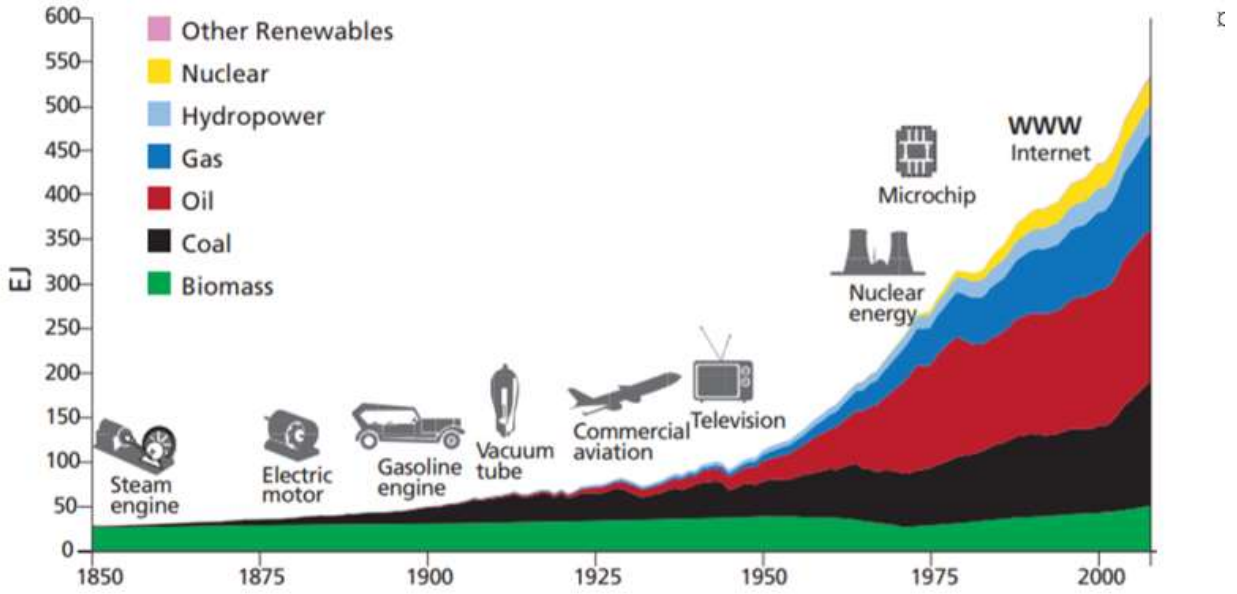

Fig. 1.1.1 The figure shows the explosive growth of global primary energy use during the last 2 centuries. (Source: Global Energy Assessment-Toward a Sustainable Future)

From the 1950 the development of our modern society has been supported by the extensive and intensive use of oil, gas, coal and nuclear power. Looking at past and thinking about the future the whole scientific community started facing three fundamental problems, never considered before:

1. The impact on the health of these sources of energy.
2. The impact on the environment of these sources of energy.
3. The period of availability of these sources of energy.

Solving these problems and ensuring the enormous amount of energy demanded by our human society is one of the biggest global challenge of the 21th century and a revolution seems to be required. This revolution, just begin but far from its end, in the world of energy is changing our mentality and touching all the aspects of life. It is composed by several factors, most important are:

- General sensitization about energy wastes and energy recovery in everyday life.
- Implementation of carbon capture and storage (CCS) for both fossil fuel and biomass.
- Shift from the “old” energy sources denominated depletable to new ones denominated renewable.

This approach is radically changing ways in which humanity uses energy, ranging from much more energy-efficient houses, mobility, products, and industrial processes to a different mix of energy supply. Electric cars appeared on the marker few years ago, and now electrification of transport is considered not only a priority in the community research program, but also a key point in the

European Economic Recovery Plan [3]. The energy the we use inside our houses is switching from electricity distributed by the line to electricity generated by solar panels which are becoming easier to be seen over our roofs. The next step is the storage of the energy provided by these panels and the resulting sharing among the various houses in the same neighborhood. The vision of a network of people sharing each other energy generated only by sun's rays was suggested by Elong Musk during the conference for the release of Powerwall® [4].

Fig. 1.1.2 The figure shows an electric car, Tesla® Model3 and a battery, Powerwall®, for the storage of solar energy. (Source: www.Tesla.com)

The transformation of how we produce and use energy is happening but there still lot of work to do. As stated in the Global Energy Assessment (GEA): "Current decision-making processes typically aim for short-term, quick results, which may lead to sub-optimal long-term outcomes" [2]. New approaches and policies are defined essential, urgent but most importantly achievable.

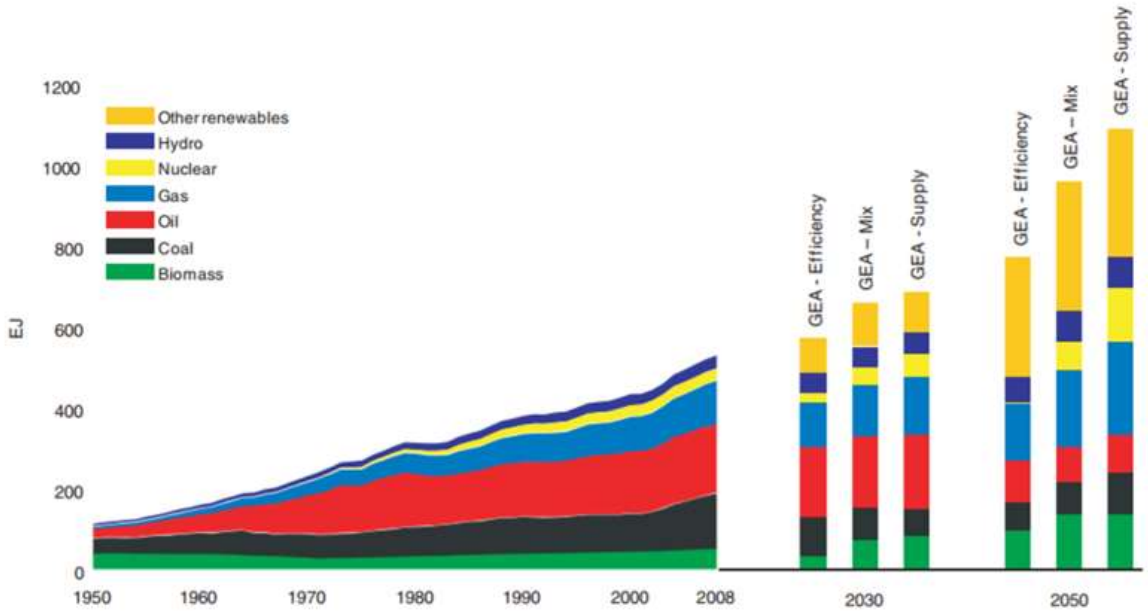

Fig. 1.1.3 The figure shows the development of primary energy from 1950 to 2008 and 3 different future sceneries of energy supplies. (Source: Global Energy Assessment-Toward a Sustainable Future)

All the pathways, indicated in the GEA, that represents alternative evolutions of the energy system toward sustainable futures forecast a much larger use of renewable energies, as shown in figure 1.1.3.

1.2 Renewable Energies

Renewable energies sources have two fundamentals advantages, regeneration in short period and absence of outtake in the atmosphere of pollutants and climate changers [5]. For these advantages in the last thirty years this sector has seen a rapid evolution, supported also by legislation. In OECD (Organization for Economic Cooperation and Development) countries, total primary energy supply from renewable sources increased from 272 Mtoe to 512 Mtoe between 1990 and 2016, an average annual growth rate of 2.5% [6].

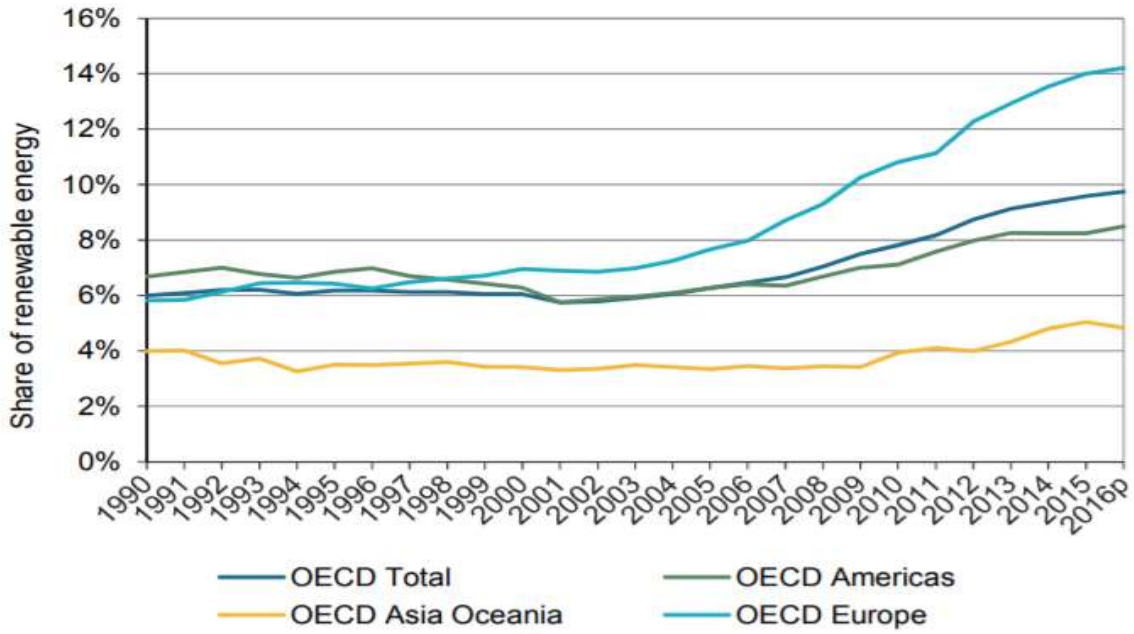

Fig. 1.2.1 The figure shows the increase of regional shares in renewable energy supplies, in a temporal window of 26 years. (Source: www.iea/publications.com)

From the graph above, can be noticed that big difference exists between OECD different regions. This difference is imputable to the different economic evolution and legislation existing in these regions.

The principal Renewable energies sources are [7]:

- Solar power
- Wind power
- Hydro power
- Geothermal power
- Marine power

Biomass, biogas, bioliquids and renewable wastes are considered renewable sources but their treatment doesn't concern this work. Nuclear fusion is also considered as an "alternative" energy source, but its implementation is far to be really used [8].

Fig. 1.2.2 The figure shows examples of renewable energy. (Source: www. costofclearenergy.com, www. redhotgrren.co.uk.com, www. windpowermonthly.com, www. renewableenergyworld.com)

Two remarks have to be made. The first remark is that the solid biofuels and hydro accounted for 59.6% of the total OECD primary renewable energy in 2016. These sources are older compared to the "new" ones, solar and wind power; which accounted for less percentage but are growing much faster. For example, solar photovoltaic experienced the highest growth among the renewables, averaging 43.3% between 1990 and 2016 as reported by the International Energy Agency (IEA) [6]. The second remark is that even if renewable energies are growing markedly their total account to the world total primary energy supply (TPES) is still restrained, as shown in figure 1.2.3.

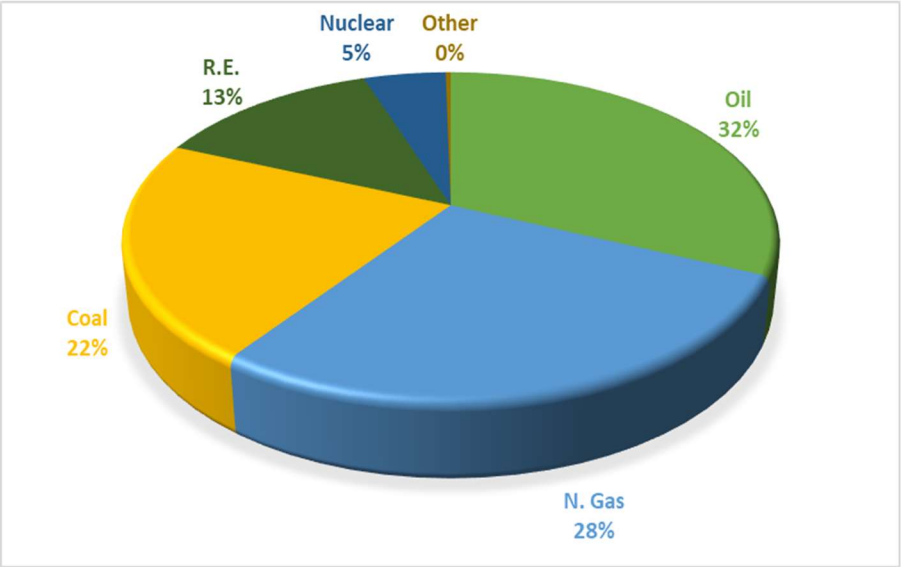

Fig. 1.2.3 The figures show the percentages of various energy form in TPES. (Source: www. iea/publications.com)

This moderate value is ascribable to the fact that these sources of power are relative new compared to the not renewable, in particular coal, oil and natural gas. This matter has an impact on the cost and efficiency of installations and so on the cost of the produced energy. By the way IEA predicts a progressive decrease in the cost of energy produced by renewable sources (especially for the "new" ones), and in a concomitant increase in the cost of hydrocarbons and coal [6].

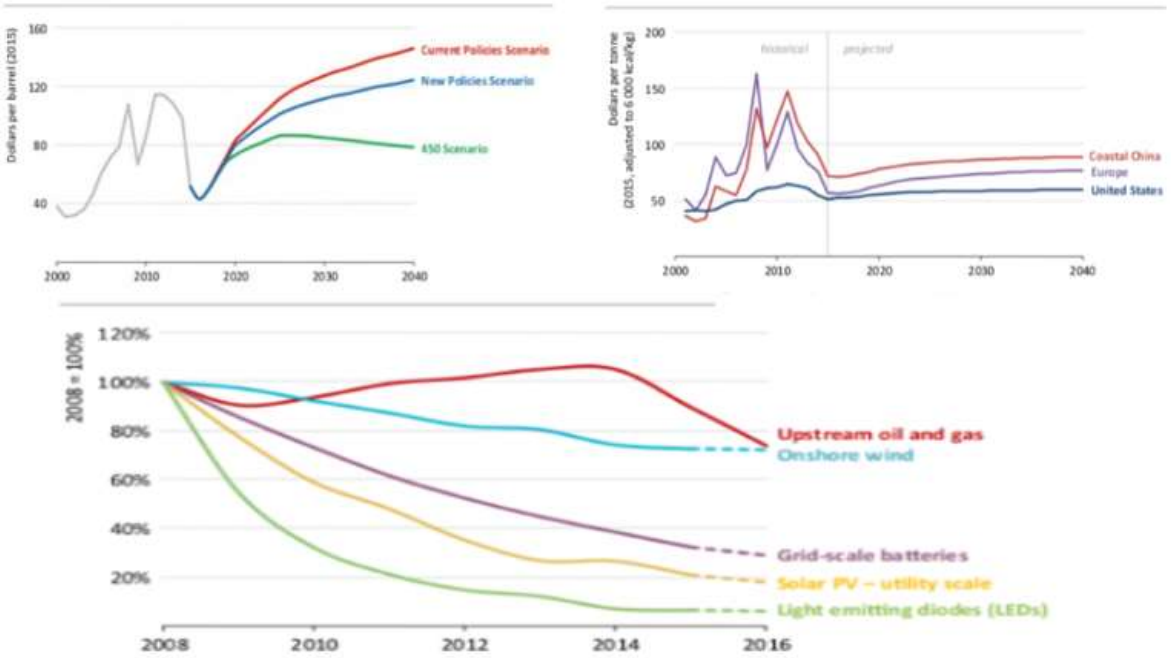

Fig. 1.2.4 The figure shows the hypothetical trends of the price for crude oil, steam coal and renewable technologies. (Source: www. iea/publications.com)

A problematic related to the use of “new” renewable energy sources is their aleatory behavior. This intrinsic characteristic generated the need of reliable storage devices. The aim is to separate the generation and utilization periods.

1.3 Storage Methods

The electricity generated from innovative source shall, have to and will fuel our world. After its generation, the electricity need to be stored in order to be used in thousands different applications when required. The development of innovative and reliable methods for storing the energy is a crucial scientific thematic [9]. For understanding the fundamental importance of economical and durable devices, capable of storing a large amount of energy, the surrounding reality and its future evolution have to be considered. The necessity of storing the electricity generated by the innovative sources. The shifting from combustion to electrical mobility. The growing dependence of men to electronic devices as smartphones, tablets, laptops and watches. All these contemporaneous phenomena required an evolution in the traditional energy storage systems. Just think about the advantage of having a smartphone whose battery lasts for three days instead of one (common duration of a smartphone’s battery with a medium utilization [10]). These are only the most common likely fields of applications which will benefit from an improvement in the storage technologies.

A wide range of storage mechanism exist. The major categories designed for use in industry and commerce are:

- Electrochemical.
- Mechanical.
- Thermal.
- Chemical.

In this work after a short presentation of batteries we will focus on supercapacitors. These electrochemical methods are widely used for lot of applications thanks to their efficiency and portability.

1.3.1 Batteries

The word battery commonly used in everyday life is very often used improperly. An electrochemical cell is a device that transform chemical energy into electrical energy and vice versa. The device only capable to turn chemical energy into electricity is called Galvanic Cell and the device only able to do the reverse is named Electrolytic Cell. Accumulator is a device able to operate both the conversion. The word Battery refers to an assemblage of cells but now is commonly used in order to designate a generic electrochemical device [11].

A battery stores energy in from of chemical reagents capable of doing a spontaneous redox reaction.

$$Ox_1 + R_2 \leftrightarrow R_1 + Ox_2 \tag{1.3.1}$$

The whole redox process can be separated in two semi-reactions which must occur in two separated spaces connected electrically only.

$$Ox_1 + n_e \leftrightarrow R_1 \tag{1.3.2}$$

$$R_2 \leftrightarrow n_e + Ox_2 \tag{1.3.3}$$

Where O and R are the oxidized and reduced forms of chemical species and n in the number of electrons involved in the process. During the years lot of batteries have been developed and used, many of them are not used anymore. From the first Daniel's battery to the last Lithium Polymer the characteristics, such as the specific capacitance, have kept growing.

Accumulator	**Cycles**	**Wh/kg**
Pb-acid	500-1000	35-40
Ni-Cd	700-1200	45-55
Zn-MnO_2	25	8-64
Zn-air	600	100-200
Ni-MetalH	700-1200	70-80
Li ion	400-1200	100-200
Al-air	n.a.	200-300

Tab. 1.3.1. The figure shows the specific capacitance and the useful number of charge-discharge cycles of some batterie's types. (source: *appunti di Elettrochimica, Professor. A. Gennaro*)

Lithium ion batteries [12] and Fuel Cells [13] are gaining more and more relevance but their handling falls outside the scope of the present work.

1.4 Capacitors

A capacitor is component made by two metal plates separated by a dielectric. Charge is stored thanks to the formation of an electrical field, between the two plates, generated by the separation of charges.

The charge C of a capacitor, in Farad (*F*), is defined by:

$$C = \frac{q}{V} \tag{1.4.1}$$

Where q is the quantity of charges, in Coulomb (*C*), accumulated between the two plates and V is the potential difference between the two plates, in Volts (*V*).

The energy U, in Joule (*J*) of a capacitor is defined by:

$$U = \frac{1}{2} \cdot C \cdot V^2 = \frac{1}{2} \cdot q \cdot V \tag{1.4.2}$$

For a capacitor with parallel plates the storable charge is mainly related to the surface area A, and the separation distance d, of the plates through:

$$C = \frac{A}{d} \cdot \varepsilon \tag{1.4.3}$$

Where ε is the absolute electrical permittivity of the material, equal to the relative permittivity of the material, ε_r multiplied for the permittivity of the vacuum ε_0 = 8,86 *pF* [14]. From equation 1.4.3 is easy to understand that if the ratio A/d is increased, the charge and so the energy stored increases too. This simple concept guided the development of supercapacitors (designated also as ultracapacitors). Same conclusions can be obtained analyzing different geometry, like cylindrical one.

1.4.1 Super/Ultracapacitors

The first tests on new capacitors, were conducted in 1957 by General Electrics. The devices as we know them have been developed later by Standard Oil company of Ohio who licensed the technology to NEC corporation. This company stat commercializing the product in 1978 to provide computer memory backup power.

Like all capacitors, electrochemical capacitors (ECs) also called supercapacitors or ultracapacitors, because of their extraordinarily high capacitance density respect to the normal ones, physically store charge. The big difference is that instead of storing charge on low-surface-area plates like conventional capacitors, ECs store charge in an electric double layer (EDL) set up by ions at the interface between a high-surface-area material and a liquid electrolyte. These double-layers consist of two layers of charges, one electronic layer is in the surface lattice structure of the electrode, and the other, with opposite polarity, emerges from dissolved and solvated ions in the electrolyte. The two layers are separated by a monolayer of solvent molecules. Solvent molecules adhere by physical adsorption on the surface of the electrode and separate the oppositely polarized ions from each other, as a molecular dielectric. The adsorbed molecules are polarized but suffered no charges transfer and so no chemical reactions take places [15]. The earliest model of electric double layer is usually attributed to Helmholtz and thus EDL is also referred to as Helmholtz double-layers. Later the Gouy-Chapman model and the Gouy-Chapman-Stern model were developed to more accurately describe the detailed structure of EDLs.

The opening of the circuit in a ECs device create two capacitors connected in series by the electrolyte. The total capacitance C_{tot} is given by:

$$C_{tot} = \frac{C_1 + C_2}{C_1 \cdot C_2} \tag{1.4.4}$$

Where C_1 and C_2 are the capacitance of the single electrode. Symmetric ($C_1 = C_2$) and Asymmetric ($C_1 = C_2$) configuration exist.

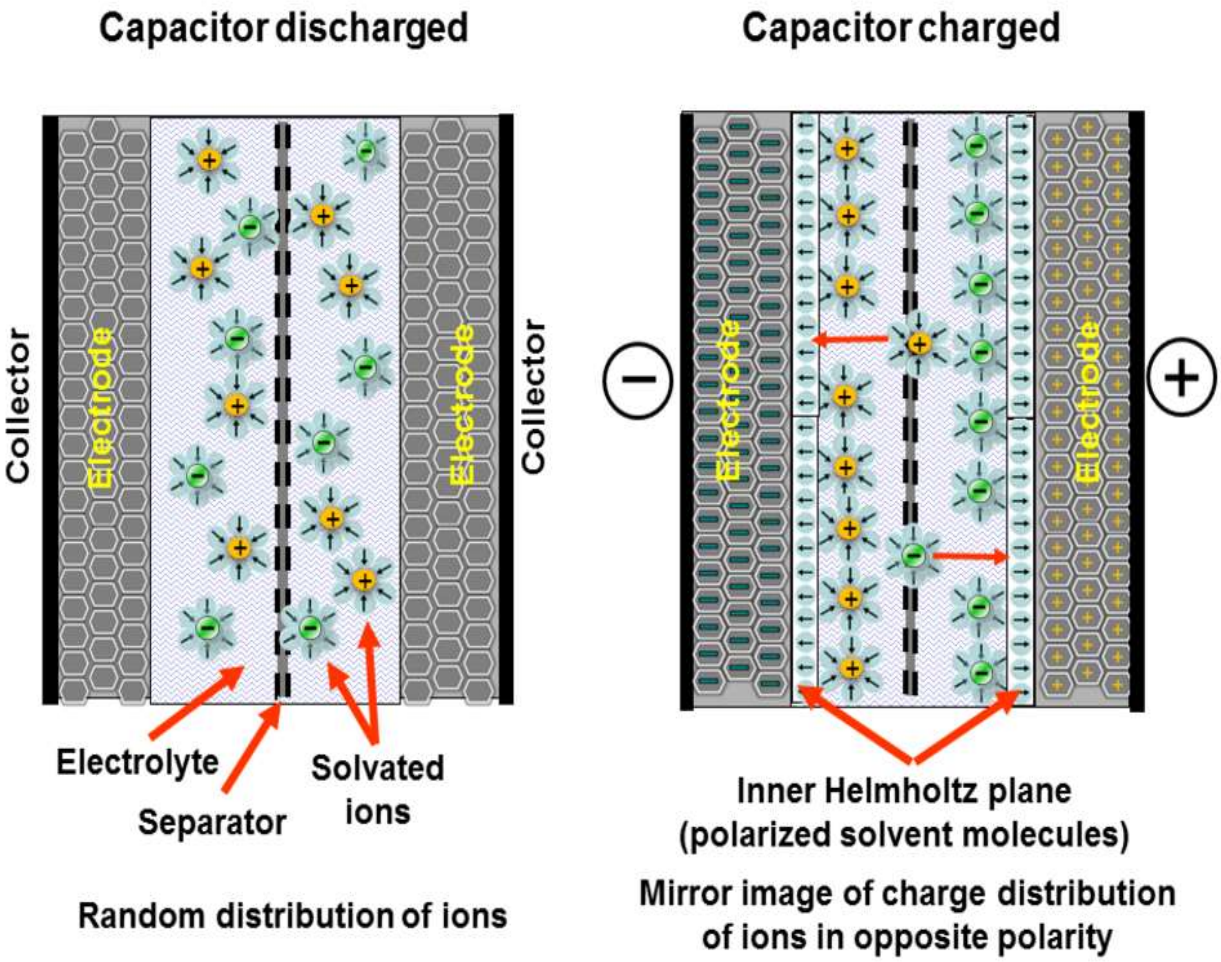

Fig. 1.4.1. The figure shows the charging mechanism of ECs (source: http: www.energoclub.org)

Looking equation 1.4.3 it is clear that thanks to the elevate surface area of the material, usually activated carbon [16], and extremely thin double-layer distance, in the order of a few angstroms (0.3-0.8 nm), devices with capacitance in order of thousands *F* (million times the capacitance offered by typical electrostatic or electrolytic capacitor) are obtainable [17].

A typical ultracapacitor unit cell is composed by two electrodes that are isolated from electrical contact by porous separator. Electrodes often contain conductive, low surface area additives such as carbon black to improve electrical conductivity. Current collectors of metal foil or carbon filled polymers are used to conduct electrical current from each electrode. The separator and the electrodes are impregnated with an electrolyte, which allows ionic current to flow between the electrodes while preventing electronic current from discharging the cell. A packaged ultracapacitor module, depending upon the desire size and voltage, is constructed of multiple repeating unit cells [15].

1.4.2 Properties and applications of Supercapacitors

Supercapacitors compared to batteries offer some advantages. The major ones are the faster storing and releasing of energy and the higher total number of utilization's cycles [18]. ECs are characterized by high power density and have a low recharging time. By contrast batteries for a given volume can store 3 to 30 times more energy [17]. These differences are generated by the different mechanism of energy storing. For ECs, it is a physically process involving only the surface of the material, oppositely for batteries the mechanism is related to chemical reaction which affect the bulk of electrode's material. We can see the different position of the two devices in the Ragone plot.

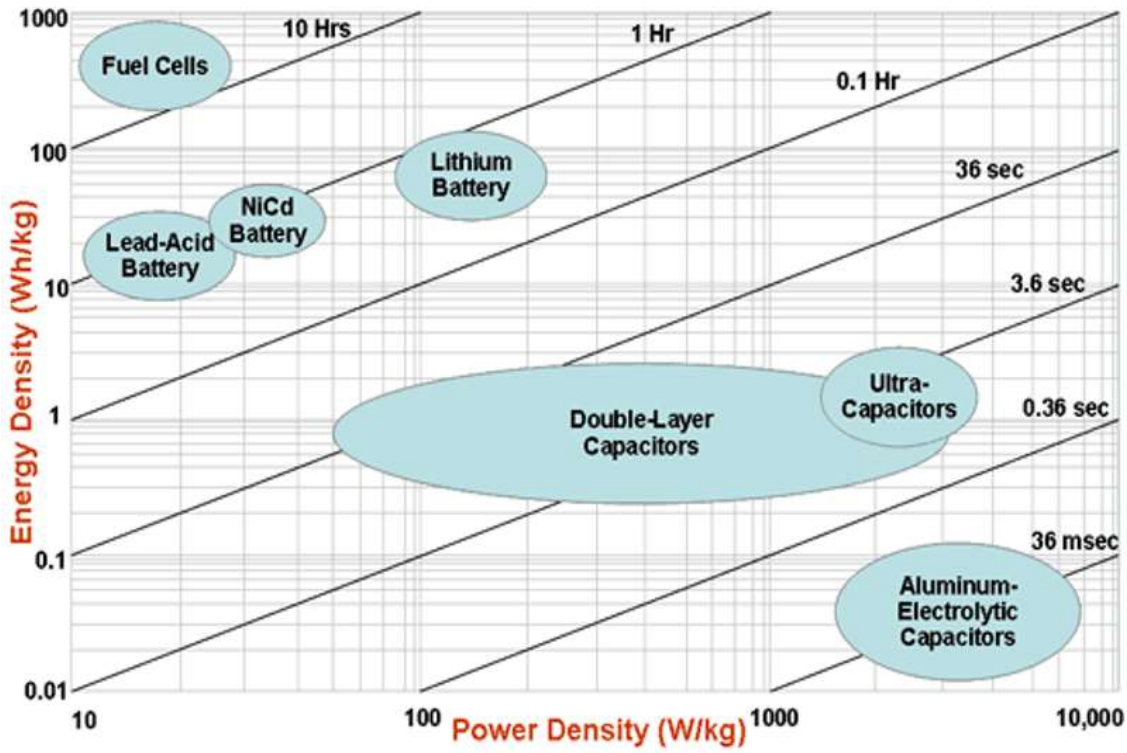

Fig. 1.4.2. The figure shows the Ragone plot for some Electrochemical storage methods (source: www.mpoweruk.com)

In super/ultracapacitors the highly reversible electrostatic charge storage exposed above does not produce the changes in volume that usually accompany the redox reactions of the active masses in batteries. Such volume changes are the main cause of the limited cycle life of batteries, up to two orders of magnitude lower respects ECs. More over Ultracapacitors can easily be integrated into electronics, can operate in more challenging environments than batteries (hot or cold environments) and generate less thermochemical heat respect to batteries. A limitation factor for supercapacitors is that the operating voltage cannot exceed the potential at which the electrolyte undergoes chemical

reactions, typically 1 to 3 V per cell. Using different types of electrolytes allows to work with different potentials. Organic electrolytes are those with the wider potential window, typically 2.5 V per cell. For higher voltage applications ECs like batteries can be series-connected [17]. In Table 1.4.1 a summary of previous conclusions can be founded.

Property	**Battery**	**Electrochemical Capacitor**
Storage mechanism	Chemical	Physical
Power limitation	Reaction Kinetics, Mass transport	Electrolyte conductivity
Energy storage	High (Bulk)	Limited (surface)
Charge rate	Kinetically limited	High, same as discharge rate
Cycle life limitations	Mechanical stability, chemical reversibility	Side reactions, electrolyte evaporation
Environments	Standard	Hot, Standard, Cold

Tab. 1.4.1. The table shows a comparison of properties of Batteries an ECs. (source: [17])

The capacity of ultracapacitors is largely determined by the electrode material and as a result research to improve the performances of electrode materials has dramatically increased [19].

The common applications for supercapacitors are those in which a large amount of energy is required in short time, a high number of charge discharge cycles and a long device's lifetime are needed or the energy's demand is highly variable and impulsive. This technology is often used coupled with another source of power, typical is the parallel coupling with batteries. Supercapacitors find utilization in electronic word as stabilizer of power supply and for memories backup. Also in renewable energies world are used as voltage stabilizers and cyclic leveler [20]. In the automotive world, they are starters for internal combustion engines and stop-start fuel saving system. In electrical vehicles like full electric or hybrid buses or cars acts as sources of power. An example of vehicles completely fueled by ECs are the terminal tractors that transport containers to warehouses. In medical fields, they find use in defibrillators. In the airplanes are the sources of power for emergency actuators for doors. Ultracapacitors find large application in innovative system for energy recovery and efficiency.

Fig. 1.4.2. The figure shows three supercapacitor's applications. (source: www.transportparis.canalblog.com, www. directindustry.com, www. Wikipedia.com)

They are used in street lights coupled with LED and a photovoltaic panel. They are employed for braking energy recovery in vehicles such as buses, trams, cars. Another example are rubber-tired gantry cranes that move and lift containers. With a capacitors system that recovers energy during load lowering their energy usage can be reduced by 40% [17].

The interest on developing ultracapacitors for energy storage devices, with all their advantages, and with the aim to obtain and energy density closer to batteries one has been underlined also by the US Department of Energy [21]. Has to be noted also that attempts over the last century to improve the energy density of rechargeable batteries have resulted in only 6-fold increase. By contrast, efforts in recent years to improve the energy density of capacitors have been extremely efficient and increase the energy density by several orders of magnitude [19].

1.4.2 Pseudocapacitors and Asymmetric capacitors.

Two additional types of devices closely related to supercapacitors but presenting substantial differences are pseudocapacitors and asymmetric capacitors.

Pseudocapacitors are capacitors which undergo electron transfer reactions, similarly to batteries. These devices store energy through highly reversible surface redox faradic reactions in addition to the electric double-layer mechanism [22]. This process is related to the charge transfer between and electrolyte's adsorbed ion and the electrode. In some cases, faradic pseudocapacitance can exceed double-layer one. Electrode's materials that exhibit this phenomenon are conducting polymer and transition metal oxides, as Ru_2O. This oxide shows the highest specific capacitance but has a prohibitive cost [17]. Efforts to develop more practical pseudocapacitative materials are now active, but the safety issue, cost, and large-scale production of the material processing route yet need to be investigated further to meet the requirement of practical applications [18].

Asymmetric capacitors are made by two electrodes, one is identical to those used in symmetric ECs, whereas the other is battery-like, relying on electron charge transfer reactions. The resulting hybrid devices combines the strengths of both batteries and supercapacitors. It presents greater capacity and operational voltages respect to a standard ECs maintaining higher cycle life and lower charging time respect to a standard accumulator [23]. A commercial example of this technology is the UltraBattery, composed by standard lead-acid battery positive electrode, standard sulphuric acid electrolyte and a specially prepared negative carbon-based double-layer electrode. The applications of this performing electrochemical hybrid device are in frequency regulation, solar smoothing and shifting, wind smoothing and other.

Chapter 2

Theory

At the beginning of this chapter Polymer-Derived ceramics and Electrospinning process are presented. Then the attractiveness of utilizing electrospinning in energy storage devices, is exposed. In the end, the electrochemical tests utilized in the present work are presented.

2.1 Polymer-Derived Ceramics

Polymer-Derived Ceramics (PDCs) are advanced ceramics, formed by the thermal treatment of particular polymers, denominated preceramic polymers. Their structure can be amorphous, crystalline or a mixture of both. The present work is focused on Si-based PDCs.

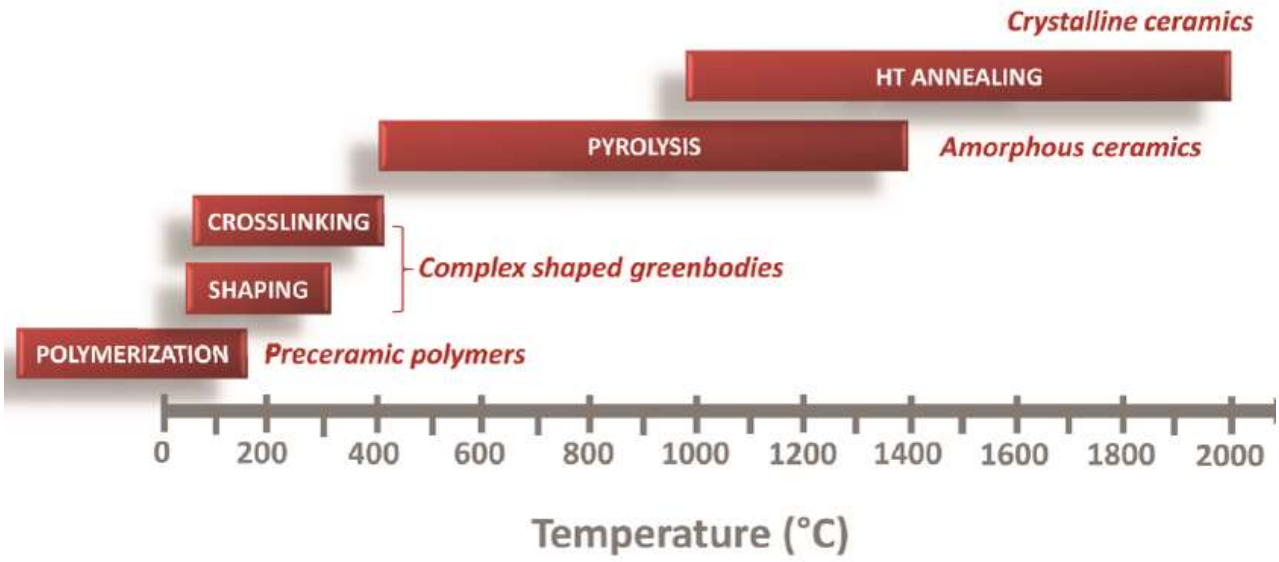

Fig. 2.1.1. The figure shows the changing of the PDCs nature with the temperature. (source: www.reseachgate.net)

The first reported polymer to ceramic transformation was presented by Verbeek and colleagues in early 1970s. They produced Si_3N_4/SiC ceramic fibers using polysilazanes, polysiloxanes, and policarbosilanes. The PDCs route is nowadays an emerging chemical process for obtaining near net-

shaped products; as attested by the increasing of commercial development of these materials and by the rising in the number of publication referred to this topic [24].

The major classes of PDCs are:

- Binary systems: SiC, Si_3N_4, AlN, BN.
- Ternary systems: SiOC, SiCN, BCN.
- Quaternary system: SiCON, SiBCN, SiBCO, SiAlCN, SiAlCO.
- Pentanary system of PDCs have been reported in recent years [25].

These materials are shaped in polymeric form using conventional or innovative polymer-forming techniques such as injection molding, extrusion, coating from solvent, resin transfer molding (RTM), polymer infiltration pyrolysis (PIP) and electrospinning. Avoiding the traditional powders formation and sintering have several benefits. First of all, binary SiC and Si_3N_4 cannot dissolve nitrogen or carbon, respectively, to form SICN compositions. Similarly, SiO_2 and SiC cannot dissolve carbon or oxygen to produce SiOC ceramics. As a result, the ternary SiOC and SiCN varieties can only be synthesized using this molecular approach [25]. More over a higher amount of materials shapes are obtainable. Ceramics fibers, layers or composite materials can be produced, while they cannot be easily obtained using the traditional route. Sintering additives which lower the thermo-mechanical properties and thus constrain technical applications, are avoided with these materials. Once formed, objects made from preceramic polymers can be converted by heating. The relatively low treatment's temperatures (lower energy consumption) of 1000-1300°C in comparison with classical ceramic powder processing technology, which requires temperatures up to 2000°C are very interesting from and economical point of view [25]. PDCs have been studied for their use as structural ceramic for high temperature applications due to their stability respect to creep, oxidation, crystallization, phase separation and chemical reactions up to 1500°C and higher. In recent years novel insights into their structure at nanoscale level have contributed to the understanding of the various useful and unique features of PDCs. As a consequence, their possible fields of applications have been extended significantly. From high-temperature-resistant materials (energy, automotive, aerospace) and hard materials to chemical engineering materials (catalyst support, filters), and most recently functional materials in electrical engineering as well as micro/nanoelectronics.

2.1.1 Preceramic Polymers

Polymer precursors are inorganic systems that provide ceramic materials with a tailored chemical composition and a defined nanostructural organization by proper thermal curing process. The type and the molecular structure of preceramic polymer influences the composition, number and distribution of phases and so the final ceramic's microstructure. For this reason, the macroscopic chemical and physical properties of PDCs can be tailored adjusting the molecular precursor [25].

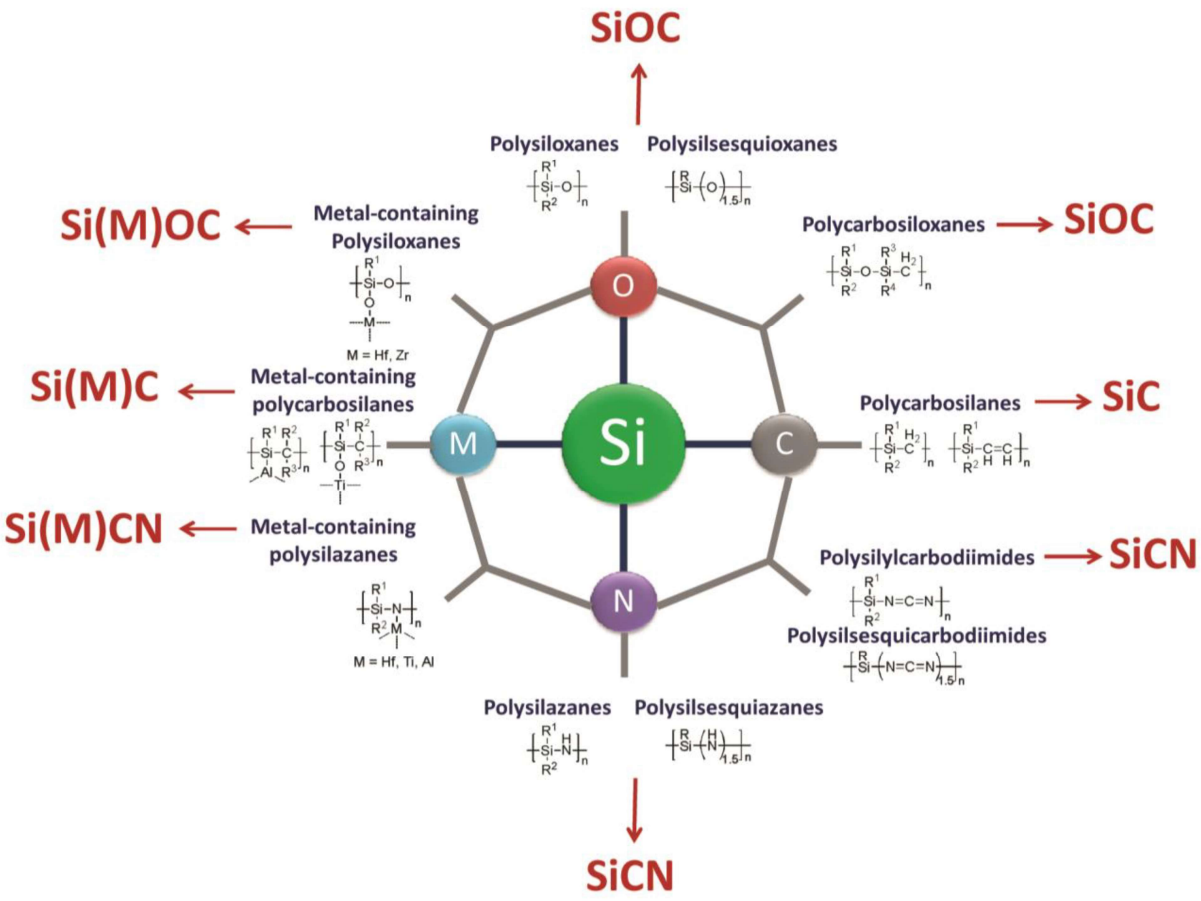

Fig. 2.1.2. The figure shows different types of polymeric precursor and, in red, the ceramics obtainable from them. (source: www.mdpi.com)

Fig. 2.1.3 shows the general formula for an organosilicon precursor polymer. The two important parameters to modify the polymer precursor and in this way the final ceramic, are group X of polymer backbone and group R_1, R_2 attached to the silicon atom. The variation of X results in different classes of Si-based polymers, exposed in figure 2.1.2. The variation of functional groups R_1, R_2 influences chemical and thermal stability, solubility and rheological, optical, electronic properties. In addition, the organic side groups allow the control of the amount of carbon in the ceramic [25].

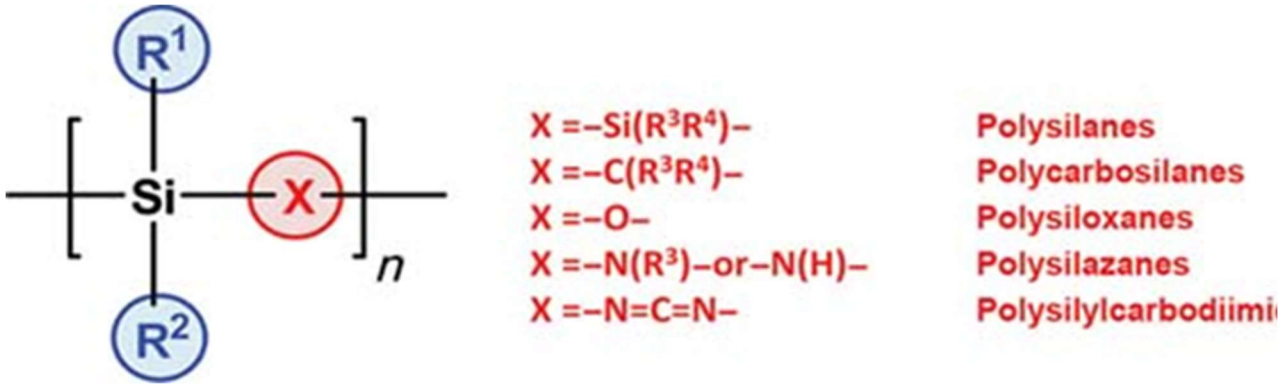

Fig. 2.1.3. The figure shows the oversimplified general formula and the different classes of organosilicon polymers. (source: www.researchgate.net)

There are several requirements for preceramic polymers. In order to avoid volatilization of low-molecular components and to be effective for the thermal decomposition process, polymer should possess a sufficiently high molecular weight. They should have appropriate solubility and rheological properties for the shaping process. They should present functional active groups which give latent reactivity for the cross-linking step. Moreover, molecular precursors have to be cheap for being competitive with traditional ceramics and their synthesis has to be selective. For these reasons, even if several alternative routes for the synthesis of the molecular preceramic polymers are reported, they are frequently produced from organochlorosilanes. These chemical compounds possess good commercial availability and low cost combined with a well-known chemistry [25].

2.1.1.1 Polysilsesquioxanes

An interesting subcategory of polyorganosiloxanes, generally denoted as silicones, are the polyorganosilsesquixanes. These branched “nanoblock” preceramic polymers with a general formula $-[RSi-O_{1.5}]_n-$ can have different configurations. Their particular structure constituted by a tridimensional disposition of atoms highly interconnected is favorable to undergo a ceramic conversion. For this reason, their ceramic yield will be elevated. On the other hand, their peculiar structure can be a problem in process like electrospinning. In this case another polymer, with a more linear structure, has to be added to the solution in order to guaranty the formations of good quality fibers [26]. In the present work three different types of polysilsesquioxanes have been used:

- MK
- H44
- RSN

These polymeric precursors, presenting different organic groups R, have different carbon content.

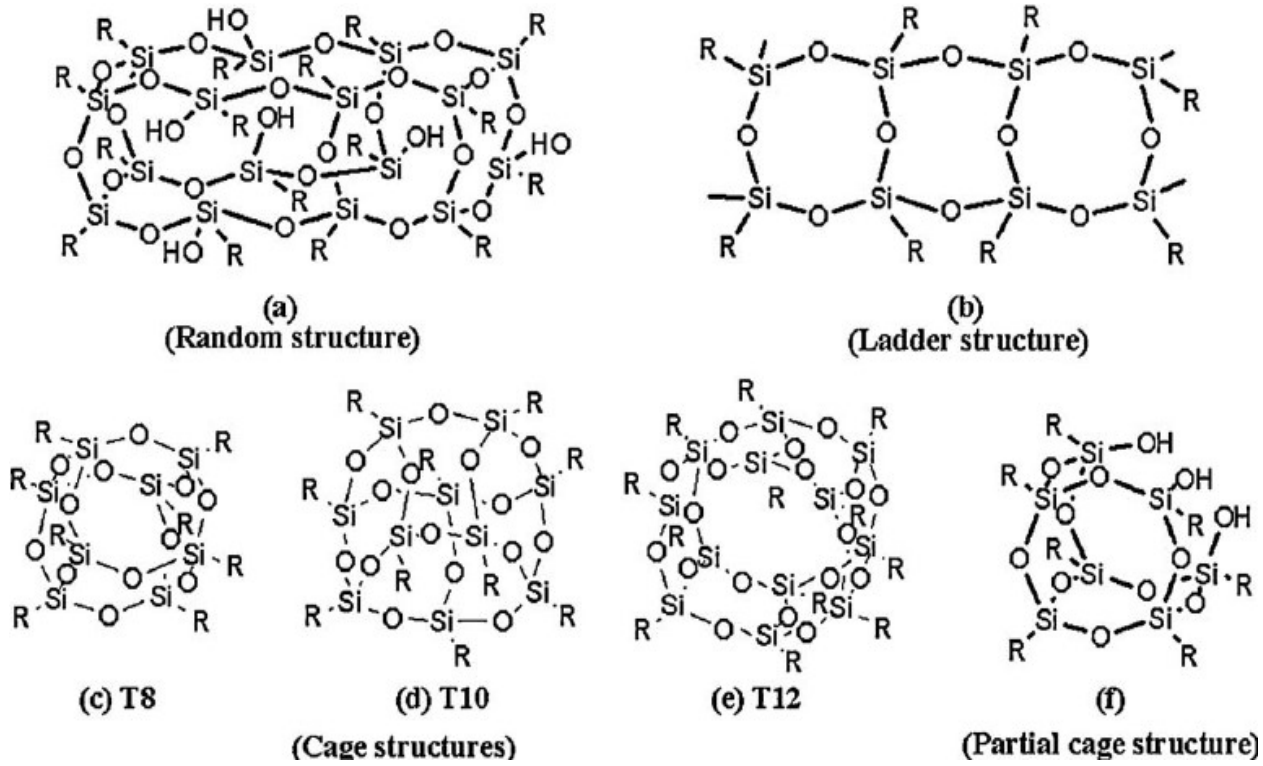

Fig. 2.1.4. The figure shows the disposition of atoms for different structural types of polyorganosilsesquioxanes. (source: www.researchgate.net)

The general synthesis method for preparation of polysiloxanes comprises the reaction of chloroorganosilanes with water. Cross-linked polysiloxanes can also be prepared by the sol-gel process through hydrolysis and condensation reactions of hybrid silicon alkoxides. This route was used by the first researchers who opened the field of silicon oxycarbide glasses. With this method extra elements (B, Al, Ti) can be introduced in the preceramic network. The drawbacks of the sol-gel process are the poor control of the viscosity, which prevents the utilization of many shaping techniques [25].

2.1.2 Cross-linking and Ceramization

Cross-linking is the first treatment which preceramic polymer undergoes after being shaped. The produced part needs to be transformed in to thermoset material capable of retaining its shape during the following ceramization process. The incorporation of active functional groups such as Si-H, Si-OH or Si-vinyl group enables the formation of a thermoset via condensation or addition that occurs

spontaneously under 200°C. The cross-linking temperature can be lowered by using catalysts, with the additional benefit of avoiding the evaporation of oligomers with formation of bubbles and so increasing the ceramic yield. Other techniques exist like oxidative and laser curing. If a large amount of fillers is added to the preceramic polymer, cross-linking might not be necessary [25].

Ceramization is the polymer to ceramic conversion and is the second treatment which preceramic polymers, already become thermoset materials, undergo. After thermal treatment at about 1000°C, amorphous SiC, $Si_xC_yO_z$ and $Si_xC_yN_z$, with tailored x/y ratio can be obtained, as shown in figure 2.1.5. This conversion leas to the decomposition and elimination of organic moieties such as methyl, phenyl, vinyl groups and Si-H, Si-OH, Si-NH_x groups [25].

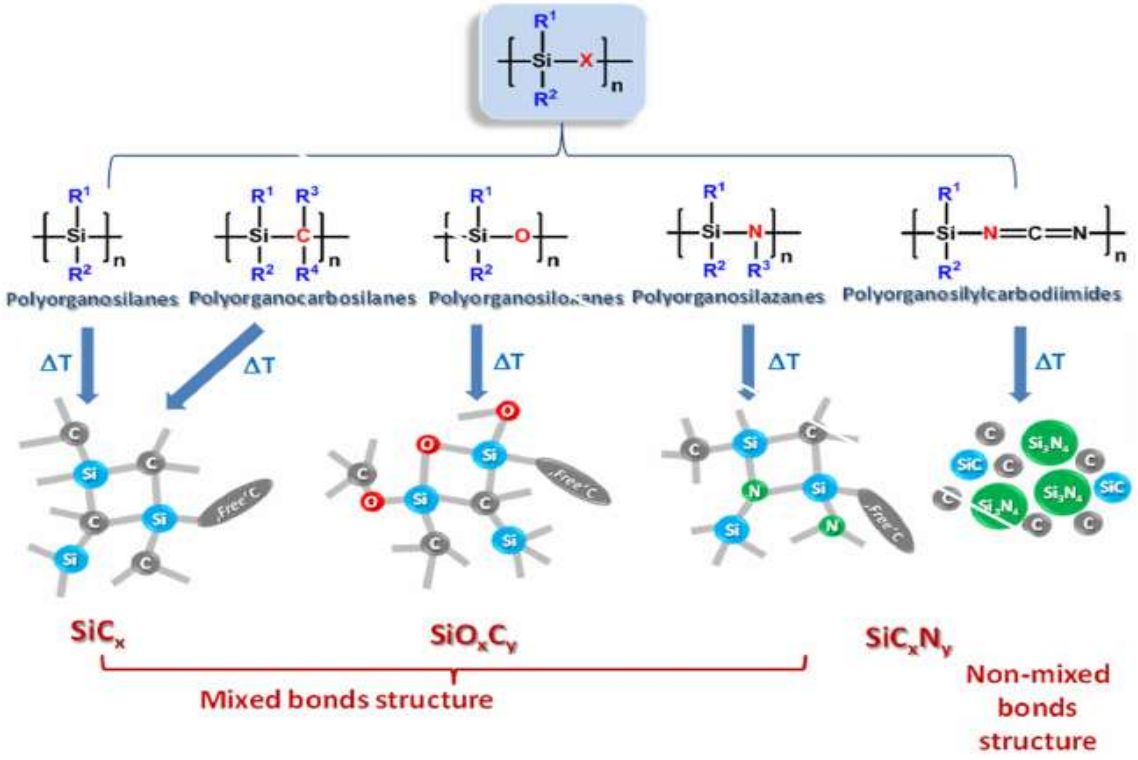

Fig. 2.1.5. The figure shows the thermal decomposition behavior of basic organosilicon polymers. (source: www.researchgate.net)

Several processes can be applied such as laser pyrolysis, microwave pyrolysis, ion irradiation, but the most widely used is oven pyrolysis, in which the flowing gas continuously removes the decomposition gaseous products generated by the material. The ceramization is a complex but versatile process. Lot of variables have to be monitored. Changing one of them can influence the final material's characteristics, such as composition, microstructure, density, ceramic yield and therefore their properties and applications [25]. Type of atmosphere can modify the composition of the resulting ceramic. If processed in air, oxygen's presence can lead to the elimination of carbon contained in the

material. Processing in high nitrogen pressure leads to the incorporation of some nitrogen in the material's structure, modifying properties as electrical conductivity [27]. Treatment atmosphere's pressure produce microstructural changes as well. Vacuum promotes carbo-thermal reduction reactions and so enhance crystallization. High pressure oppositely hinders these reactions and so leads to a suppression of crystallization. If working in controlled atmosphere also the flow rate of the gas has to be controlled. A too fast removing of decomposition gas can lead to a lower ceramic yield. Temperature-related processing parameters such as heating rate dwelling time and temperature affects the extent of crystallization, carbothermal reduction reactions and fillers reactions and so influence the final composition and microstructure. The heating rate is crucial because a fast releasing of decomposition gasses can lead to cracks. It has to be low especially in polymer-ceramic transformation region. If net-shaped processing is required polymer-ceramic transformation can be not carried out completely.

2.1.3 Structure of PDCs

The microstructure of PDCs is a complex mix of crystalline nanodomains in an amorphous matrix. Quantity and dimensions of these domains are affected primarily by the structure of initial preceramic polymer and then by the temperature and the time of the pyrolysis. For example, SiCN ceramics obtain through the same route from different preceramic polymer such as polysilazanes and polysilylcarbodiimides, presents different microstructures. At elevated temperature, the devitrification process of the initial amorphous network starts and leads to local crystallization of different phases. The process begins with a redistribution of chemical bonding then the material undergoes to a phase separation and at the end crystallization occurs. In many cases there is a releasing of gaseous product such as CO, SiO, or N_2. Regarding the microstructural evolution of PDCs from the amorphous state to the partially crystalline state the following major aspects can be highlighted [25]:

- During annealing, the entire bulk of the material undergoes a phase separation process.
- Separation of a "free" carbon phase which is subjected to a graphitization process.
- Increasing the temperature, local formation of nanocrystal occurs.

It was proposed that the nature of the nanodomains is the basis for the remarkable resistance of PDCs to crystallization even at ultrahigh temperature. Typical structural features of SiCO and SiCN (most common system) are listed in table 2.1.1.

Atomic and Nanostructure	SiOC	SiCN
Si atoms	Tetrahedrally bonded to C and O	Tetrahedrally bonded to C and N
C atoms	-sp^3 when bonded to Si atoms -sp^2 when bonded to other C atoms	sp^3 when bonded to Si atoms -sp^2 when bonded to other C atoms - not bonded to N atoms
Size of nanodomains	1-3 *nm* gradually increase in size with annealing	1-3 *nm* gradually increase in size with annealing

Tab. 2.1.1. The table shows structural features for SiCO and SiCN systems. (source [25])

The introduction of further elements, such as boron or aluminum, into preceramic polymers can increase the high temperature stability, creep and oxidation resistance, which are features directly correlated to the nanostructure of the ceramics.

2.1.3.1 Structure of SiOC ceramics

The present work is focused on SiOC ceramics. Silicon oxycarbide is an amorphous covalent ceramic material whose composition can be expressed as $SiCxO_{2(1-x)} + {}_yC_{free}$ where the first term refers to the amorphous silicon oxycarbide network and the second term is free carbon not bonded to Si or O atoms [28]. The microstructure depending to the preceramic polymer utilized and to the annealing parameters (temperature and time) evolves from a homogeneous amorphous network to a more complex network. The microstructure, shown in figure 2.1.6, is characterized by the presence of:

1. Amorphous network composed by mixed bonds between Si, C, O atoms.
2. Regions depauperated by C atoms and so rich in silica SiO_2. These regions can be etched with hydrofluoric acid leaving a porous structure as reported in [29].
3. Regions enriched in C atoms.
4. Regions of “free” turbostratic graphite.

in particular “free” carbon clusters play a key role, which has not been completely understood yet, in the polymer to ceramic transformation and in tuning the properties of PDCs materials.

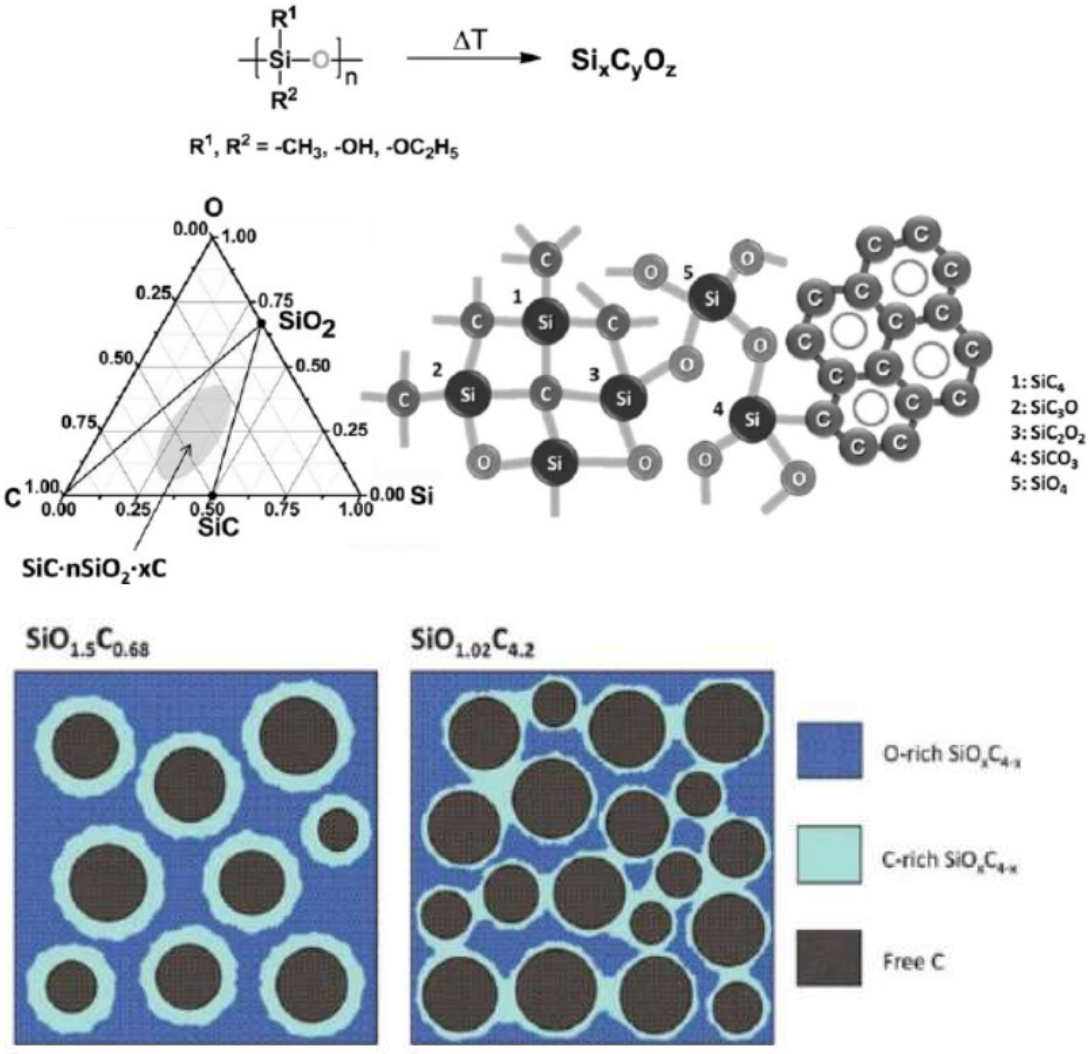

Fig. 2.1.6. The figure shows two schematic illustrations of SiOC microstructures. (source: www.researchgate.net)

The understanding of such disordered and variable structure is not completed yet. For comprehending the PDCs microstructure, characterization methods such as Raman spectroscopy, FT-IR, XRD, TEM, SEM, SAXS, and theoretical modeling are being used.

2.1.4 Properties of PDCs

As exposed so far properties of PDCs are intrinsically related to their peculiar structure. Tuning the structure will affect also their properties. These materials have captured interest for their chemical and mechanical stability in extreme environment (presence of reactive species and high temperature).

2.1.4.1 Mechanical properties

The mechanical properties of PDCs in form of fiber or bulk samples have been widely studied. Regarding the fibers, lot of articles treat SiC, Si(O)C (where oxygen is incorporated during annealing), SiBCN, SiAlON, and BN. Tailoring the annealing temperature and the starter polymer value of tensile strength and elastic modulus are being constantly increased (SiC fiber with tensile strength of 2.5GPa and elastic modulus of 400 GPa have been reported [30]). For the aims of present work, mechanical properties of fiber mats are important in order to make a self-standing electrode. If no supporting metallic plates are required the specific capacitance of the assembled cell (battery or supercapacitor) is enhanced. The handling of bulk PDCs samples falls outside the scope of the present work.

2.1.4.2 Chemical properties

PDCs, like SiOC, exhibit greater durability then the pure silica glass, SiO_2 in both basic and acidic media. This thanks to the presence of mixed bonding, Si-C bonds are less sensible to nucleophilic attack, higher compositional disorder, and cross-links due to the presence of carbon atoms. Increasing the amount of carbon enhances chemical durability. For PDCs pyrolyzed at high temperatures, parabolic oxidation rates and formation of a dense and continuous oxide layer, with sharp interface, are observed. The parabolic αK_p constants increase with the amount of "free" carbon present [25]. The elevated chemical stability, which can prevent detrimental reactions, is useful to unsure a long electrode's working life in energy storage devices [31].

2.1.4.3 Electrical properties

Although electrical properties of PDCs have been reported since the early discover of these new materials, these studies were neglected for almost one decade and were undertaken only form 2000. The room-temperature dc conductivity of PDCs varies up to 15 orders of magnitude (typically in the range 10^{-10} to 1 $(\Omega cm)^{-1}$), depending on the polymeric precursor, composition, pyrolysis temperature and atmosphere. Their behavior passes from insulator, for low pyrolysis temperature (600°C) to semiconducting at medium temperature (800°C). The Increase in conductivity is attributed to the loss of residual hydrogen accompanied with an increase in the sp^2/sp^3 ratio. For higher temperature

(1400°C) the formation of a percolation network of C_{free} ensure a metallic-like electron conductivity. For high-carbon SiCO, such as those obtained from phenyl-containing polysiloxane, the development of a continuous C network occurs at a lower temperature (1100°C). The conductivity of PDCs can also be changed by adding filler particles to the preceramic matrix. It is reported that introduction of $MoSi_2$ to methyl-containing siloxanes leads to the drastic increase in the conductivity of the $MoSi_2$/SiOC composites by the formation of a percolation paths through fillers particles. More recently MW-CNTs have been homogeneously dispersed into an insulating PDCs with a corresponding increase of the electrical conductivity up to 7 orders of magnitude for a volume fraction of CNTs < 1%. [25]. Possessing high electrical conductivity is a fundamental requirement for the use of these material as electrodes for supercapacitors and batteries. Electron conductivity is related to the capacitance of the material and to the impedance of the resulting storage device.

Even if there are lot of studies related on the magnetic and optical properties shown by PDCs their handling falls outside the scope of the present work.

2.1.5 Applications of PDCs

Polymer-Derived Ceramics has found application in several key fields thanks to their unique physical, chemical and functional properties coupled with their ability of being shaped using a wide variety of processing methods. PDCs have been widely used in ceramic-matrix composites (CMC) lowering the amount of time and money required in order to achieve a component with low residual porosity and good mechanical properties. Preceramic polymers are suited for producing porous ceramics which can be used in thermal protection, impact absorption and 3D reinforcement. With preceramic polymers processed by various lithographic methods, miniaturized ceramic components are obtainable. Thanks to their chemical and thermal stability these components are used as sensor and probe for extreme environments. As stated previously, ceramics in fibers or coating shapes are easier obtainable via polymer route than the traditional one. In particular, there is a strong interest in low temperature, cost effective ways of protecting metal surfaces against oxidation, wear and corrosion [32]. Other applications are layers with controlled porosity for catalyst support or biomedical devices. The growing interest in using preceramic polymer as joining medium in CMC and ceramic monoliths have to be reported as well. Fibers represent the oldest and the most successful commercial application of preceramic polymers. SiCO fiber with boron and nitrogen show superior oxidation and creep resistance and have been used in CMC. Ceramic fibers functionalized with anantase's particles, showing high photocatalytic activity, have been used for purification of industrial wastewater.

Recently application of PDCs in energy storage have been studied. Experimental results indicate that SiCN phase is active in terms of lithium intercalation/deintercalation because it contains disordered carbon that can act as a percolation path for lithium as well as for electrons. SiCN ceramics, used as anode material, can therefore combine the role of binder phase for graphite and conductive additive in one material. Moreover, the chemical stability of this material prevents the degradation during the use [25]. SiOC ceramics seem to be giving not encouraging results as electrode material in Li-ion batteries. For their easy shaping methods, their low price and their chemical stability they are possible attractive materials for supercapacitors electrodes.

2.2 Electrospinning

Electrospinning is an electrostatic process in which molten or solubilized polymer is spun in form of thin fibers with micro and nano dimensions. The first studies related to the process of electrospinning were conducted in 1914. The first patent related to the electrospinning of cellulose acetate fibers with micrometric sizes, was obtained by Formhals in 1934. More studies conducted in the last years of the century and driven by the growing interest of the possible application of this technique, have been focused on the determination of the major processing parameters and their influence [33].

2.2.1 Electrospinning process

The process consists in the application of a strong electric field between a needle, usually of a syringe, with an orifice and a metallic collector. The polymeric fluid is feed through the orifice by a volumetric pump. The potential's difference generates an electrical force, which produce a charges separation in the solution, and prevailing on the surface tension of the solution leads to the formation of a jet from the orifice to the collector. The electrically charged jet is accelerated and tapered by the electrical field which also promote the evaporation of the solvents and thus generates the polymeric fiber. Increasing the potential's difference, the liquid meniscus of the solution at the needle's hole assumes a conic shape, called Taylor's cone, in which the charges concentrate themselves. Increasing again the voltage leads to the formation of the jet form the cone's tip and start the electrospinning process. The charges transported by the jet, which direction is determined by the electric field, are dissipated by the earthed collector. The viscous forces of the polymeric fluid stabilize the jet and allow the

formation of thing fibers instead of droplets. The high charge density on the jet's surface makes the fiber oscillating. The jet's oscillation is so fast it looks like there are multiple fibers. In reality, it is a single oscillating fiber which covers the collector with a random orientation and produces a mat. The diameters of the fibers are in micro or nano scale and are much more smaller compared to the mechanically extruded ones. The earthed collector dissipates fiber surface's charges and allow the detachment of the fibers membrane. An illustration of the process is provided in figure 2.2.1.

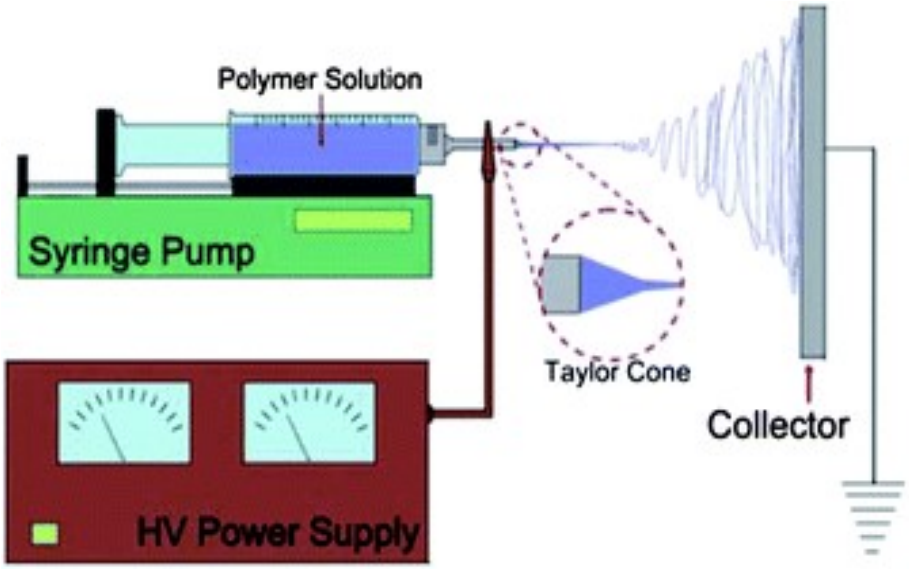

Fig. 2.2.1. The figure shows a scheme of electrospinning process. (source: www.rsc.org)

Various collectors with different shapes can be adopted depending on the final aimed result.

2.2.2 Fibers Formation

The formation mechanism of electrospun fibers is complex and can be divided in different stages.

The first stage is jet's start. Droplets of polymeric solution keep forming, at the tip of the syringe, and falling down. The only two forces that act on the drops are surface tension, γ and gravity, Fg. When these two forces balance each other the radius of the droplet at the tip's end r_0 is:

$$r_0 = \sqrt[3]{\frac{3R\gamma}{2\rho g}} \qquad (2.2.1)$$

Where R is the internal radius of the tip, ρ is the density of the liquid and g is gravitational acceleration.

If an external electric field is applied, the surface tension become balanced by the sum of gravity and electrostatic force, Fe. With Fe equal to:

$$F_e = \frac{4\pi\varepsilon V^2}{\ln(4L/R)^2} \tag{2.2.2}$$

Where V is the applied voltage, L is the distance between the tip and the collector and π is the permittivity of the medium, generally air.

The radius of the droplet is now r with $r < r_0$. With r equal to:

$$r = \sqrt[3]{\left\{\frac{3}{2\rho g}\left[R\gamma - \frac{2\varepsilon V^2}{\ln(4L/R)^2}\right]\right\}} \tag{2.2.3}$$

The electric field produces a charges separation in the solution's drop situated at the needle's orifice. The surface, as the needle, is positively charged while negative charges moves inside the drop. This separation generates a force opposite to the surface tension. The electrically charged droplet remains stable as long as the surface tension (inwardly directed) prevails upon repulsive electric force (outwardly directed).

An increase in the voltage produces a decrease in the drop's radius. At the critic voltage's value, Vc instability arises and the shape of the droplet switch form spherical to conical, denominated cone of Taylor and a little vessel is generated. Vc in *kV* is equal to:

$$V_c = \sqrt{\{(2h/L)^2[\ln(2h/L) - 1.5](0.117\pi R\gamma)\}} \tag{2.2.4}$$

Where h is the distance between capillary vessel and the earthing, L and R are the length and radius of the vessel respectively and γ is the surface tension of the liquid. Equation 2.2.4 is valid for solution presenting low value of viscosity and conductivity.

This is a crucial step that decides the formation of the fiber or its subdivision in droplets.

The second stage is vessel's elongation. When the voltage exceeds critical value, Vc the capillary vessel turns in to a real jet. The separation of charges in the vessel contributes, combined with the evaporation of solvent, to the elongation and stretching of the jet. In this stage, the jet is defined stable and the flow behavior is laminar. Stability is given by the entanglements of the polymer.

The third stage is the instability region. The jet, stable and straight in the previous step, becomes now curved because of several instabilities denominated Raleigh, symmetric and whipping ones. These instabilities are determined by the intensity of the electrical field. Intense electric fields produce Jet's oscillations similar to whip's lashes that happens within a geometrical cone-shaped space. At this point the increase of surface area and solvent's evaporation reach their maximum. As a consequence,

the whipping instability is the one which produce the major reduction in the size of fibers during the electrospinning process [34]. In this stage lot of strong and highly variable forces act contemporaneously. Gravity, surface tension, electrostatic force, repulsive coulomb's forces, viscoelastic forces, friction forces influence the jet's diameter and contribute to the determination of the final dimensions of the fibers.

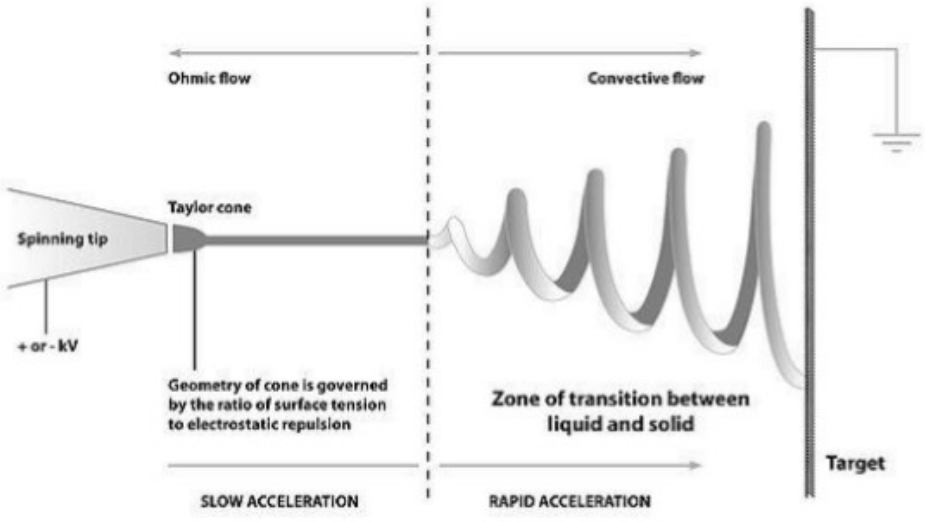

Fig. 2.2.2. The figure shows a scheme of Taylor's cone and whipping instability. (source: www.rsc.org)

The last stage is the solvent's evaporation. The evaporation starts at the beginning of the jet and as exposed, have a pick during the instability region. Ideally all the solvent has to be already gone when the fiber touches the collector in order to prevent defects in the electrospun material.

2.2.3 Processing parameters

Despite the simplicity of the instrumentation required for the electrospinning technique, the processing variables that have to be controlled in order to have a fruitful result are numerous. These parameters can be ideally divided on the base of their nature into three groups: solution's parameters, process parameters, environmental parameters [35].

The polymeric solution's parameters have the greatest effect on the results of electrospinning process. These parameters are:

- Viscosity. The viscosity of a polymeric solution is linked to the molecular weight of the polymer in the solution and to his concentration. A higher molecular weight increases the numbers of entanglements between polymeric chains as a higher concentration does. If the solution doesn't present adequate viscosity the jet breaks into droplets or the fibers morphology will present surface defects.
- Surface tension. A low surface tension, achievable with the use of proper solvents or surfactant, hinders the aggregation of solvent's molecules and produces defect-free smooth fibers.
- Conductivity. A high electrical conductivity, obtainable through the addition of a salt, is related to an elevated number of charges in the jet. The stretching of the jest is produced by the repulsion of the charges, thus increasing their number produces a stronger stretching and so thinner and smoother fibers. Attention has to be paid because an excessive conductivity can lead to excessive instability and to the jet's breakup.
- Dielectric constant. A high dielectric constant produces an extended instability region which generates a bigger deposition area. This produces smoother and thinner fibers.

The process parameters can also produce significant effects on the electrospun fibers, thus they have to be carefully set. These parameters are:

- Voltage. The applied voltage and the resulting electric field directly influence stretching and acceleration of the jet. Elevated voltages ideally increase elongation of the jet and solvent evaporation but also decreases the transit time toward the collector. If this time is not sufficient the stretching and elongation of the jet cannot happen properly and the final diameter of the fiber will be greater. This means that, a balance in the applied voltage is required to achieve a good fibers dimension and morphology.
- Flow rate. The effect of the flow rate and so of the amount of solution available for the spinning process is complex. If the amount of solution pumped is equal to the amount of solution pulled from the jet, an increase in the flow rate produces a higher number of charges and so a stronger stretching. The resulting fibers will be thinner. If the flow rate increases excessively there will be an increase in the fiber's diameter and a possible incomplete evaporation of the solvent. This can lead to their re-solubilization on the collectors.
- Collector's type. Different collectors with different shapes and sizes are utilized for the electrospinning process, depending on the designated application of electrospun mats. If the collector presents a pattern, fibers will be deposited following that pattern. With moving

collectors, more aligned fibers are achievable. This gives more time for the solvent evaporation.

- Distance tip/collector. The distance between the tip and the collector affects the transit time and electric field intensity. If the distance is short, transit time is low and jet's acceleration is high. These conditions can produce instability and an incomplete evaporation of the solvent resulting in fibers with defects or large diameter. If distance is long, transition time is sufficient to provide a good stretching; but If the distance is too much the electric filed cannot produce a good stretching and the fiber diameters will grow. If the distance exceeds a critical value, related to the applied voltage, there will be no jet formation and deposition.
- Needle's size. A needle with small orifice produces thin and defect-free fibers. If the orifice is too small it is not possible to generate a droplet form its tip.

The last type of parameters are environmental parameters. Their influence is not completely understood and so it is still under evaluation.

- Temperature. Increasing the temperature makes viscosity decrease and enhances the evaporation of the solvent leading to a greater stretching of the spray. In general, conducting electrospinning process at high temperatures is fruitful.
- Humidity. A low level of humidity enhances solvent's evaporation. If the evaporation speed exceeds the speed of flowing solution through the orifice, obstruction of the syringe can occur. On the other hand, a high level of humidity can lead to the formation of pores on the fiber surface, which dimensions are related to the percentage of humidity. This phenomenon happens due to the evaporation of water previously condensated on the fiber. Fiber surface after the evaporation of the solvent cool down and this way the formation of water can occur. The effect of humidity on the distribution of charges is not completely clear.
- Pressure. Vacuum condition produces instabilities in the initial stage of the process due to a backwash of the droplet. Usually electrospinning is conducted under atmospheric pressure
- Atmosphere. Different gasses behave differently in presence of electric fields. Usually electrospinning is conducted in air.

Several studies report quantitative methods for the evaluation of the optimum conditions for the process. These methods are based on the equations of conservation of mass, motion and charge.

2.3 Electrospun architectures for energy storage

Electrospinning is attracting close interest as a versatile fabrication method for “one dimensional” mesostructured organic, inorganic (ceramic, metallic, composite) and hybrid materials of controlled dimensions and morphologies, such as core-sheath, hollow, porous, dense or even multichanneled microtube arrangements. Dimensionality and compositional flexibility of electrospun micro or nano fibers and mats, are increasingly being investigated for the targeted development of electrode materials where the properties associated with nanoscale features such as high surface area and aspect ratios, low density and high pore volume allow performance improvements in energy conversion and storage devices [33]. This growing interest has to be contextualized in a scenario where energy from renewable sources is bound to play an increasingly relevant role and so efficient energy conversion and storage devices are required to constantly improve their performance in terms of cost, ease of fabrication, durability, energy stored and power delivered. These demands can be obtained by performance improvement in ionic conductivity, cyclability, reversibility, chemical stability, interfacial resistance as well as mechanical strength of the electruspun materials. The studied applications of electrospun material in energy are numerous; nanofibers for fuel cells, support materials for electrocatalysts, electrolyte membranes and still photoanodes, counter electrodes, electrode materials for lithium-ion batteries and for supercapacitors. Among the methods for generating fibrous nanostructure, electrospinning is a top-down approach that is simple, versatile and cost-effective allowing the fabrication of nanofibers in a continuous process and at long length scales [33]. As previously exposed ECs are suitable energy storage devices with high power density, rapid charge/discharge rate and high durability. They are used in lot of field for delivering high power pulses, load levelling or fast and reliable energy storage. The present work is focused on electrospun PDCs fibers for double layer supercapacitors The Coupling of material (SiOC ceramics), with morphology (fibers), produced by technology (electrospinning), for the application (supercapacitor) is expected to be fruitful for several reasons summed in the figure 2.3.1.

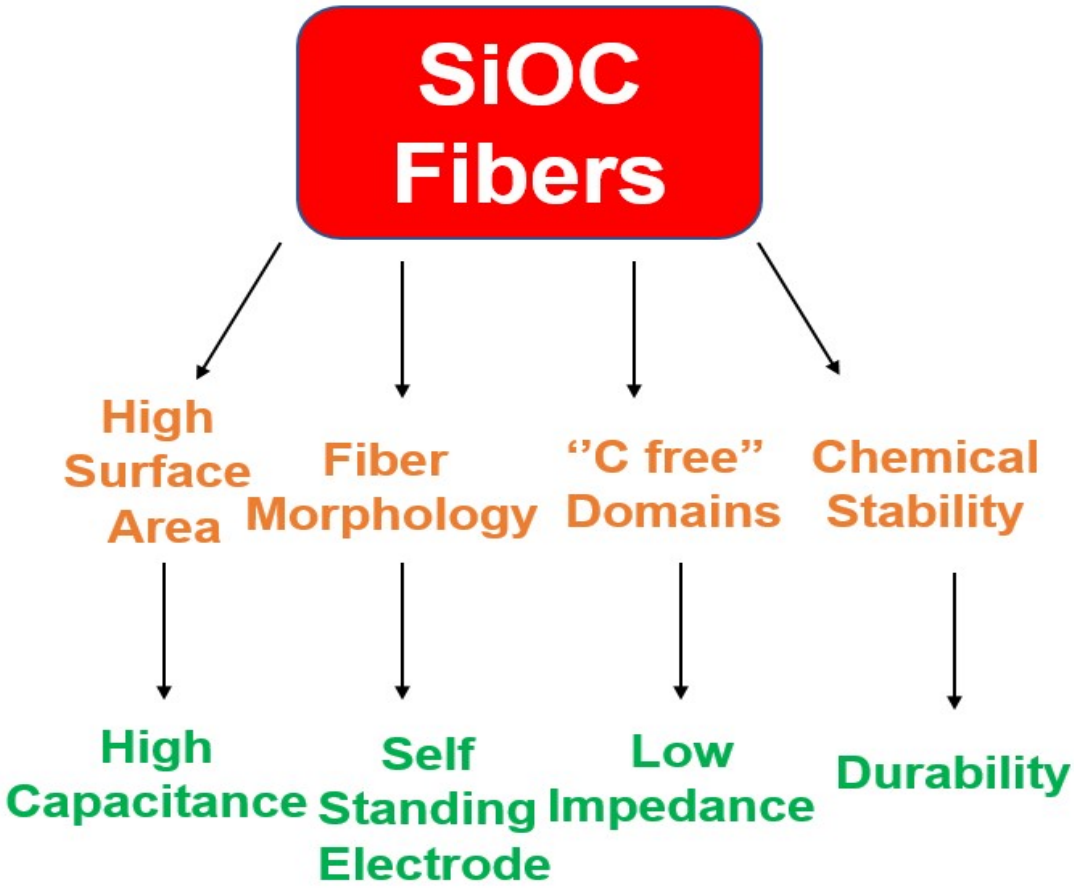

Fig. 2.3.1. The figure shows the characteristics of SiOC fibers (orange) and correlated electrode's properties sought (green) (source: personal figure)

Coupling a flexible production method and variable type of material allow to precisely change the chemical-physical properties and so to rapidly and easily adapt the material for the selected application.

2.4 Electrochemical analysis methods

The performance of a supercapacitor can be characterized by a series of key parameters. To accurately measure these parameters, a variety of methods have been proposed and are used in academia and industry. Unfortunately, methodology to reliable measurement of supercapacitor's performance is not well standardized [36]. As a result, some confusion has arisen due to the inconsistence between different evaluation methods and practice. The present work is focused on Materials, and not device, properties. The electrochemical methods used to determine the electrode's material properties are

cyclic voltammetry (CV), constant current charge/discharge (CCCD) and electrochemical impedance spectroscopy (EIS).

2.4.2 Cyclic Voltammetry (CV)

CV test is used to characterize supercapacitor devices or electrode's materials under the application of ramping voltage. Differentiating equation 1.4.1 with respect to *t* and assuming that capacitance is constant we obtain:

$$\frac{dq}{dt} = C\frac{dE}{dt} \tag{2.4.1}$$

Where *dQ/dt* is an expression for current and *dE/dt* is the potential scan rate ν. The test consists in the application of a linearly changed electric potential between positive and negative electrodes. Potential change with a scan rate ν into a set potential window. The resulting output is a plot of current calculated in *A* against potential *V* that depends on the set scan rate and potential window. Knowing the electrode's mass or area the result can be expressed in specific current, as shown in figure 2.4.1.

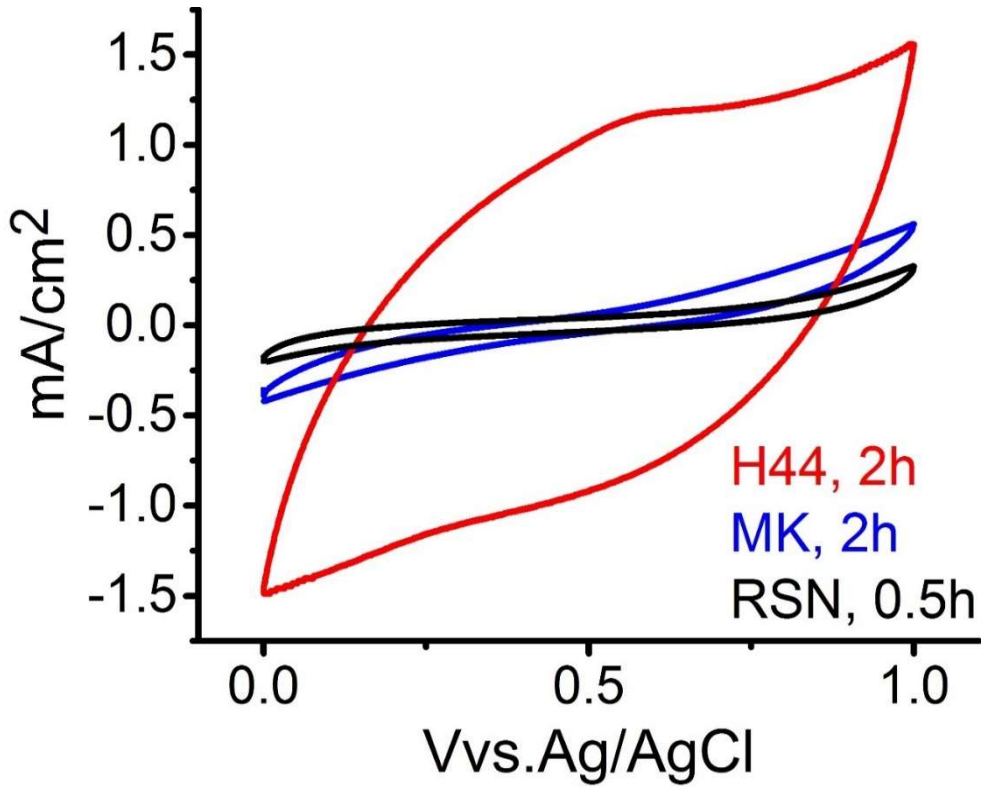

Fig. 2.4.1. The figure shows CV plots at various scan rate (source: experimental graph)

The test results can first be analyzed by examining the shape of the CV curves. For EDLC materials the shape of the resulting CV curves is rather rectangular [36]. From this test, specific capacitance C_s *F/g* of the electrode material is obtainable:

$$C_s = \frac{2\int idV}{\nu V} \tag{2.4.2}$$

Where:

- The integral is equal to the area of the CV curve, where current is expresses as *A/g* or A/cm^2.
- ν is the scan rate calculated in *V/s*
- V is the potential window, calculated in *V*

2.4.2 Galvanostatic Charge Discharge (GCD)

Galvanostatic charge discharge (GCD), called also constant current charge discharge (CCCD), is a test used to characterized supercapacitor devices or electrode's materials under direct current. It consists in the repetitive charge and discharge of the supercapacitor cell at a constant current level with or without a dwelling point in correspondence of the peak voltage. The resulting output is a plot of Potential calculated in *V* against time in *s*. The resulting curve depend by the applied current, as shown in figure 2.4.2.

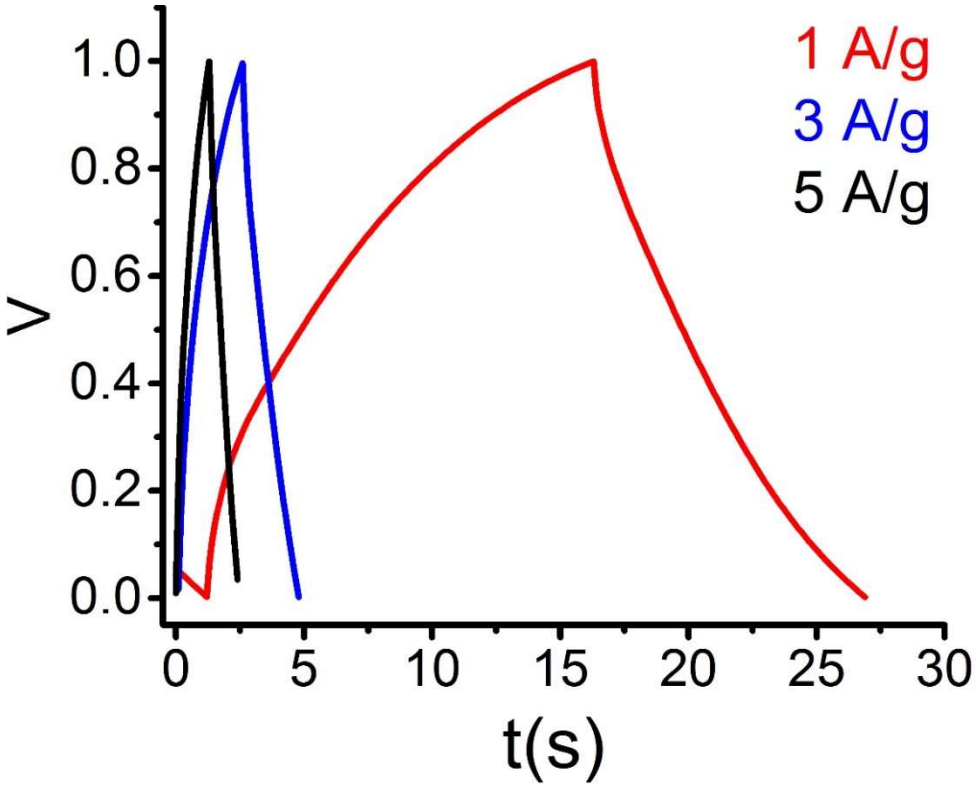

Fig. 2.4.2. The figure shows a CCCD plot (source: experimental graph)

From this test, specific capacitance C_s *F/g* of the electrode material is obtainable:

$$C_s = 2I/[m \cdot (\Delta V/\Delta t)] \quad (2.4.3)$$

Where:

- *I* is the applied current, calculated in ampere *A*.
- *m* is the mass of a single electrode, calculated in grams *g*.
- ΔV is the potential window during discharging process, calculated in volts *V*.
- Δt is the discharging time, calculated in seconds *s*, excluding the *iR* drop.

A couple of problems have to be mentioned. Driving a cell above its true maximum operating voltage can lead to an over-estimation of specific capacitance. Cells operating at these levels will have shortened lifetimes and poor efficiencies due to the non-reversible reactions within the cell. Very low rates of discharge also lead to large errors. Charge and discharge rates should be specified in units of current per electrode mass with the duration of charge and discharge corresponding to typical ultracapacitor applications. Current should be adjusted to provide charge and discharge times of approximately 5 to 60 seconds [37].

This test is widely and conveniently used also for determining the cycling stability of supercapacitor devices or electrode's materials [36]. The test consists in repeating a large amount of charge and discharge cycles. Capacity retention is evaluated comparing the specific capacitance calculated for first and last cycle.

2.4.2 Electrochemical Impedance Spectroscopy (EIS)

Electrochemical impedance spectroscopy EIS test is used to characterize the impedance of devices. The Impedance is a measure of the ability of a circuit to resist the flow of electrical current. Electrochemical impedance is usually measured by applying an AC potential with a fixed frequency to an electrochemical cell and then measuring the current through the cell. The resulting output, called Nyquist plot, is a plot of the imaginary part of the impedance -Z''[Ω] against the real part of the impedance Z'[Ω], as shown in figure 2.4.3.

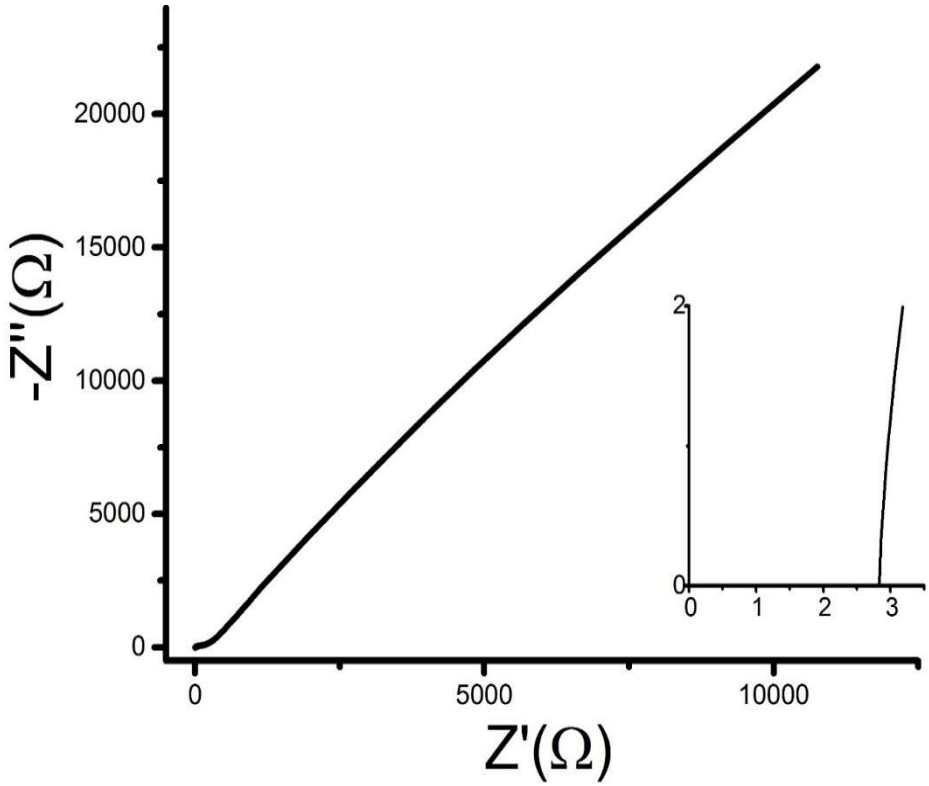

Fig. 2.4.2. The figure shows a Nyquist plot (source: experimental graph)

The left intercept of the real axis is a measure of dominant resistive behavior due to the interface between the electrolyte, electrode, and current collector, commonly referred to interfacial resistance. The right intercept of the real axis, fitted if not present, is a measure of internal resistance due to several factors as electrical conductivity and diffusion path length of ions [38].

Chapter 3

Materials and Methods

In this chapter are exposed the experimental procedures followed for the synthesis and characterization of SiOC electrospun mats. The first section regards the electrospinning of the polymeric mats. The second section regards the curing and pyrolysis treatments. The third section is related to the chemical and morphological catherization (FT-IR, Raman, OM, SEM, TEM). The last section concerns the electrochemical characterization of the materials.

3.1 Electrospinning of fibers mats

In order to produce a mat composed by fibers with a good and uniform diameter, electrospinning process has to be carefully set. This means to control not only the variables related to the spinning process but also to accurately formulate the polymeric solutions. Thin and uniform fibers that doesn't present beads or melted points are required for having high surface area and good mechanical properties, which are characteristics needed for a self-standing electrode.

3.1.1 Preparing the solutions

It is possible to obtain fibers by directly electrospinning a solution that only contains inorganic precursor and a solvent. However, in order to adjust the rheological properties and so to facilitate the process, a polymer is often introduced into the solvent. In this work, polyvinylpyrrolidone (PVP) is used because of his high solubility in a variety of solvents. Selecting an appropriate solvent is also important for electrospinning. A solvent with high solubility for PVP is necessary because the electrospinnability of the solution is mainly determined by PVP concentration. On the other hand, in consideration of the large loss weight of the silicon resin during the polymer-to-ceramic transformation, it is better to select the solvent that also shows a high solubility for the inorganic precursor, in order to increase the preceramic content [28]. In the present work 3 different solution, one for each preceramic polymer have been formulated:

1. Polymethyl-silsesquioxane, MK resin.
2. Polymethylphenyl-silsesquioxane, H44 resin.
3. Polyphenyl-silsesquioxane, RSN resin.

Characteristic of Silicone resins are listed in table 3.1.1.

Precursor	Chemical formula	Crosslinking groups	M_w(*g/mol*)
MK	$[(CH_3)_{0.96}(OR)_{0.04}SiO_{1.5}]_n$	OR = -OH and OC_2H_5	9100
H44	$[(C_6H_5)_{0.62}(CH_3)_{0.31}(OR)_{0.07}SiO_{1.5}]_n$	OR = -OH and OC_2H_5	2100
RSN-0217	$[(C_6H_5)_x(OR)_ySiO_{1.5}]_n$ $x > 0.9$; $y < 0.1$	OR = -OH and OC_2H_5	2500
Tab. 3.1.1. The table shows. (source: chemicals specifications)			

3.1.1.1 MK solution

Chemicals used in the MK solution are:

- Silicone resin (MK), Wacker Chemie AG, Munich, Geramany. Ceramic precursor.
- polyvinylpyrrolidone (PVP, M_w = 1300000 Da), Sigma-Aldrich, Saint Louis, Missouri, USA. Polymer added for increasing the electrospinnability of the solution.
- Isopropanol (Iso-P, anhydrous 99.5%), Sigma-Aldrich, Saint Louis, Missouri, USA. Solvent for MK and PVP.
- N, N-dimethyl formamide (DMF, anhydrous 99,8%), Sigma-Aldrich, Saint Louis, Missouri, USA. Solvent added for increasing the electrospinnability of the solution.

Like polyvinylpirrolidone thedimethyl formamide has been added in order to increase the electrospinnability of the solution and so to obtain fibers with smaller diameters and with a narrow size distribution. Introducing a small quantity of DMF, which has low surface tension (35.2 *mN/m* at 25°C) and high relative dielectric constant (36.7 at 20°C), adjusts the same properties of the solution producing benefic effects on the resulting material [28].

Chemicals ratio used in the MK solution are:

- Volumetric ratio for solvents: Iso-P/DMF = 80/20.
- Weight ratio for polymers: MK/PVP = 75/25.

- Total polymer weight ratio: Polymer/solvent = 30/70.

225 *ml* of solution has been prepared every time in order to avoid the solution's aging. First of all, a volumetric flask with total capacity of 500 *ml* has been washed with water and acetone. Then Isopropanol has been poured into the flask and gently stirred with a magnetic anchor. After that MK and PVP have been slowly introduced with a metal spoon. The agitation was needed in order to promote the mixing of all components and the formation of a uniform liquid phase. In the end DMF has been added. The spinning solution once formed has been leaved stirring for whole night. Figure 3.1.1 show a solution in a volumetric flask being stirred.

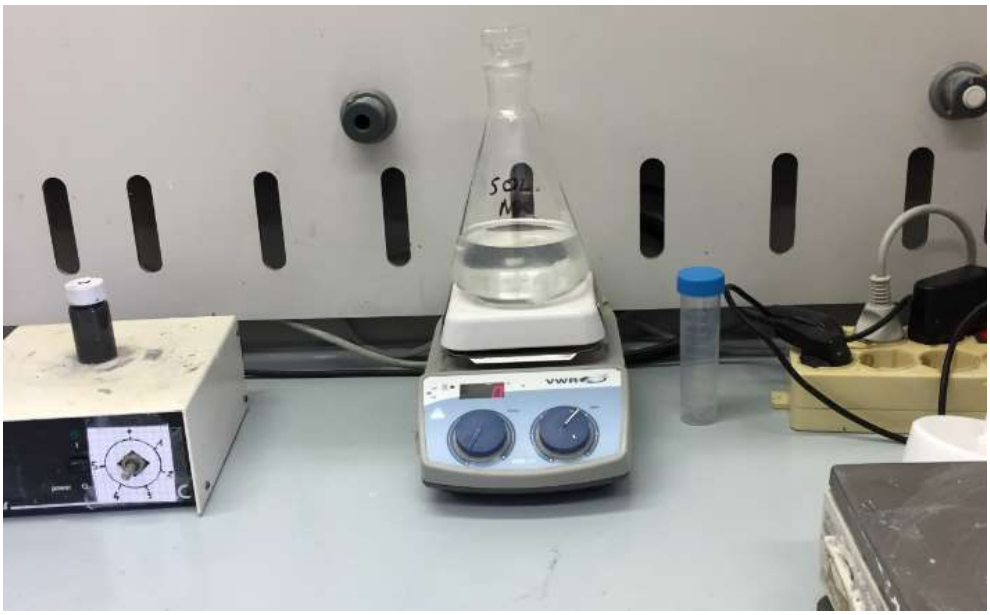

Fig. 3.1.1. The figure shows the stirring of a spinning solution. (source: experimental figure)

3.1.1.2 H44 solution

Chemicals used in the H44 solution are:

- Silicone resin (H44), Wacker Chemie AG, Munich, Geramany. Ceramic precursor.
- polyvinylpyrrolidone (PVP, M_w = 1300000 Da), Sigma-Aldrich, Saint Louis, Missouri, USA. Polymer added for increasing the electrospinnability of the solution.
- Chloroform (CF, anhydrous > 99%), Sigma-Aldrich, Saint Louis, Missouri, USA. Solvent for MK and PVP.
- N, N-dimethyl formamide (DMF, anhydrous 99,8%), Sigma-Aldrich, Saint Louis, Missouri USA. Solvent added for increasing the electrospinnability of the solution.

H44 and PVP are highly soluble into dimethyl formamide. Problems could arise during the process because of high boiling point (153°C) and low vapor pressure (0.38 *kPa* at 20°C) of DMF. Chloroform, which present low boiling point (61.3°C) and high vapor pressure (21.1 *kPa* at 20°C) has been added in order to balance the DMF and improve the solvent evaporability [28].

Chemicals ratio used in the H44 solution are:

- Volumetric ratio for solvents: DMF/CF = 50/50.
- Weight ratio for polymers: H44/PVP = 75/25.
- Total polymer weight ratio: Polymer/solvent = 35/65.

225 *ml* of solution has been prepared every time in order to avoid the solution's aging. First of all, a volumetric flask with total capacity of 500[ml] has been washed with water and acetone. Then DMF has been poured into the flask and gently stirred with a magnetic anchor. After that H44 and PVP have been slowly introduced with a metal spoon. Before adding the Chloroform, the as prepared solution has been stirred for a whole night at 75°C. The agitation and the temperature were needed in order to promote the mixing of all components and the formation of a uniform liquid phase. In the end CF has been added. The spinning solution once formed has been leaved stirring for whole night.

3.1.1.3 RSN-0217 solution

Chemicals used in the RSN-0217 solution are:

- Silicone resin (RSN-0217), Dow Corning, Midland, Michigan, USA. Ceramic precursor.
- polyvinylpyrrolidone (PVP, M_w = 1300000 Da), Sigma-Aldrich, Saint Louis, Missouri, USA. Polymer added for increasing the electrospinnability of the solution.
- Chloroform (CF, anhydrous > 99%), Sigma-Aldrich, Saint Louis, Missouri, USA. Solvent for MK and PVP.
- N, N-dimethyl formamide (DMF, anhydrous 99,8%), Sigma-Aldrich, Saint Louis, Missouri, USA. Solvent added for increasing the electrospinnability of the solution.

Chemicals ratio used in the RSN-0217 solution are:

- Volumetric ratio for solvents: DMF/CF = 50/50.
- Weight ratio for polymers: RSN/PVP = 75/25.
- Total polymer weight ratio: Polymer/solvent = 35/65.

The same consideration taken for H44 solution can be taken for the RSN-0217 (from now on called RSN) solution.

Fig. 3.1.2. The figure shows the three spinning solution after preparation and solubilization (source: experimental figure)

3.1.2 Spinning the solutions

Before starting the process, catalyst has to be added to the aliquot of solution, which will be spun, taken from the volumetric flask and poured into a glass phial. Catalyst is inserted in the solution in order to facilitate the following thermal treatment of cross-linking. The catalysts used in the present work are:

- For MK solution: Genosil® GF 56 (GS-cat), Wacker Chemie AG, Munich, Germany.
- For H44 solution: Zr-acetylacetonate (Zr-cat, 97%), Sigma-Aldrich, Saint Louis, Missouri, USA.
- For RSN solution: Zr-acetylacetonate (Zr-cat, 97%), Sigma-Aldrich, Saint Louis, Missouri, USA.

Catalysts ratio used in the three solutions:

- GS-cat/MK = 1/100
- Zr-cat/H44 = 4/100
- Zr-cat/RSN = 4/100

Once added the catalysts into the phial, the final solution has to be mixed for 5 and 10 minutes respectively for MK and H44, RSN solution. After mixing the solution a degassing period of 5 minutes is required for letting the air-bubbles reaches the surface. Then the solution is ready for the electrospinning.

An aliquot of final solution is taken form the glass phial and loaded into a 5 *mL* syringe fitted with a 0.7 *mm* diameter stainless steel and fed at 0.5 *mL/h* with a syringe pump. Electrospinning process is carried out at a voltage of 10 *kV*. A carbon steel plate (width 8 *cm* and height 8 *cm*) covered with aluminum foil has been used as collector, and the nozzle-collector distance has been set 12 *cm*. Figure 3.1.3 shows the electrospinning process.

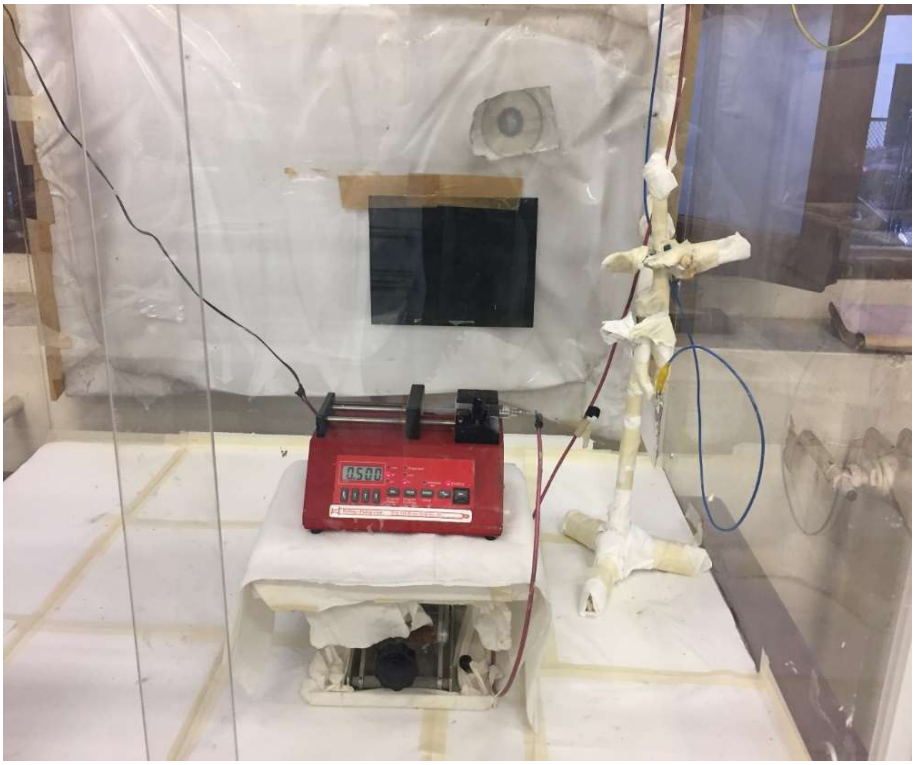

Fig. 3.1.3. The figure shows the electrospinning process. (source: experimental figure)

Red and blue cables provide electrical contact between the needle and the collector.

Devices used are:

- Syringe pump, NE-300, New Era Pump System, USA.
- Power Supply, ES100R-20W, Kansai Electronics, Japan.

Spinning times have been set:

- MK solution → 2 hours.

- H44 solution → 1.5 hours.
- RSN solution → 1.5 hours.

After these temporal windows solutions tend to become too viscous, fibers and drops starts obstructing the needle's tip and so blocking the process.

Once completed the process, the aluminum foil with fibers mat on his surface has been removed from the steel plate. Figure 3.1.4 shows an example of as-spun fiber mat presenting a withe color. The upper damaged area is due to the hooking of the collector to the electrospinning device.

Fig. 3.1.4. The figure shows an aluminum foil with a fibrous mat (width 8 *cm* and height 8 *cm*). (source: experimental figure)

The Fibers obtained from this process are composed by Preceramic Polymer (MK, H44, RSN) and PVP. Fibers were homogeneously distributed on the metallic foil and the mats presented an adequate thickness, needed for their handling in the following operations.

3.2 Thermal treatments

Once produced fibers are in a polymeric state in ordered to transform them into ceramic materials two thermal treatments are required: Cross-linking and Pyrolysis.

3.2.1 Cross-Linking

The first thermal treatment needed is cross-linking. High temperatures (from 100°C to 300°C) and the action of a catalyst promotes chemical reaction between single blocks (shown in figure 2.1.4) which constitute the silicone resin. These chemical bonds turn the polymeric fibers from a thermoplastic into a thermoset material, capable of retain the fiber morphology during the pyrolysis. Fibers mats has been subdivided into pieces (shown in figure 3.2.1) with a scissor, previously washed with water and acetone.

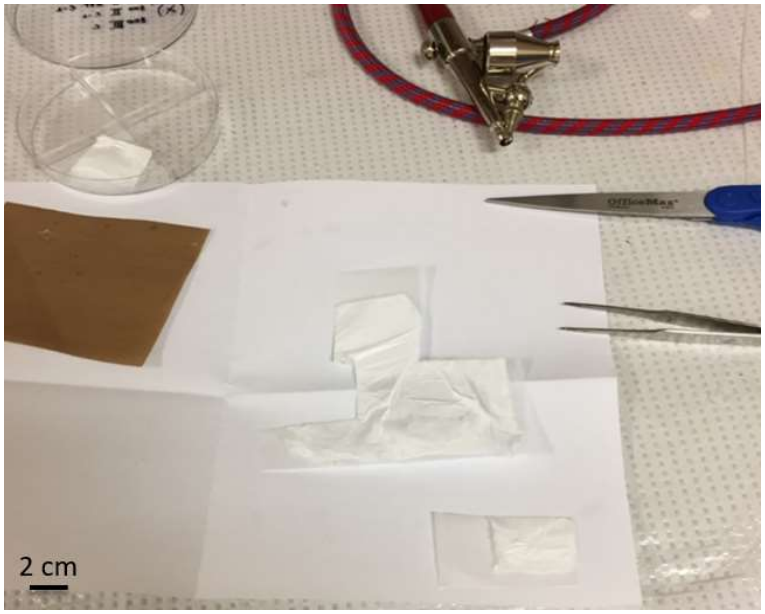

Fig. 3.2.1. The figure shows pieces (width 4 *cm* and height 3 *cm*) of fibrous mat. (source: experimental figure)

Then mat's pieces have been weighted, in order to control the mass reduction during each thermal treatment, and laid down on a graphite sheet inside a glass petri dish as shown in figure 3.2.2. Then petri dish has been inserted into the curing oven and the thermal treatment started.

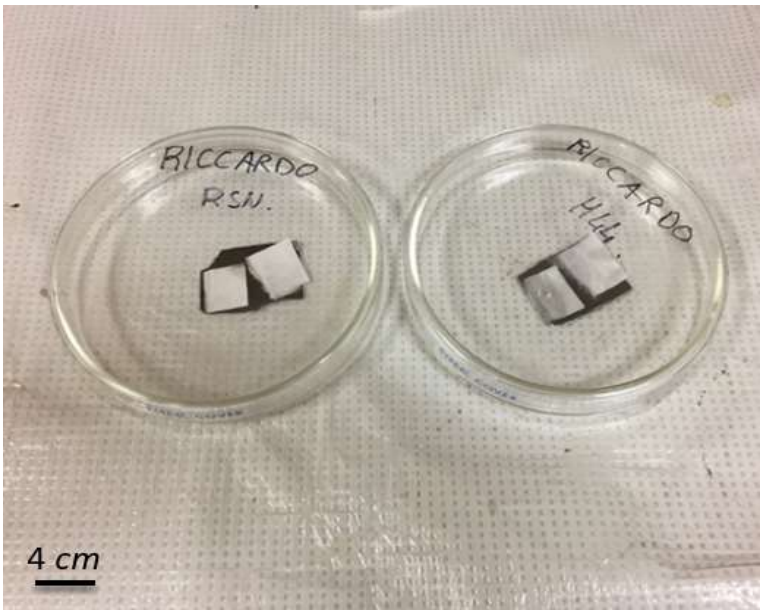

Fig. 3.2.2. The figure shows a subdivided fibrous mat (dimensions of the pieces: width 4 *cm* and height 3 *cm*, approximately). (source: experimental figure)

The heating has to be slowly applied because time is required for the formation of bridging chemical bonds, even with the presence of a catalyst. If the heating rate is too high fibers will melt losing their morphology, becoming useless for the purpose of the present work. In figure 3.2.3 the difference between well cross-linked pieces of mat and melted one can be appreciated. At the end of this process, thermoset materials show switch in color from white to brown-yellow, as can be seen comparing figure 3.2.2 to figure 3.2. In literature for these materials a cross-linking treatment of 200°C, reached with a heating rate of 5 *°C/min*, lasting 1 hour has been reported [28].

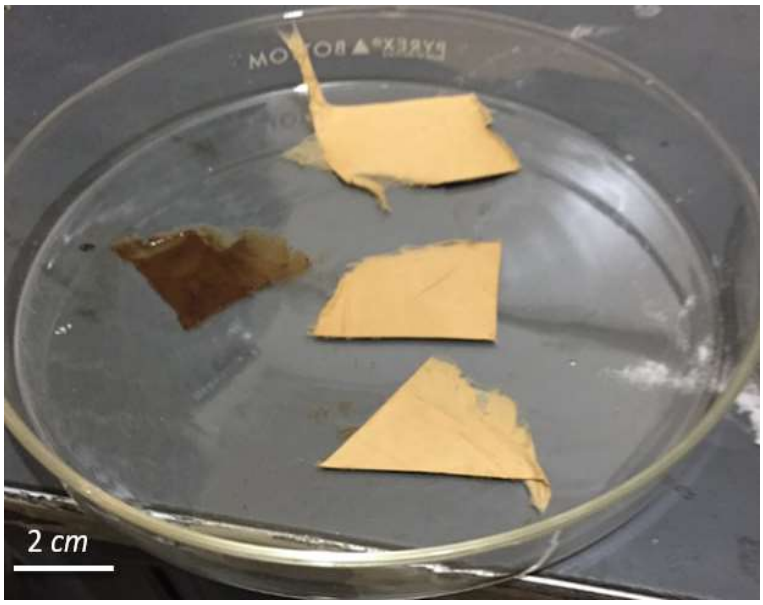

Fig. 3.2.3. The figure shows well cross-linked materials, on the right and melted one on the left (dimensions of the pieces: width 4 *cm* and height 3 *cm*, approximately) (source: experimental figure)

The oven utilized for the cross-linking process is a Precision™, ThermoFisher scientific, Waltham, Massachusetts, USA, shown in figure 3.2.4.

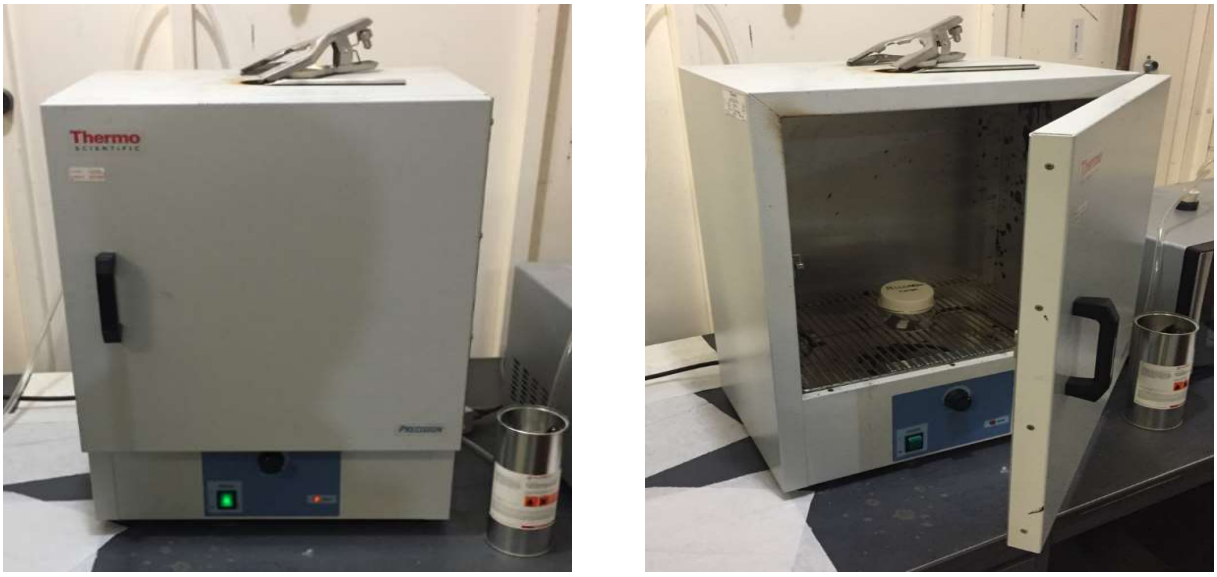

Fig. 3.2.4. The figure shows the oven used for the cross-linking (source: experimental figure)

This particular oven cannot be programmed with a fixed heating rate, dwelling time at maximum processing temperature and final cooling step. Temperature has been risen manually turning the designated control knob from value 2, which corresponds to a temperature of 30°C, till the value of 10, which corresponds to a temperature of 300°C. For guarantying a slow heating, knob has been turned off half level every 30 minutes, only level 7 has been leaved for 1 hour. This level of temperature has given problems to some samples. In order to avoid these problems, spacing between the heating elements of the oven and sample surface has been increased. At maximum temperature materials has been leaved for 3 hours in order to ensure a complete cross-link. Different mats (MK, H44, RSN) has presented different behavior. For example, MK fibers show less susceptibility to the heating ratio. This can be attributed to a better mixing of the catalysts, which is in liquid form instead of a solid one.

3.2.2 Pyrolysis

The second thermal treatment needed is pyrolysis. During the pyrolysis treatment, as previously exposed, redistribution of atoms, elimination of organic moieties and formation of nanodomains turn the thermoset resin into a ceramic material with complex microstructure. The treatment has been conducted in an alumina tube furnace STT-1600°C-12, Sentro Tech, Cleveland, Ohio, USA shown in figure 3.2.5. All materials have been treated in argon atmosphere in order to prevent oxidation of the fibers.

Fig. 3.2.5. The figure shows the furnace used for the pyrolysis (source: experimental figure)

Crosslinked piece has been weighted and placed into an alumina boat (width 4 *cm* and height 5,5 *cm*) which has been inserted in the tube.

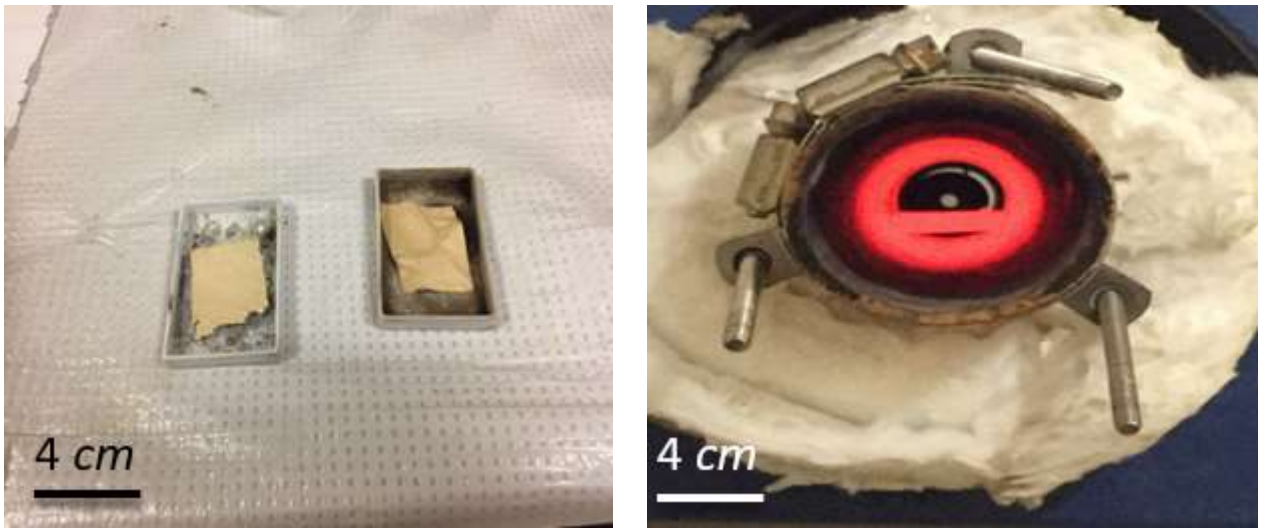

Fig. 3.2.6. The figure shows alumina boats within crosslinked pieces (dimensions of the pieces: width 4 *cm* and height 3 *cm*, approximately) and a view of the pyrolysis process (source: experimental figure)

After having sealed both sides of the tube, and having applied argon flux, the pyrolysis has been started. The thermal treatment is composed by three parts. The first is a heating, with controlled rate, until a fixed temperature. The second is a holding time at maximum temperature during which the ceramization occurs. Figure 3.2.7 shows a scheme of the pyrolysis treatment.

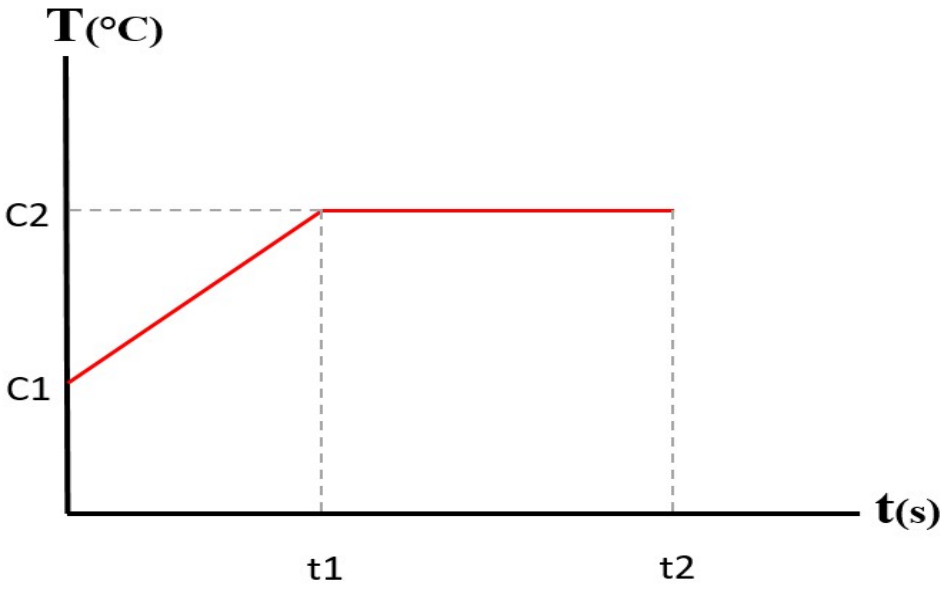

Fig. 3.2.7. The figure shows a scheme of a generic pyrolysis treatment (source: experimental figure)

Treatment's parameters C1, C2 and t1,t2; which depends on the treatment applicated, are listed in table 3.2.1. For MK and RSN two further treatment has been used in order to observe the influence of the processing parameters on the electrochemical characteristics.

Material	C1°C	C2°C	t1 *min*	t2 *min*
MK	68	1000	466	586
MK	68	800	366	586
H44	68	1000	466	586
RSN	68	1000	466	496
RSN	68	1000	466	469

Tab. 3.2.1. The table reports the variables C and t for all the pyrolysis conducted. (source: experiment table)

The treatment has to happen in absence of oxygen in order to avoid oxidation and the loss of material's carbon content. Heating rate and inert gas flow are also very important. High heating rate can lead to a fast gas release and so the development of cracks. In order to avoid this fact a heating rate of 2°C has been adopted (as reported in literature [28]). An excessive gas flow can lead a very fast removal of decomposition products and so to a lower ceramic yield. After the pyrolysis, fibers have completed their transformation form polymers to ceramics. This last thermal treatment produces a change in color form brown to black, as we can see in figure 3.2.8.

Fig. 3.2.8. The figure shows a ceramic fiber mats (dimensions of the pyrolyzed pieces: width 2 *cm* and height 1 *cm*, approximately) (source: experimental figure)

3.3 Chemical characterization

Fourier transformation infrared spectroscopy (FT-IR) and Raman spectroscopy (RS) methods have been used in order to follow the changing in the material's nature, from polymer to ceramic, and to characterize the presence of graphitic carbon, respectively.

3.3.1 Infrared spectroscopy

Infrared spectroscopy is based on the capability of molecules of vibrating, changing their distance (stretching) and their angle (bending) by absorbing electromagnetic wave with fixed energy. The energy required, which is related to the wave length, depends on the particular chemical bond and on the particular movement. So, observing the amount of radiation absorbed by one sample it is possible to understand the types of chemical bond present. Information on their quantity are also obtainable. Infrared spectrometers which are based on Fourier transformation use a Michelson interferometer in order to rapidly change the radiation hitting the sample. FT-IR can work both in absorption or in reflection. In the present work, single bounce reflection setup with diamond plate is adopted on a IR spectrometer, Nicolet IS5, ThermoFisher scientific, Waltham, Massachusetts, USA on wavelength window from 2000 to 500 cm^{-1} (64 scansion with 4 cm^{-1} resolution). Figure 3.3.1 reports the device utilized in the present work and a scheme of how an interferometer works.

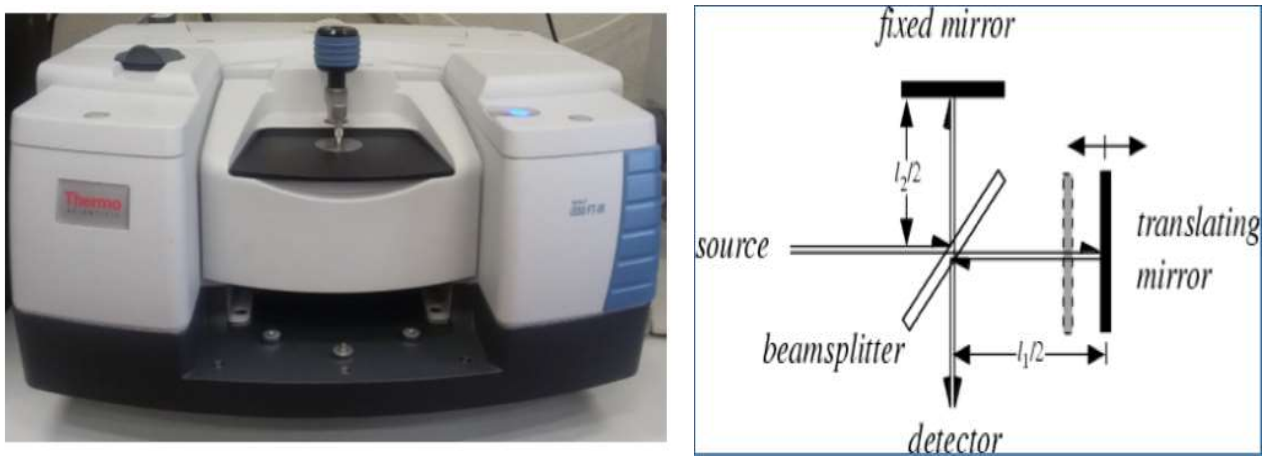

Fig. 3.3.1. The figure shows the IR spectrometer used, on the left and a scheme of a Michelson interferometer, on the right (source: experimental figure, www.chem.libretexts.org)

In the present work FT-IR analysis has been used in order to follow the evolution of the materials (MK, H44, RSN PDCs); which nature, as stated several times, turns from thermoplastic workable polymer to thermoset polymer, capable of retaining his shape during pyrolysis, and finally becomes ceramic material with tailored composition and morphology. This evolution can be seen from the disappearance of peaks related to chemical bonds present in the electrospun polymer and form the appearance of peaks related to chemical bonds present in the final ceramic material.

3.3.2 Raman spectroscopy

Raman spectroscopy as infrared spectroscopy is based on the interaction between an electromagnetic radiation and the material analyzed. Energy of the photons, which have undergone "inelastic scattering", changed depending on the material that has caused the collision. Thanks to the analysis of this energy's change, information about chemical phases inside the material are obtainable. The spectrometer used in the present work is a inVia^{TM} confocal Raman microscope by Renishaw,Wotton-under-Edge, Gloucestershire, UK. Figure 3.3.2 reports the device utilized in the present work and a scheme of different scattering interactions.

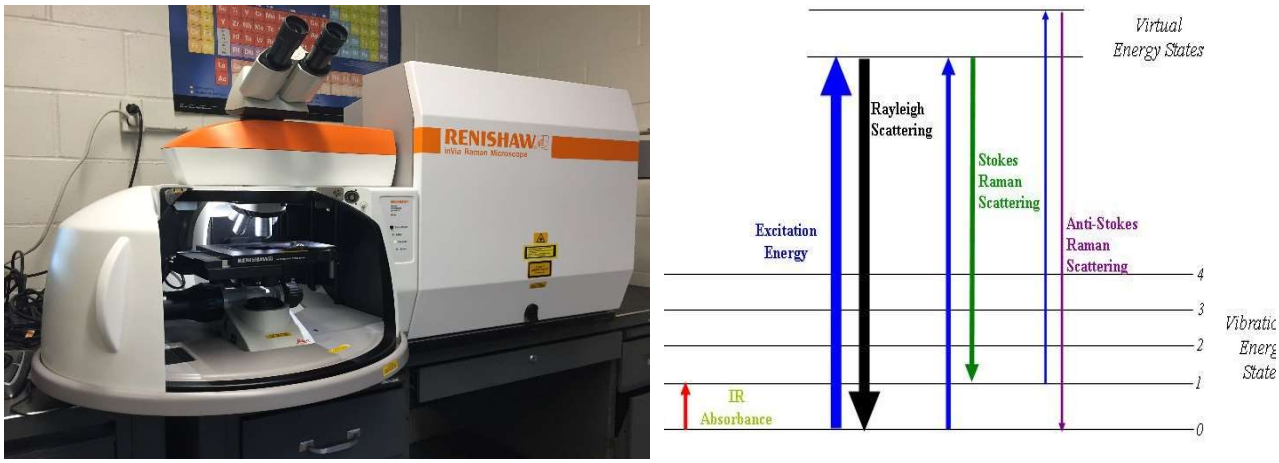

Fig. 3.3.1. The figure shows the Raman spectrometer used, on the left and a scheme of energetic transitions, on the right (source: experimental figure, www.chem.libretexts.org)

Raman spectroscopy is intrinsically a "local" method because the laser beam is focused on areas of only a few micrometers of the sample. Nevertheless, the local variations in compositions or phase content mostly occur on the nanometer scale and Raman data are acquired with the lateral resolution of a few micrometers, giving an average signal over that specimen volume [25].

In the present work Raman analysis has been used in order to observe the difference in the content of graphitic carbon between all the materials (MK, H44, RSN PDCs). Nanoscale “free” carbon clusters are known to play a significant role in tuning the properties of PDCs.

3.4 Morphological characterization

For the morphological characterization of the fibers scanning electron microscope (SEM) has been used. Then, after samples preparation, ceramic fibers have been looked also at transmission electron microscope (TEM).

3.4.1 SEM

Scanning electron microscopy utilizes an electron beam (energy in the range of 1-30 *kev*), accelerated by electromagnetic field and focused by electromagnetic lenses, which interacts in a vacuum chamber with the sample and generates various signals like X-rays, auger electrons, secondary electrons and backscattered electrons. After the collection of these signals by different detectors, information regarding composition and structure of the tested material’s surface are obtainable. In particular, secondary electrons (energy < 50 *keV*), produced by inelastic scattering interactions between the primary electron beam and the sample, give information of the morphology of sample’s surface. The scanning electron microscope used in the present work is a EVO MA10, Carl Zeiss, Oberkochen, Germany with incident voltage of 5-30 *kV*. Figure 3.4.1 reports the device utilized in the present work and a scheme of how a SEM works.

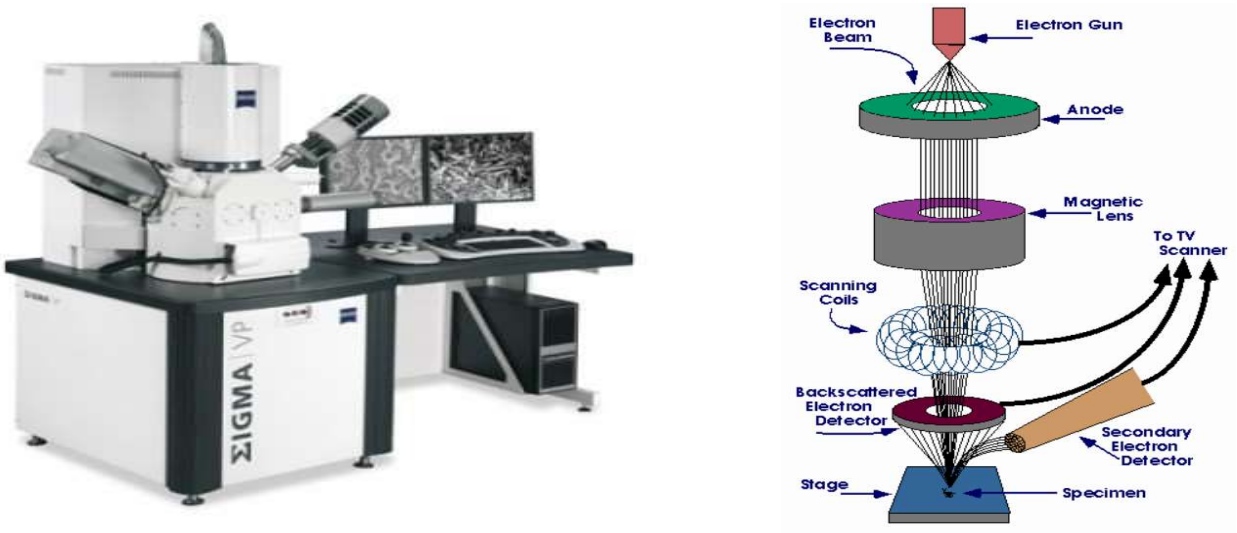

Fig. 3.4.1. The figure shows the SEM used, on the left and a scheme of a generic SEM, on the right (source: experimental figure, www.enfo.agt.bme.hu)

In the present work SEM has been used in order to observe the morphology of the ceramic fibers and to understanding if electrospinning and ceramization have happened properly. Moreover, trough SEM fibers dimension, which have been reported to be on average 1 micron for MK and H44 system [28], can be studied. One of the numerous advantages of electron microscope is the simplicity of preparation of the samples. The only requirements needed by a specimen to be analyzed are conductivity and to not release particles or humidity. A small piece of mat has been cut and stuck on a conductive double-sided scotch tape. The tape has been laid on a metallic carrier which has been inserted in the SEM chamber.

3.4.2 TEM

Transmission electron microscopy uses an electron beam (energy in the range of 100-300 *keV*) accelerated by electromagnetic fields and focused by electromagnetic lenses, which hits the specimen and passes through it. Interaction of the electrons with the sample generates an image on a device such as a fluorescent screen. The TEM is a complex and multifunctional device which possess several imaging methods, each of them can provide extremely useful information about the tested material. Bright filed imaging mode is the most common mode of operation and it is the one adopted in the present work. In this mode, the contrast formation comes from the sample having varying thickness or density, resulting in images with different tonalities of gray and black. Electron microscopic studies have been conducted on PDCs for studying first stage of local crystallization, analyzing nanocrystalline phases and also for identifying the presence of turbostratic or graphitic carbon. The transmission electron microscope used in the present work is a CM-100, Philips/FEI, Amsterdam,

Netherlands, with incident voltage of 40-100 *kV*. Figure 3.4.1 reports the device utilized in the present work and a scheme of the different parts of a TEM. Unlike SEM with TEM the sample preparation is complex and requires a delicate procedure. In order to produce specimen for the TEM little piece from fiber mat has been cut and immersed in a small quantity of 2-propanol (IsoP, anhydrous 99,5%), Sigma-Aldrich, Saint Louis, Missouri, USA. After 10 minutes of sonification a small amount of solution has been picked up with a plastic pipette and one single drop has been deposited over a metallic grid, grid size 1000 mesh × 25 *μm* pitch, copper, by Sigma-Aldrich, Saint Louis, Missouri, USA. Once organic liquid has evaporated single fibers have been found stacked on the grid, and after that analyzed.

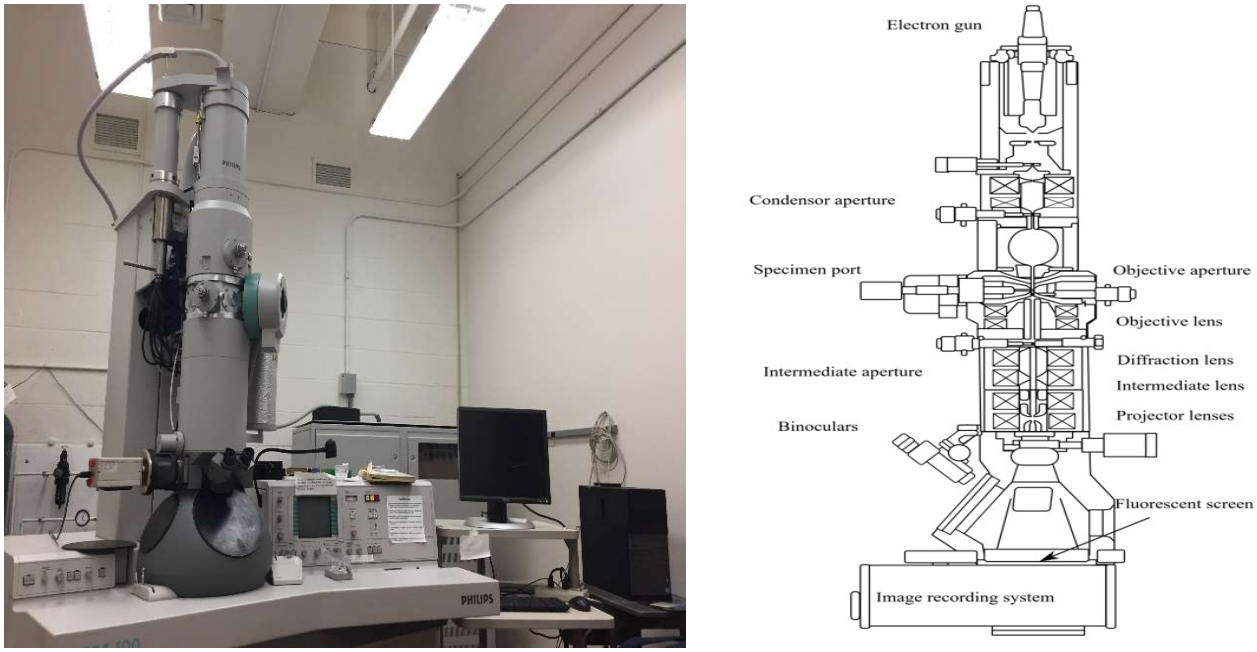

Fig. 3.4.2. The figure shows the TEM used, on the left and a scheme of a generic TEM, on the right (source: experimental figure, www. www.enfo.agt.bme.hu)

In the present work TEM has been used, in addition to the SEM, to have a better understanding of the fibers morphology, structure and dimensions. Even if the edges of the fibers can be passed through by electron beam their bulks, due to their width, absorb all the incident radiation, producing a completely black image. Except this limitation, several useful information can be obtained from this analysis.

3.5 Electrochemical characterization

For characterizing the electrochemical performance as supercapacitor's electrodes of the three ceramics materials (MK, H44, RSN) produced and studied in the present work, electrochemical workstation CHI660E, CH instruments, Inc, Austin, Texas, USA, has been used. Specimens for three-electrode setup have been prepared and cyclic voltammetry has been used for an approaching analysis. Then samples for two-electrode setup have been assembled and cyclic voltammetry (CV), galvanostatic charge/discharge (GDC) and Impedance spectroscopy (EIS) has been performed. The difference between the two setups is that on the three electrodes the counter and the reference electrode are separated. The reference electrode act only as a reference in measuring and controlling the working electrode's potential, so its potential can be easily kept constant. The counter electrode passes all the current needed to balance the current observed at the working electrode. It is always possible, with a single workstation, to switch between the two different setups.

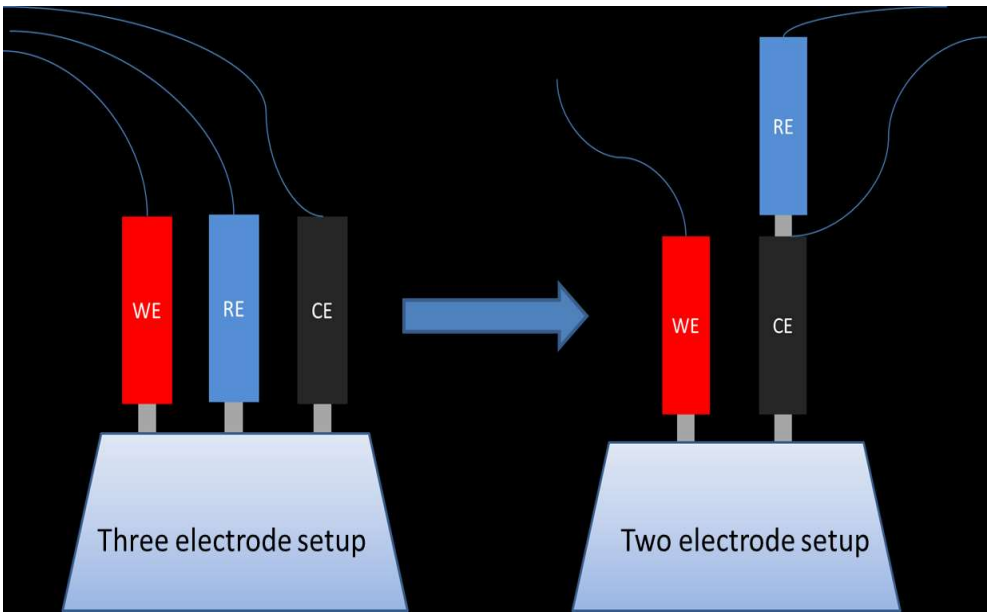

Fig. 3.5.1. The figure shows the three-electrode setup, on the left and the two-electrode setup, on the right. (source: www.kanopytech.com)

The two testing methods can generate various difference on the same tested material as reported in literature [37]. For a given potential range on the x-axis of the CV the working electrode of a three-electrode cell has twice the potential range applied the same applied to the electrodes in a two-electrode cell. This results in a doubling of the calculated capacitance [37]. Other differences are present but not involved in the present study.

3.5.1 Electrodes preparation

Different working setups need different electrodes; thus, two different assembling routes have been followed in the present work.

3.5.1.1 Electrode for three-electrode setup

First of all, the metal carrier has been produced and weighted. A stainless-steel coil has been cut into the form of a square, with a total area of 1 cm^2, with a protrusion of 4 *cm* in order to be connected to the workstation. Then the active material has been prepared. A little piece of fibers mat, of 10 *mg* has been cut, weighted and then inserted in a ceramic mortar in which has been added a mass of Polyvinylidene fluoride (PVDF, M_w = 534000 *Da*, Sigma-Aldrich, Saint Louis, Missouri, USA) equal to the 5% of fibers mass and a mass of Carbon black (CB, Sigma-Aldrich, Saint Louis, Missouri, USA) equal to the 10% of fibers mass. CB and PVDF have been added for enhancing electrode's conductivity and for ensuring a proper grip to the metal carrier, respectively. A slurry has been prepared in the ceramic mortar grinding the three components and adding 10 drops of N-Methyl-2-pyrrolidone (NMP, > 99%, Sigma-Aldrich, Saint Louis, Missouri, USA) as ligand.

Fig. 3.5.2. The figure shows the chemicals needed for electrode preparation and the black slurry. (source: experimental figure)

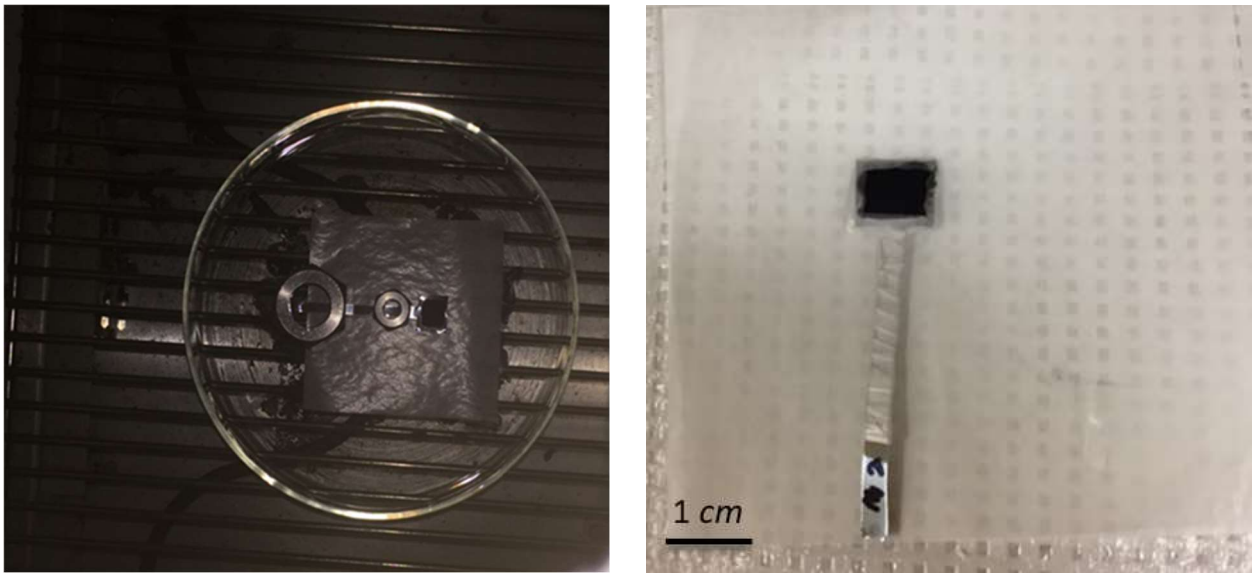

Fig. 3.5.3. The figure shows the drying stage and a final electrode (dimensions:1x5 *cm*). (source: experimental figure)

After 10 minutes of sonication, required for a proper mix of all the components, the slurry has been deposited on the metal carrier. The as-prepared electrode has been leaved for a whole night in an oven at 30°C for drying the slurry, and so obtaining the final active material. The as-prepared electrode has been weighted and this way, comparing the two different measurements of the mass, the active material has been calculated. After having wrapped with plastic parafilm the metallic parts of the collector not covered with the active material the electrode has been tested.

3.5.1.2 Electrode for two-electrode setup

First of all, two similar current collectors have been cut from a copper (commercially pure) foil and glued to two plastic plates (dimensions: width 4 *cm* and height 4 *cm*) with a plastic tape. A little piece of fiber mats has been cut and weighted, then it has been split into two parts in order to constituted the active material of the supercapacitor. The two fibers pieces have been placed on the copper collectors and both the as-prepared electrodes have been sandwiched between a Whatman filter paper (Grade 1, Sigma-Aldrich, Saint Louis, Missouri, USA) which has been previously immersed in the electrolyte for 5 minutes.

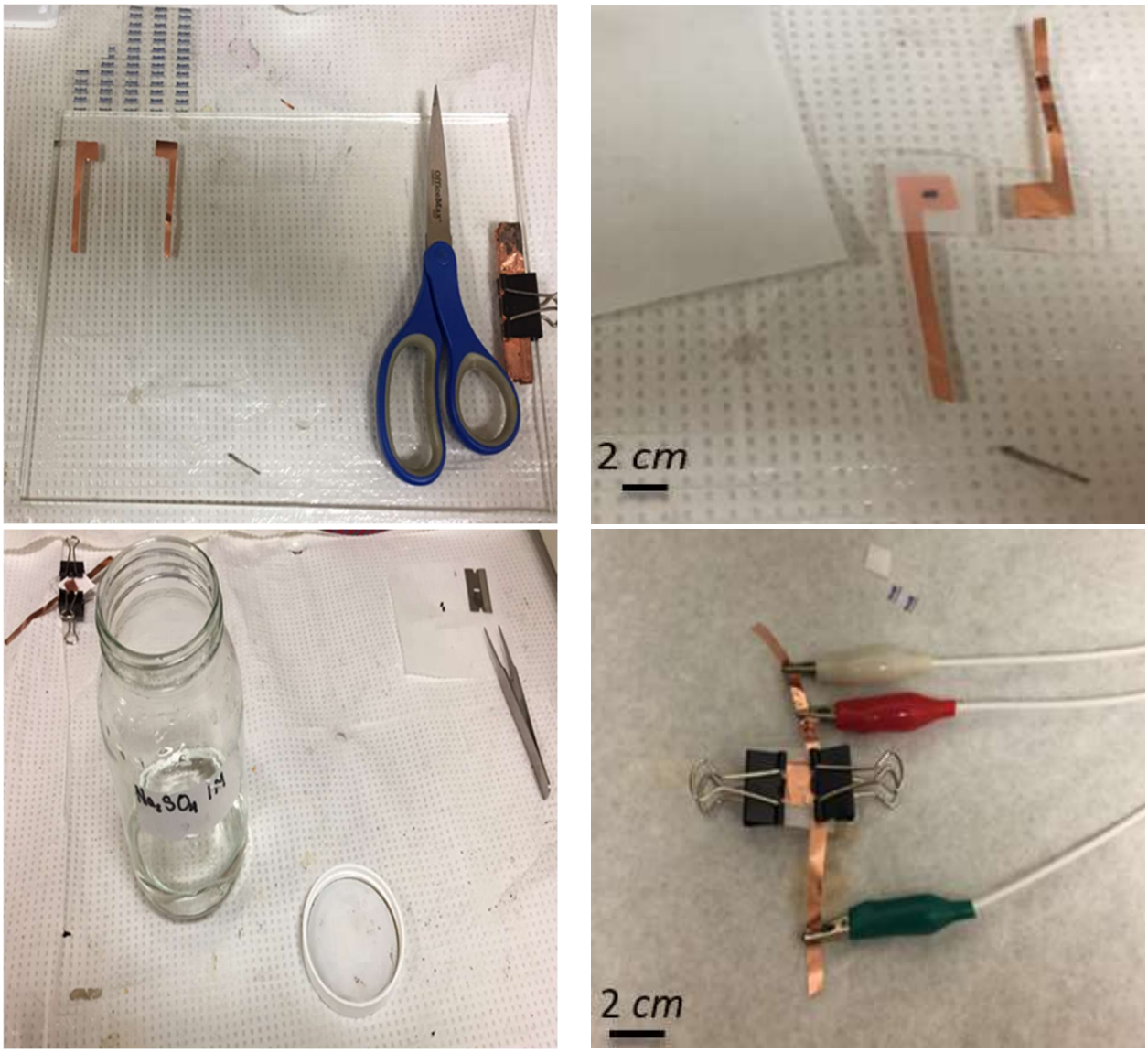

Fig. 3.5.4. The figure shows, in order, instruments for the electrode preparation, cell preparation, electrolyte and filter paper, and the final supercapacitor cell. (dimensions: width 2,5 *cm* and height 2,5 *cm*). (source: experimental figure)

Once assembled the supercapacitor's cell, plastic plates have been closed between two clothespins for ensuring a good handling, and the device has been tested with the electrochemical work station.

3.5.2 Electrochemical test

The electrolyte utilized in the present work for both the setups adopted is an aqueous solution of Sodium sulfate 1 *M*, produced using current water and anhydrous Na_2SO_4 (anhydrous, Sigma-Aldrich, Saint Louis, Missouri, USA). In the three-electrode setup the Counter electrode is a platinum wire and the reference electrode is Silver/ Silver Chloride.

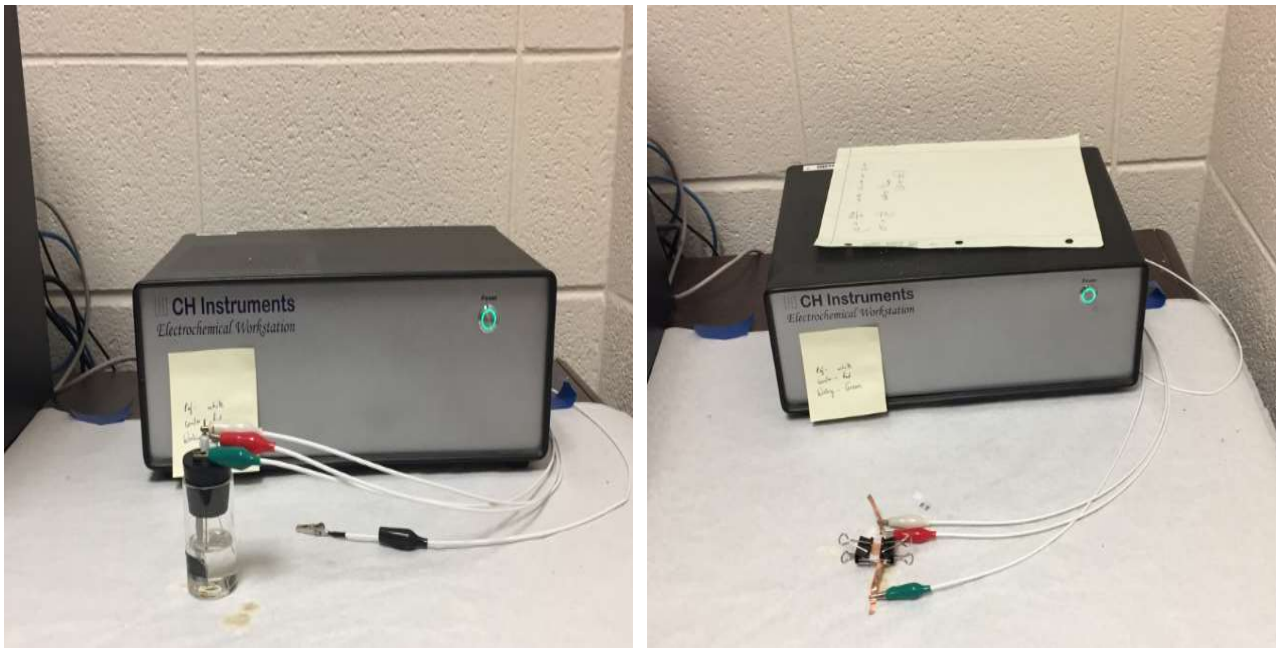

Fig. 3.5.5. The figure shows the test being performed on the two different configurations. (source: experimental figure)

The CV test has been performed identically on the two different setups, while GCD and EIS tests have been performed only on two-electrode setup. In the present work three electrode setup has been used for a first analysis and for comparison reasons.

For the CV test, operative settings are:

- Potential window: 0-1 V
- Scan rate: 500, 200, 100, 50, 20, 10 mV/s
- Sensibility: 0,01 mV

For the GCD test, operative settings are:

- Potential window: 0-1 V
- Current: 1, 3, 5 A
- Sensibility: 0,01 mV

For EIS test, operative settings are:

- Frequency: form 0,01 to $1x10^6$ Hz
- Sensibility: 0,01 mV

Before starting testing session 10 minutes of CV has been run in order to stabilize the working station.

Chapter 4

Results and Discussion

In this chapter, the results of the characterization techniques and of the tests performed on the different materials are presented and discussed. First, we analyzed the images produced by SEM and TEM, in order to see the successful production of homogenous fibers by electrospinning. Then results from FT-IR and RS are illustrated. Thanks to infrared analysis we can follow the chemical changes during the different steps and the polymer to ceramic transformation. With Raman spectroscopy insight on the free carbon domain presented by the fibers are obtainable. Lastly The result from electrochemical characterization are presented and the performances of the different PDCs (MK, H44, RSN) as supercapacitor's electrodes are discussed.

4.1 Morphological characterization results

Before analyzing the SEM and TEM images of ceramic fiberous mats and single fibers respectively; optical microscope has been utilized for observing the polymeric fibers after electrospinning and before the thermal treatments. This analysis is necessary in order to prove the success of solutions preparation and fiber formation. As can be seen in figure 4.1.1 the electrospinning process has led to the formation of fibers with homogenous distribution, sizes and morphology. The careful formulation of polymeric solutions and the operative parameters set, have avoided the formation of typical defects such as solubilized zones or beads on the fibers surface. The spinning process have been conducted under room temperature and humidity. So, verified the good morphology presented by the fibers, the resulting process for these solutions seems to be poorly affected by these two parameters, which have not been set to specific values during the process. For a reduction of the electrospun fibers diameters the influence of the temperature and humidity should be take into account. As expected fibers in the mat don't present any particular orientation.

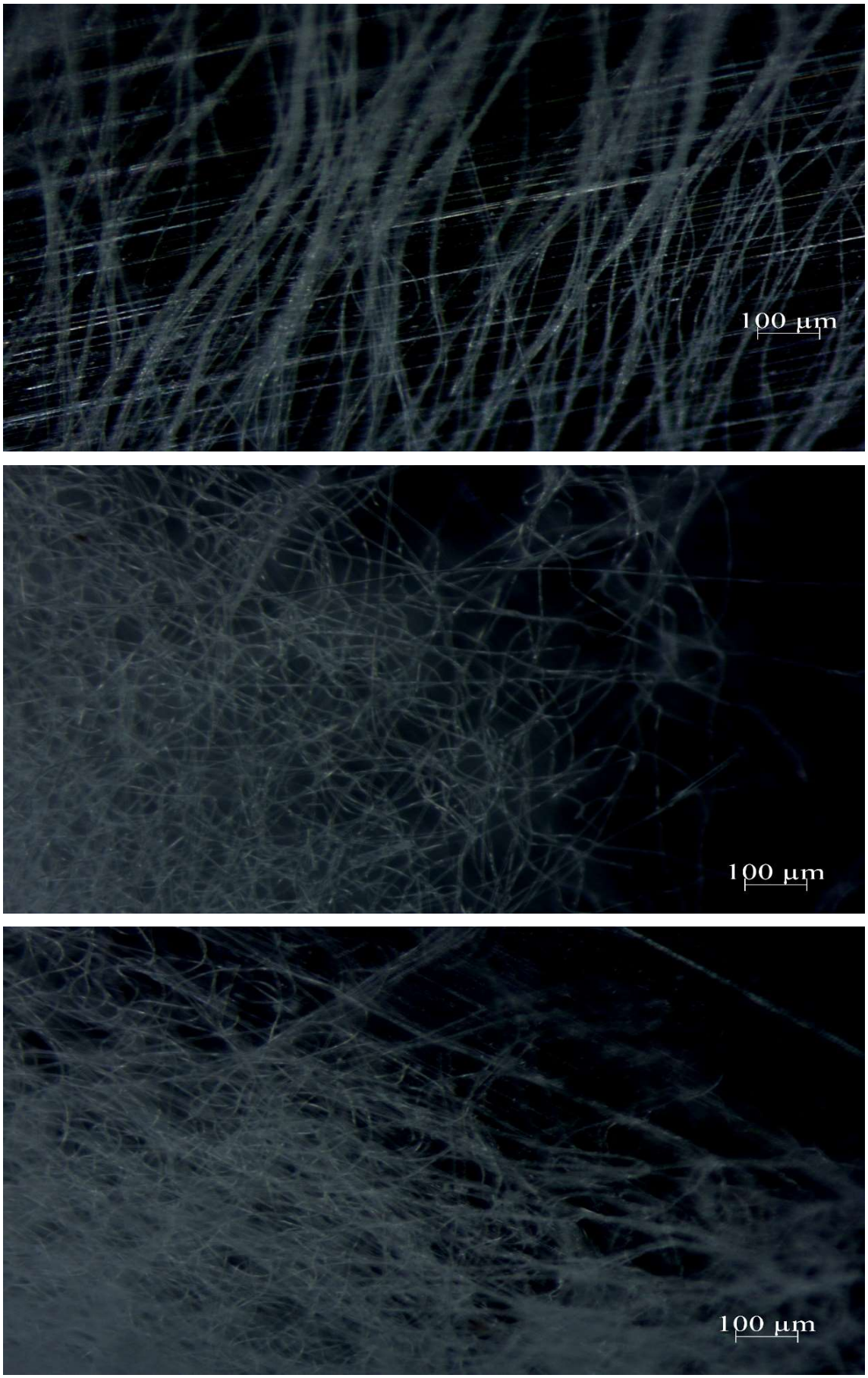

Fig. 4.1.1. The figure shows MK, H44 and RSN as spun fibers. (source: experimental figure)

After the formation, electrospun mats have to undergo two thermal treatments, the first one in order to transform fibers form thermoplastic to thermoset polymer and the second in order to mineralized them and so obtaining ceramic fibers. During these treatments, as stated in Chapter 2 and as can be seen form the FT-IR analysis, the materials undergoes heavy transformation, which leads to the developing of gaseous products. This process produces a mass loss, estimated by comparing the weights of the same mat's piece after electrospinning, curing and pyrolysis, respectively. A decrease of the fibers dimension is always coupled with the reduction of their mass so, the final average fibers diameter is not equal to the one presented by the as-spun mats, but lower. The changing of material's nature during the three steps could be seen also from a macroscopic view noting the changing in the color of fiber mats. After electrospinning, thermoplastic fibers present a withe color. This turns into yellow-brown during cross-linking. After ceramization their color passes from yellow-brown to completely black. The chromatic changes ae related to the evolution of the material and so the modification of its atomic bonds (discussed with FT-IR results). The Three different materials (MK, H44, RSN) show the same behavior just described. In figure 4.1.2 single pieces of the three PDCs, belonging each one to a different processing step, are reported.

Fig. 4.1.2. The figure shows chromatic changes of the three PDCs. (source: experimental figure)

Mass loos will be discussed in the FT-IR paragraph.

4.1.1 SEM images

Thanks to the SEM analysis of MK, H44, RSN samples, information related to the porosity of the mats and to the average size of the fibers have been obtained. These two aspects possess a capital importance in the perspective of maximizing the material's capacitance in applications as supercapacitors electrode. This importance can be explained analyzing the mechanisms involved in the formation of the electrical double layer (physical storage of charges). Porosity of the fibers mats is important in order to let the liquid electrolyte coming in contact with all the surface of the fiber. Diameters of the fibers are important because having the same amount of material with lower fibers size means having more surface and so, as previously exposed, having more capacitance.

Figure 4.1.3 shows an electrode prepared for the three-electrode setup. A previously exposed, in this case the fibers have been milled and mixed with conducting agent (carbon black) and a ligand (Polyvinylidene fluoride), which function is ensuring a good electron conductivity and a good adhesion on the metal collector, respectively. Utilizing the fibers morphology, instead of particles, gives some advantages. Ligands are no longer required. The absence of the ligands and the different processing route for fibers electrodes are positive for aspects like:

- Easier and faster electrode production: mixing and drying phases are not required.
- No ligands added: reduction of the inactive mass and so parallel increase of specific capacitance.
- No metal collector required: reduction of the inactive mass and so parallel increase of specific capacitance.

Presence of ligand can also generate problems as limitation in electron transport, loss of electrical contact [31] as well as screening electrodes surface, suitable for electrical double layer and so decreasing total capacitance.

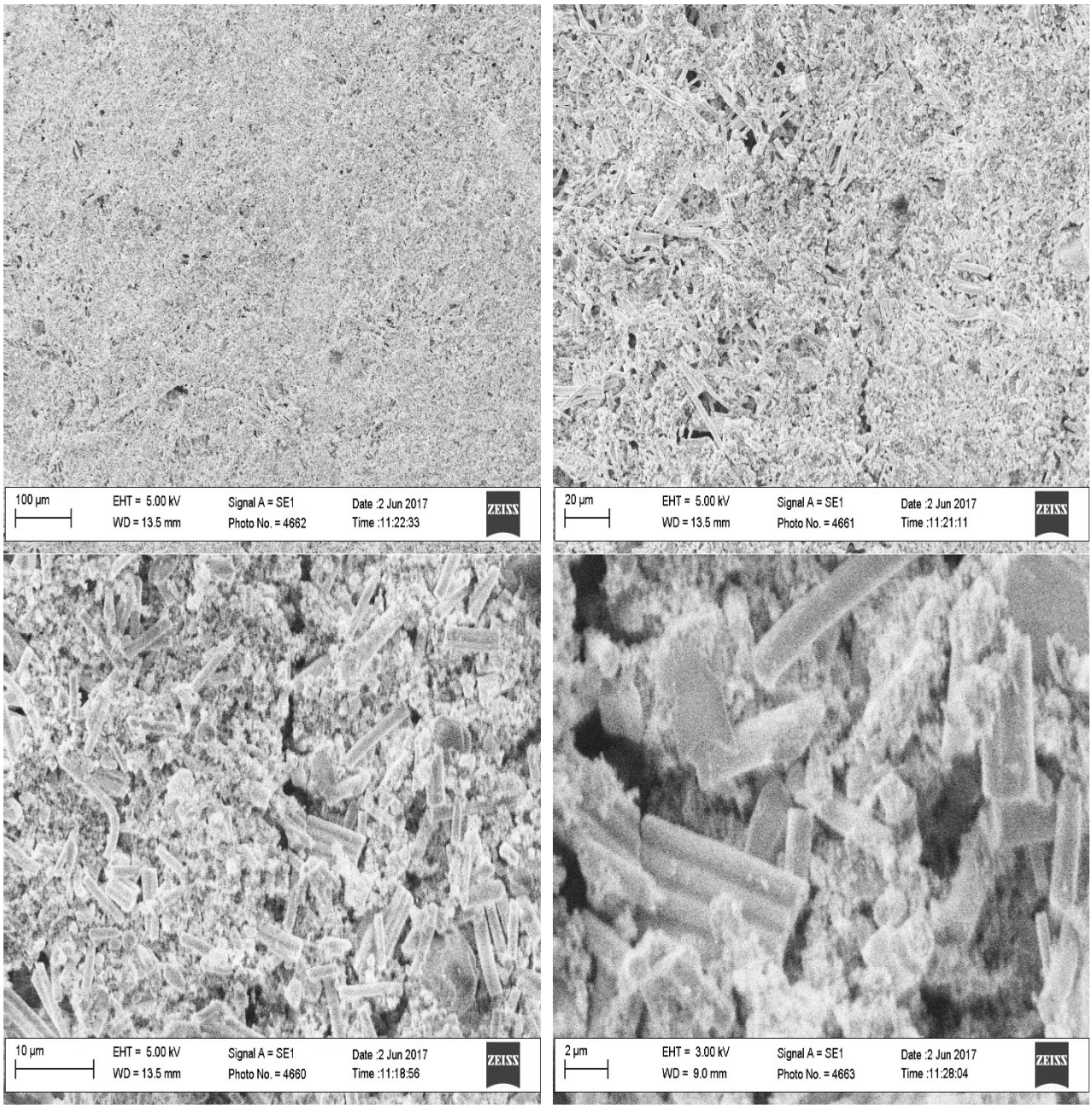

Fig. 4.1.3. The figure shows SEM Pictures of the electrode for three-electrode setup. (source: experimental figure)

Figures from 4.1.4 to 4.1.12 report the SEM images for MK, H44 and RSN fibers, respectively. For each material image of the cross-linked and pyrolyzed fibers at different magnification are provided. Comparing the different images, information about orientation, morphology and size of fibers, before and after the last thermal treatment, can be obtained.

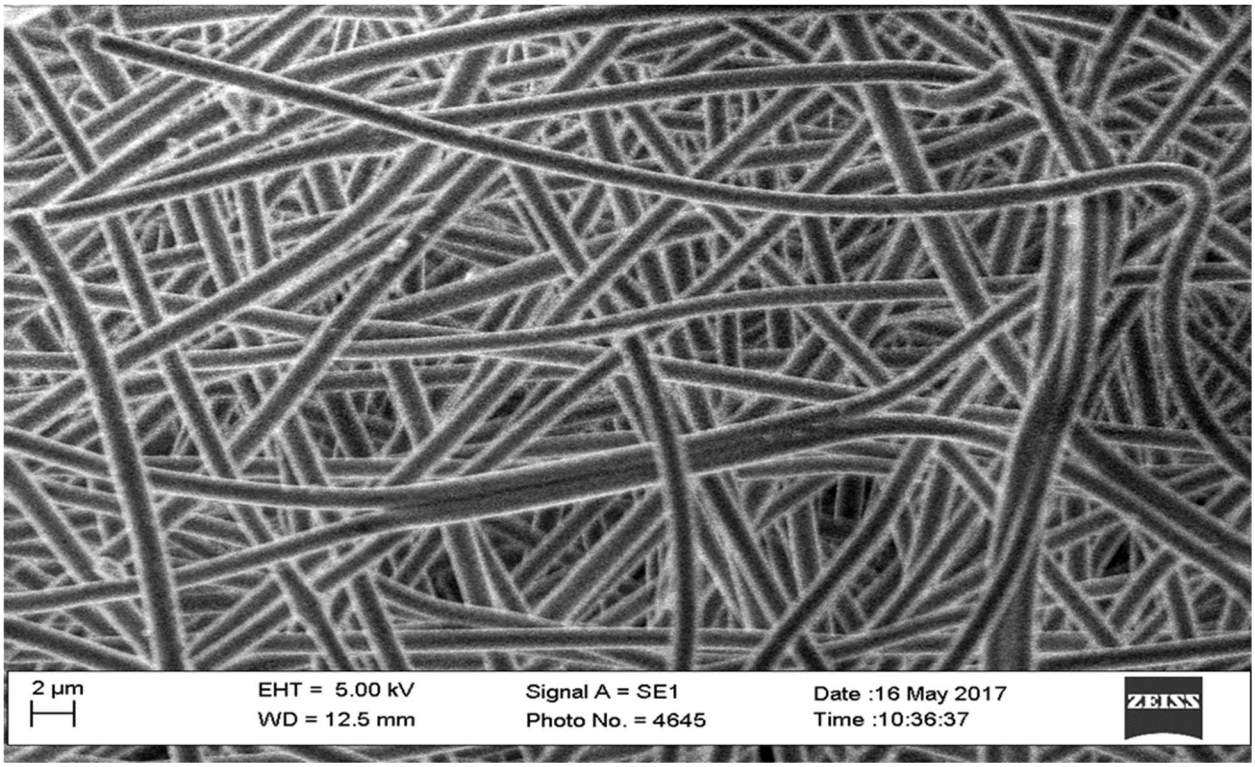

Fig. 4.1.4. The figure shows SEM Picture of MK cross-linked fibers. (source: experimental figure)

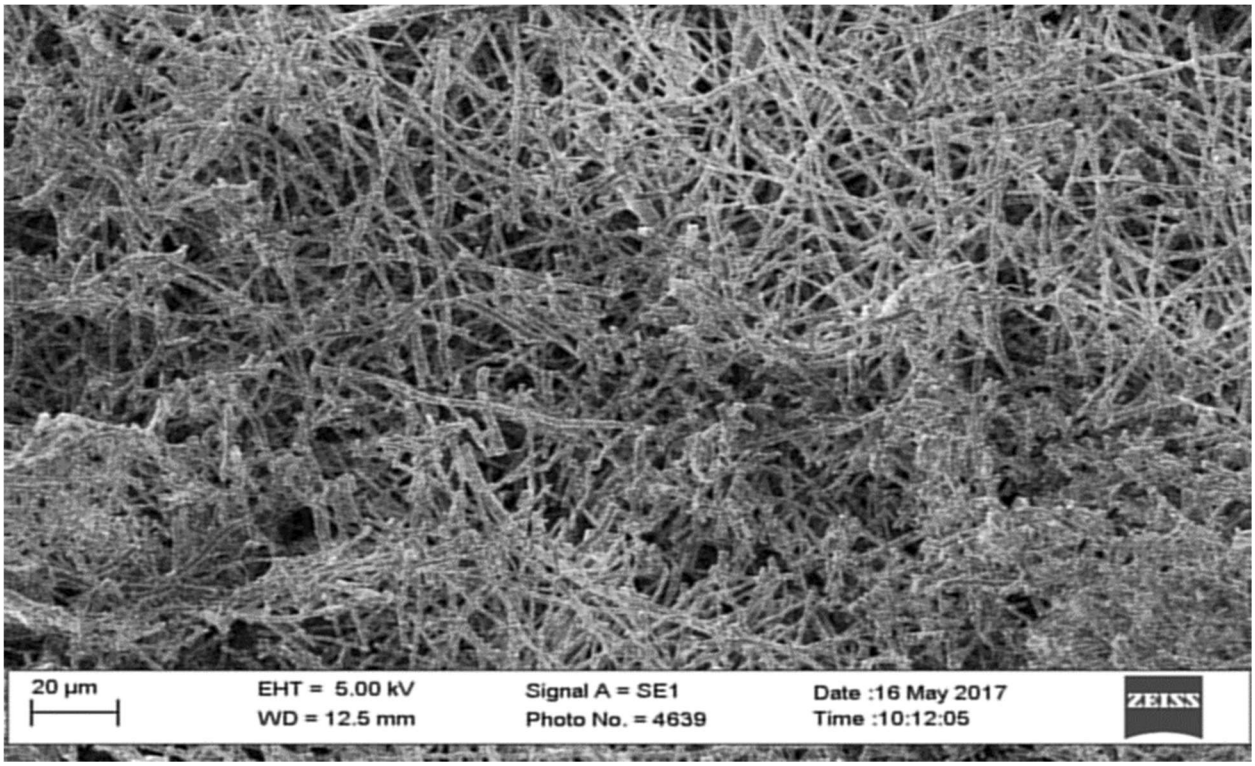

Fig. 4.1.5. The figure shows SEM Picture of MK ceramic fibers (low mag). (source: experimental figure)

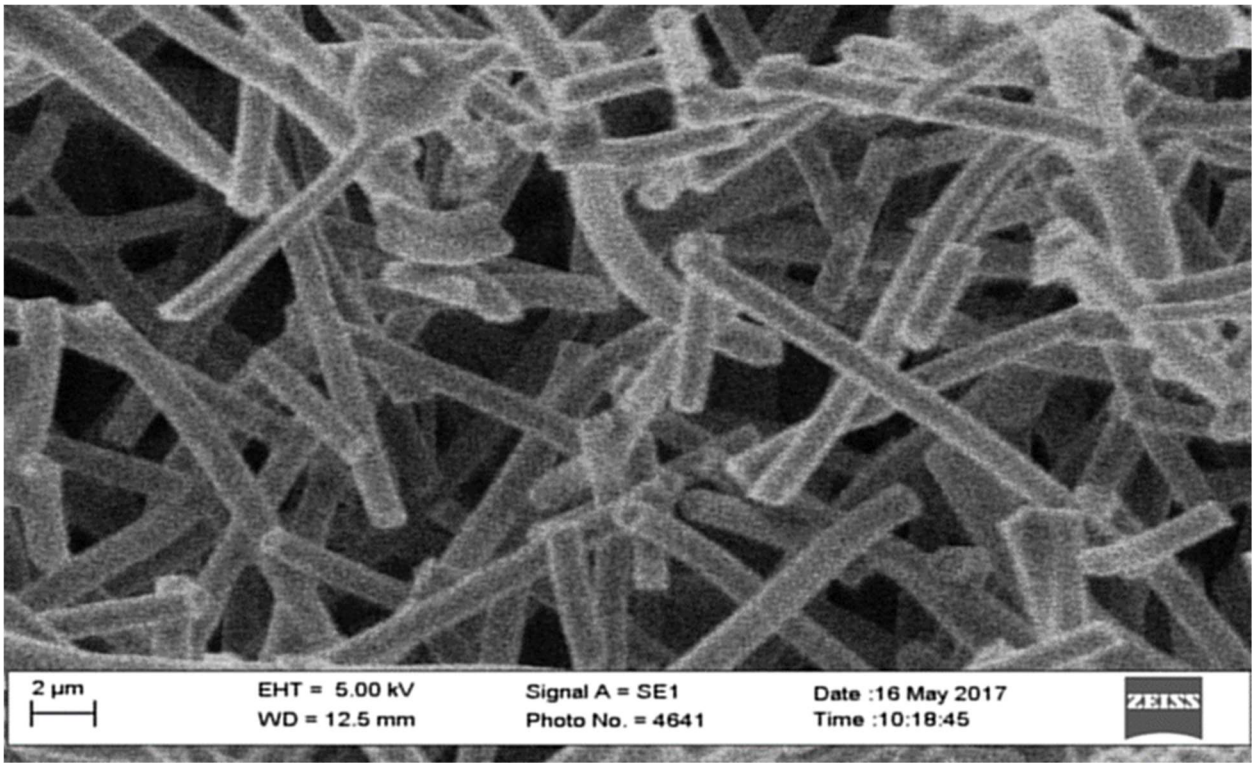

Fig. 4.1.6. The figure shows SEM Picture of MK ceramic fibers (high mag.). (source: experimental figure)

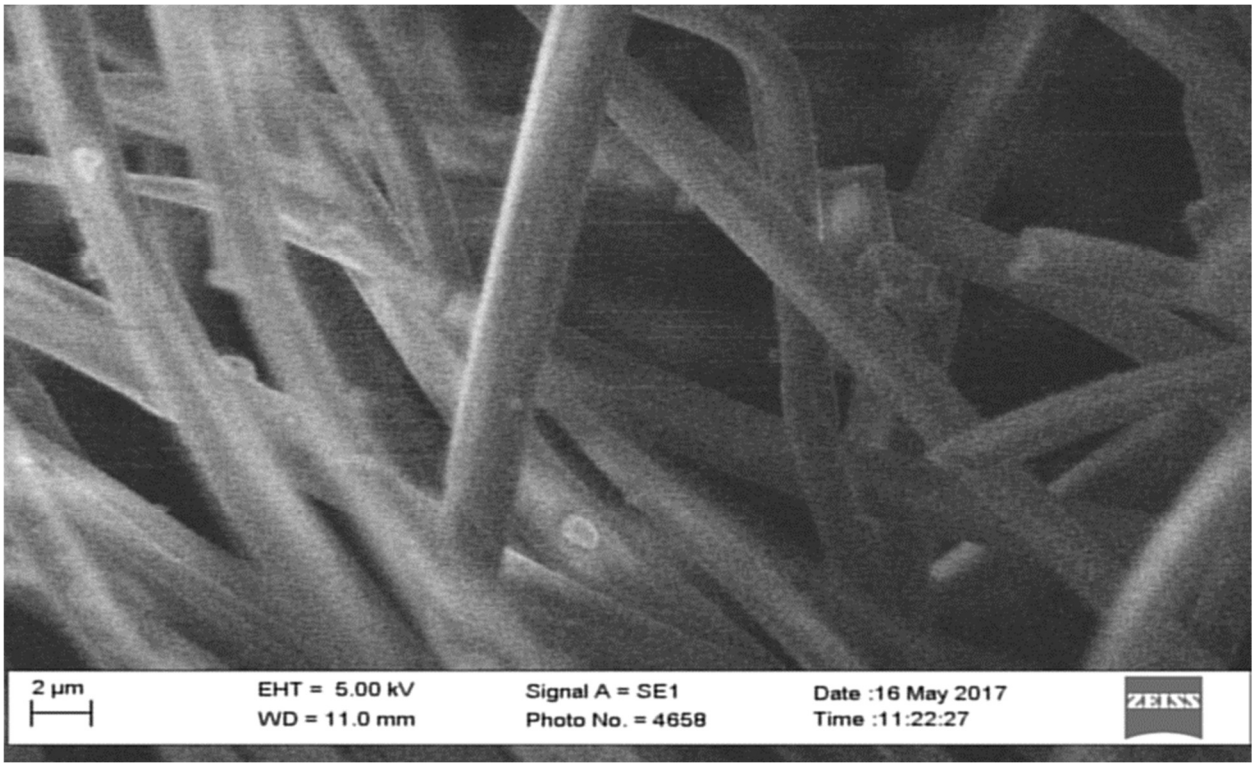

Fig. 4.1.7. The figure shows SEM Picture of H44 cross-linked fibers. (source: experimental figure)

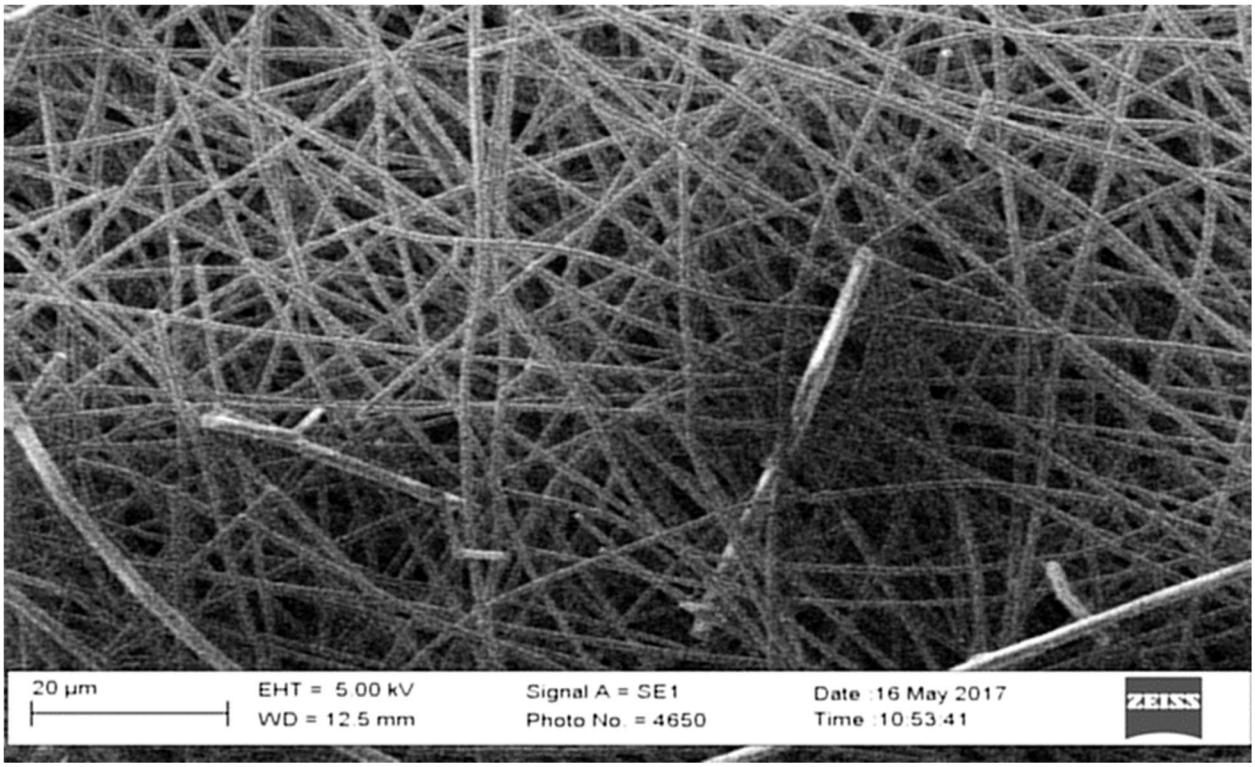

Fig. 4.1.8. The figure shows SEM Picture of H44 ceramic fibers (low mag). (source: experimental figure)

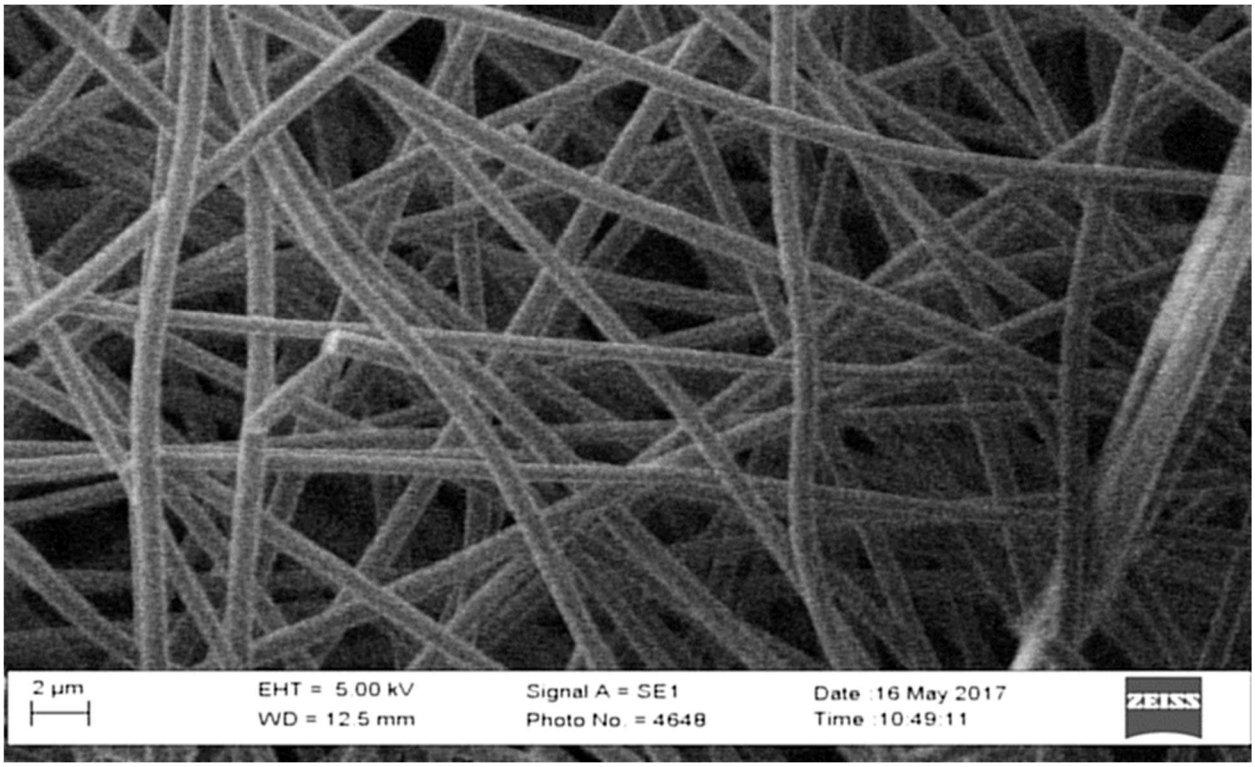

Fig. 4.1.9. The figure shows SEM Picture of H44 ceramic fibers (high mag.). (source: experimental figure)

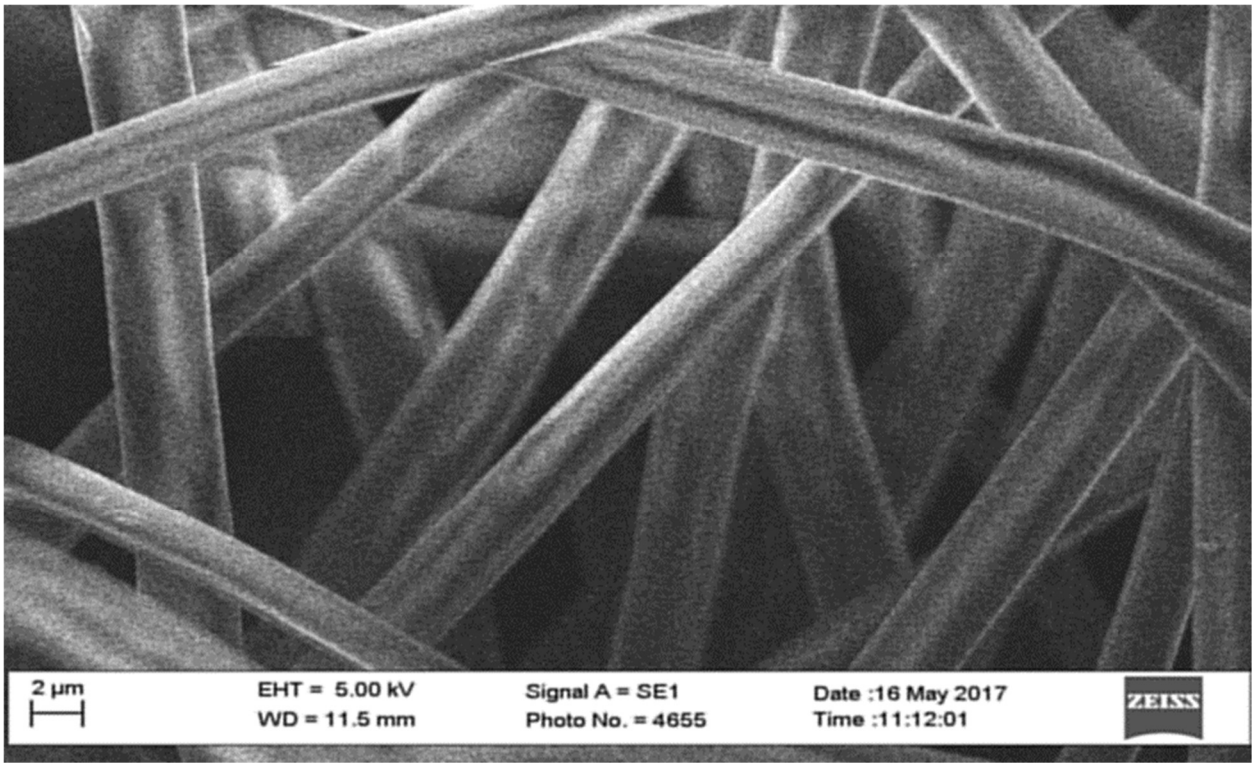

Fig. 4.1.10. The figure shows SEM Picture of RSN cross-linked fibers. (source: experimental figure)

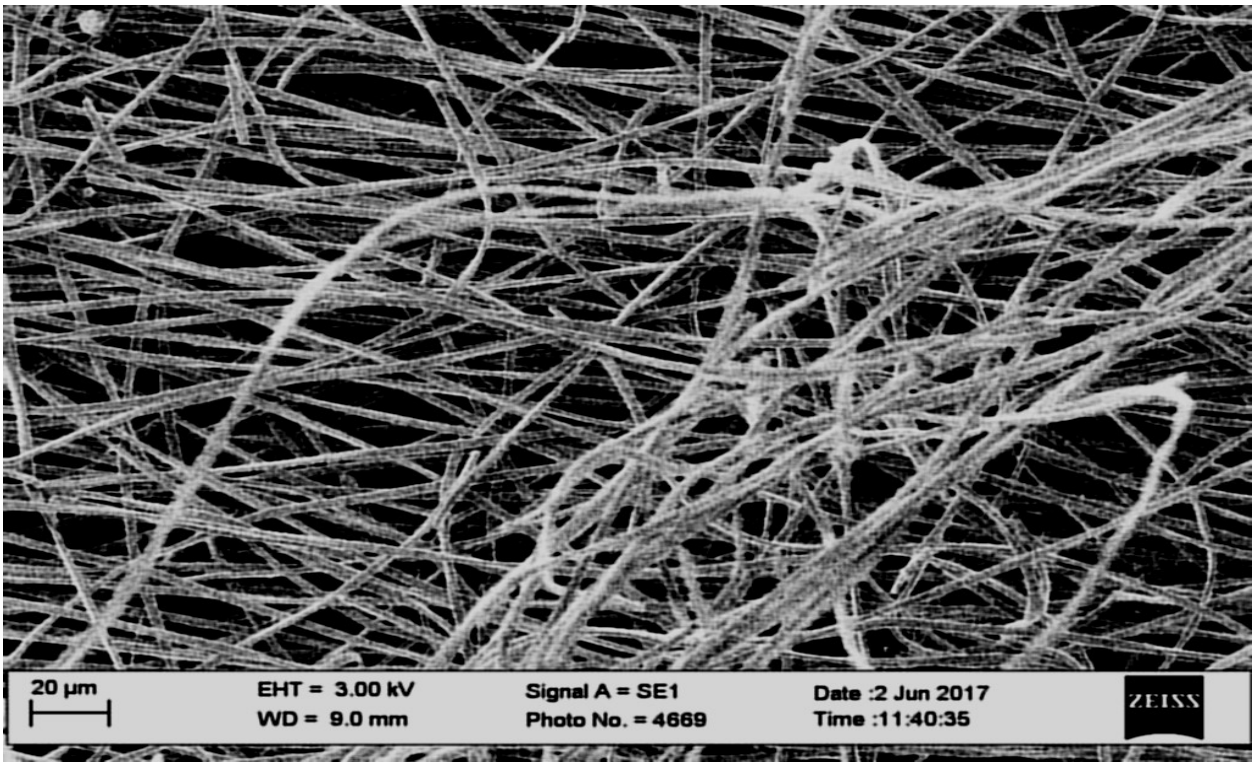

Fig. 4.1.11. The figure shows SEM Picture of RSN ceramic fibers (low mag). (source: experimental figure)

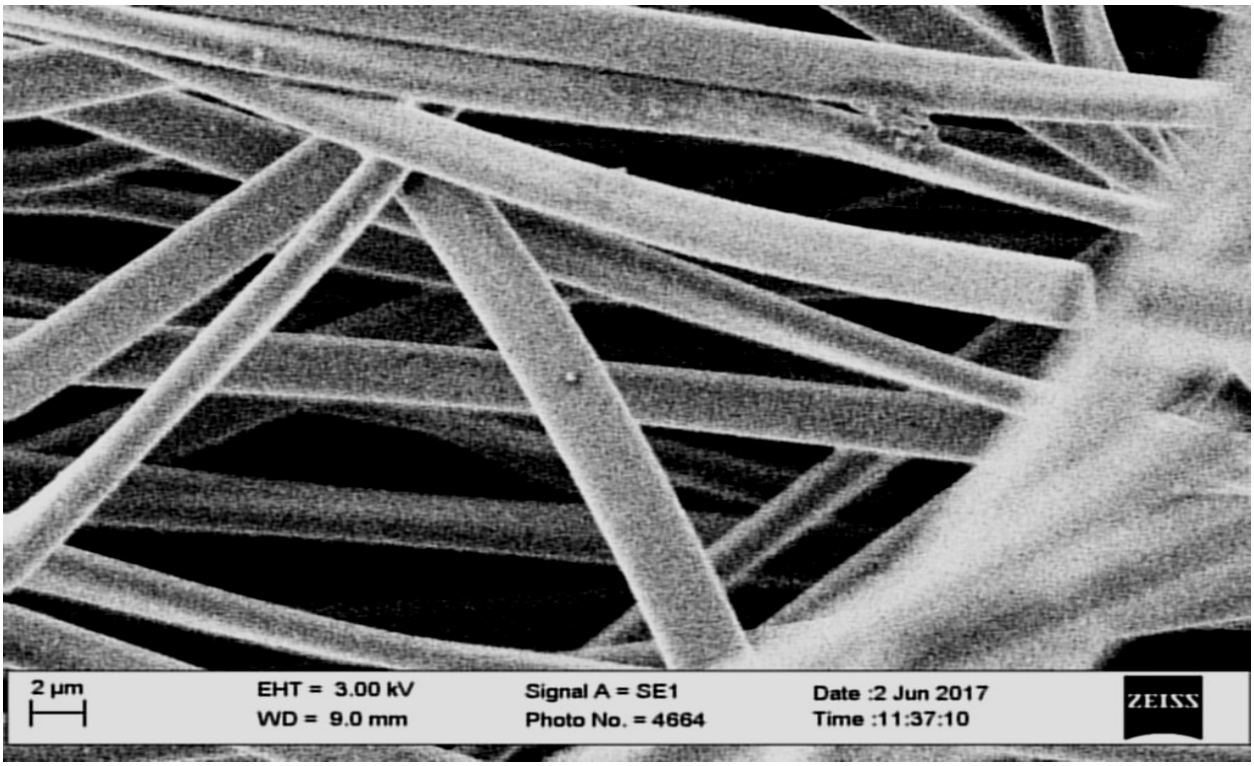

Fig. 4.1.12. The figure shows SEM Picture of H44 ceramic fibers (high mag.). (source: experimental figure)

Analyzing the images, we can notice the good level of porosity present, largely sufficient to ensure a good contact of the liquid aqueous electrolyte. The porosity is referred to the fibrous mats and not to the fibers themselves, which appear dense. In literature, the porosities of those fibers mat are reported to be higher than 80% [39]. A further analysis of the porosity of fibers mats for the aim of the present work is not required.

The nonwoven fibrous network with random orientation is preserved after pyrolysis and all the three material presents a homogeneous and defect free structure. Fibers with abnormal diameters are not present in the mats as well as typical defects like beads or solubilized/melted zones. Moreover, fibers surfaces seem to do not present particular irregularity. In all the three materials, a reduction of the fibers diameters can be noticed, comparing the SEM images of cross-linked fibers (the first reported for every set of three images) and pyrolyzed ones (last 2 reported every set of three images). For the different materials fibers sizes change:

- For MK: from about 1.5 μm to aproximately1 μm.
- For H44: from about 1.5 μm to aproximately1 μm.
- For RSN: from about 3 μm to approximately 2 μm.

Utilizing ImageJ, an image processing program, a more precise analysis has been conducted and the medium value of fibers diameter has been calculated. Figure 4.1.13 report the average diameters of fibers before and after pyrolysis for the three systems.

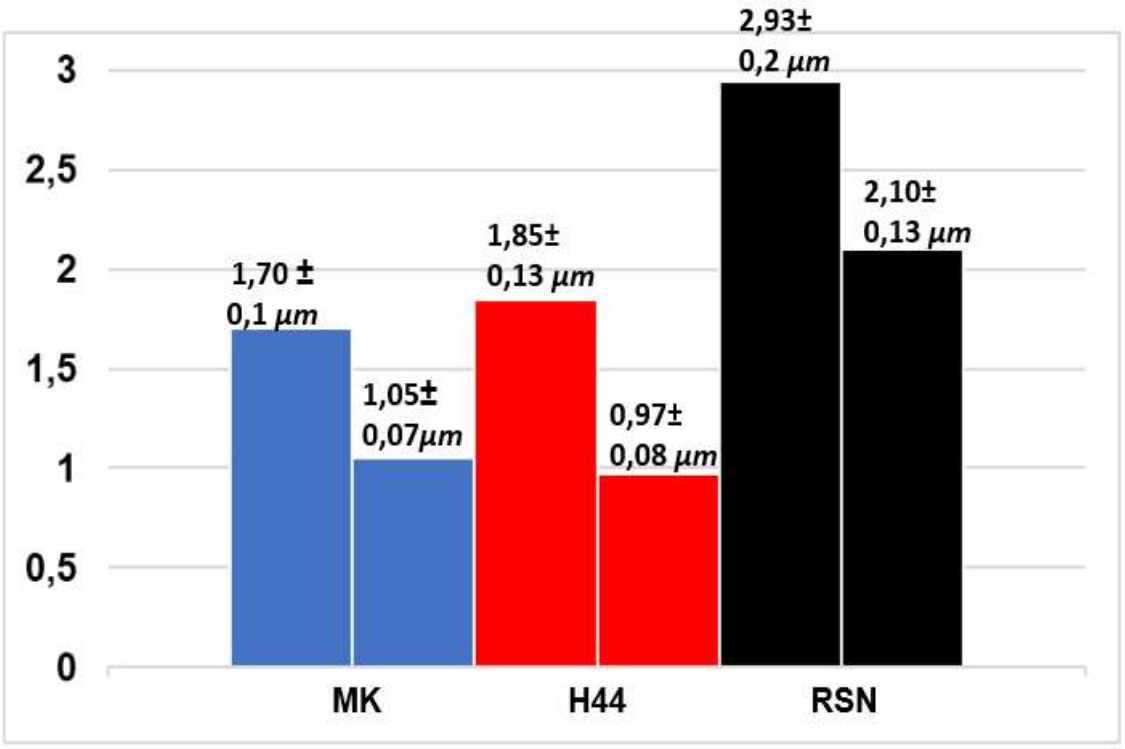

Fig. 4.1.13. The figure shows the average diameters for MK (blue), H44 (red) and RSN (black) fibers. (source: experimental figure)

Those values are consistent with those reported in literature for analogous systems [28].

MK and H44 present lower fibers size with respect to RSN after the ceramization. This can be attributed to two main factors. The first factor is the diameter possessed from the fibers after the electrospinning process. Higher is the diameter presented by polymeric fibers at the beginning of the route that will transform them from polymers to ceramic, and higher will be the final diameter of the ceramic fibers. The initial diameter of the fiber, as previously exposed, depend by the optimization of the electrospinning process. A better solution formulation and process parameters setting lead to lower medium diameter. The value of medium diameter after spinning process represents the maximum value that ceramic fibers will present, because during the mineralization process only reduction of fibers size can occur. The second factor is the maximum temperature and dwelling time of the pyrolysis treatment. An increase of one or both these two variable causes a more marked decrease of sample's mass and diameter. Looking at the reported SEM images, the influences of both

the factors exposed previously can be seen. As spun RSN mat presents bigger fibers diameters probably related to the fact that the spinning process for this resin (RSN) is not well balanced as the process for the other two (MK, RSN). The different thermal treatment which the mats have undergone has produced differences as well. The dwelling time of RSN material has been set equal to 0.5 *h* instead of 2 *h* like MK and H44. Reducing the temporal window spent by the material at the maximum temperature (1000°C for the three material) ideally produces a lower mass loss and a lower decrease in the value of medium diameter of the fibers.

In the specific application of the present work fibers diameters have a crucial importance. Lower is the medium value of fiber's diameter, higher will be the specific area of the material. Having larger surface in contact with the electrolyte means having wider electrical double layer and so more charge stored by the material. The sizes reduction of the fibers constituting the electrode's material, produce an increase in his specific capacitance. Two supercapacitor devices, built with the same amount of fibrous material and so presenting the same cost, will present different properties if the fibers sizes of the material are not equal. The device with lower fibers diameters in the same operational conditions will present higher capacitance and so will provide more electricity.

4.1.2 TEM images

For a further analysis of the produced fibers, transmission electron microscope has been used. With the TEM instead of SEM single fibers are analyzed but at higher magnification. The diameter possessed by the fibers are too wide and so the electron beam is completely adsorbed by the bulk of the material, thus the resulting image are completely black. Figures from 4.1.14 to 4.1.19 report the SEM images for MK, H44 and RSN fibers respectively. For each material two images of pyrolyzed fibers at different magnification are provided.

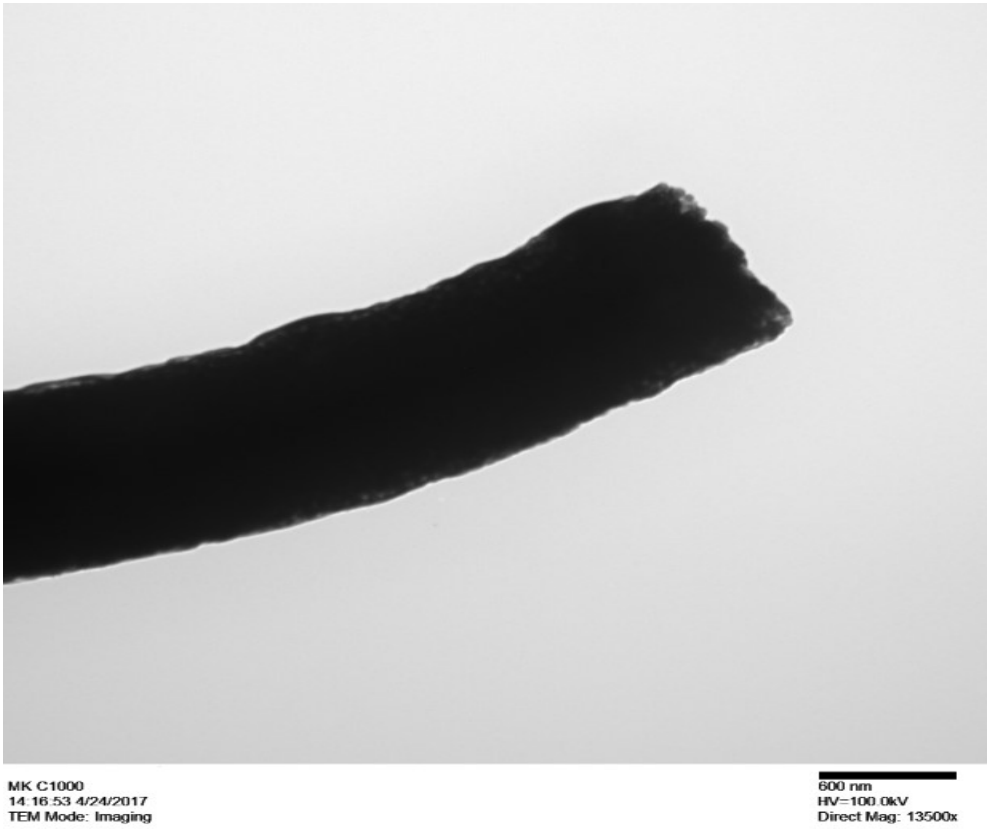

Fig. 4.1.14. The figure shows TEM Picture of MK ceramic fiber (low mag.). (source: experimental figure)

Fig. 4.1.15. The figure shows TEM Picture of MK ceramic fiber (hig. mag.). (source: experimental figure)

Fig. 4.1.16. The figure shows TEM Picture of H44 ceramic fiber (low mag.). (source: experimental figure)

Fig. 4.1.16. The figure shows TEM Picture of H44 ceramic fiber (hig. mag.). (source: experimental figure)

Fig. 4.1.17. The figure shows TEM Picture of RSN ceramic fiber (low mag.). (source: experimental figure)

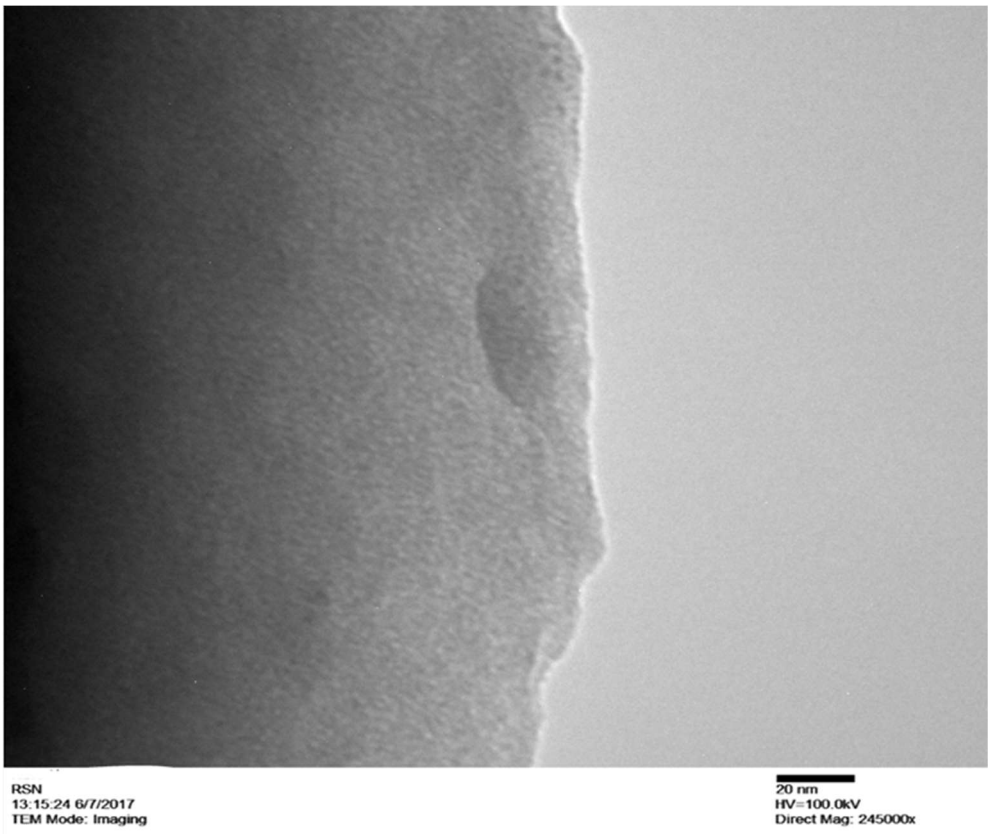

Fig. 4.1.18. The figure shows TEM Picture of RSN ceramic fiber (hig. mag.). (source: experimental figure)

At high magnification, when the electron beam is focused on the fiber's edge, the superficial roughness of the fibers can be seen. In the SEM images, fibers appear completely smooth, due to the lower magnification achievable. The releasing of volatiles from the silicon resin and the thermal decomposition of PVP lead to a grained and cracked surface, as can be easily seen in the figures exposed above. It could be observed that analyzing the TEM images, conclusions in agreement with the SEM analysis can be drawn. After the pyrolysis treatment fibers shown a decrease in the diameter, which depend by the treatment's parameters. The final ceramic fibers diameters are in the range of 1 micron for MK and H44 system and the double for the RSN system. The SiOC fibers produced in this work shown exhibit both a smaller average diameter and a more controlled morphology than those reported in previous literature [28].

In the present work ceramic fibers presenting low diameter ($\approx 1\ \mu m$), good (defect-free) and homogeneous morphology has been produced, starting from low-cost, available materials using inexpensive facilities and adopting a cost effective, reproducible and industrially suitable route.

4.2 Chemical characterization results

FT-IR has been used in order to follow the ceramization of the polymeric fibers. Comparing the weight of the same piece of fibrous mat before the electrospinning and after the pyrolysis the loss in mass of the materials has been evaluated. Raman spectra for the three materials (MK, H44, RSN PDCs) have been taken in order to observe the presence of C_{free} domains with sp^2 hybridization.

4.2.1 FT-IR result

FT-IR spectra of the samples, reported in figures 4.2.1, 4.2.2, 4.2.3 for MK, H44, RSN polymer derived ceramics, respectively; clearly indicate the transformation in the material's nature. As already state in chapter 2, the spinning fibers are thermoplastic materials constituted by a mixture of PVP and preceramic resin. After the cross-link, the material becomes a thermoset polymer capable of retain his shape in the pyrolysis treatment during which the ceramization occurs. For each material three spectra are reported. One belonging to the as-spun polymeric material, the second belonging to the cross-linked polymer and the third to the ceramic fibers after pyrolysis.

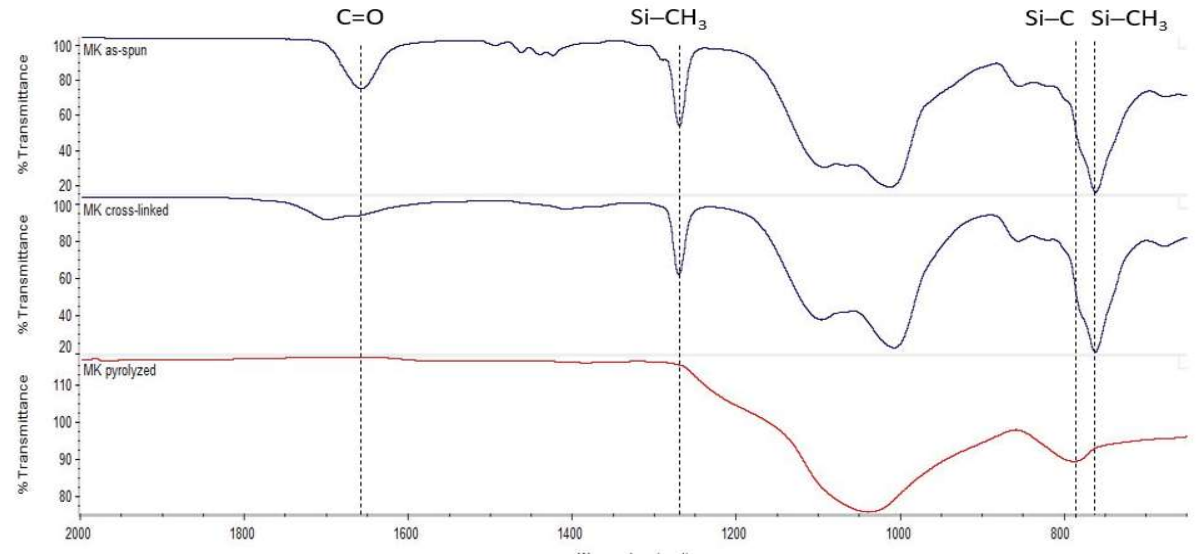

Fig. 4.2.1. The figure shows FT-IR spectrum for MK fibers. (source: experimental figure)

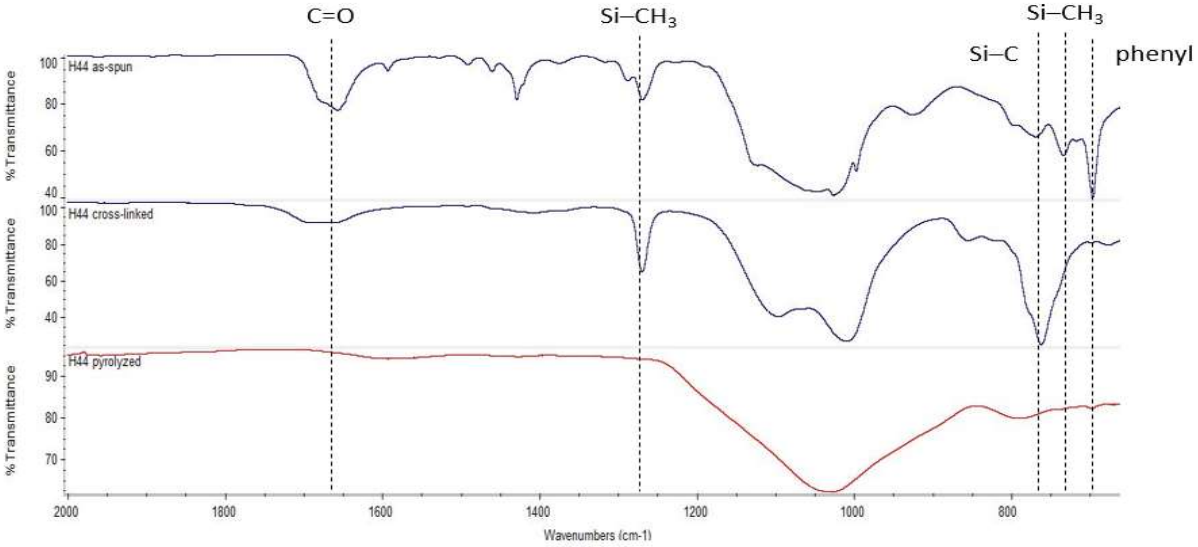

Fig. 4.2.2. The figure shows FT-IR spectra for H44 fibers. (source: experimental figure)

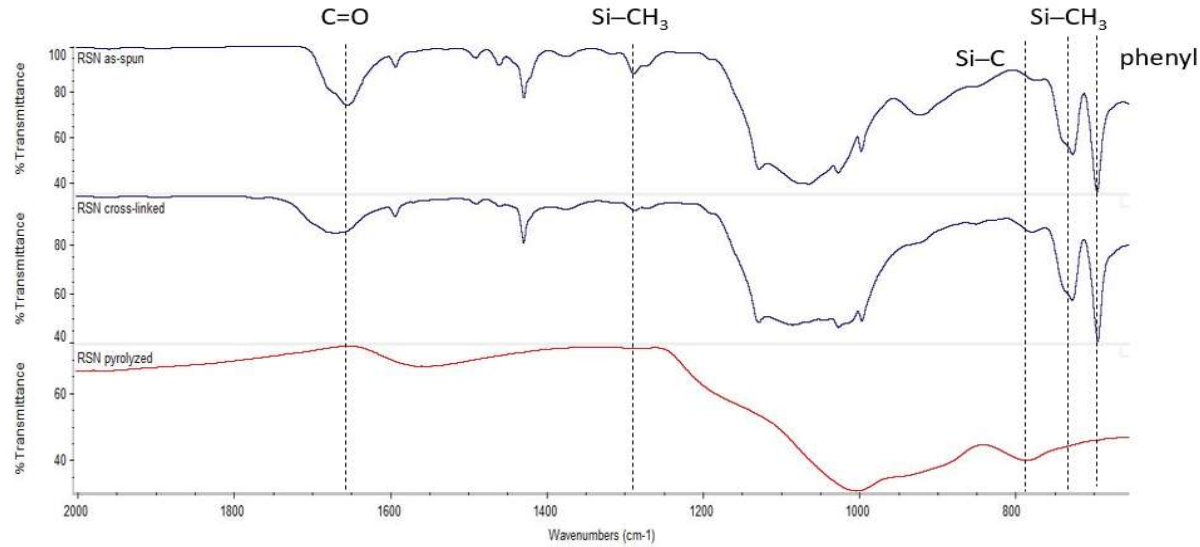

Fig. 4.2.3. The figure shows FT-IR spectra for RSN fibers. (source: experimental figure)

In all the three systems, the characteristic absorption peaks of PVP at 1670 cm^{-1} and 1290 cm^{-1} corresponding to the C=O and C─N on the pyrrolyl ring disappear after pyrolysis treatment at 1000°C. On the other hand, the disappearance of the signal related to Si─CH_3 at 1270 cm^{-1}, C─H in Si─CH_3 at 760 cm^{-1}, and phenyl at both 1590 cm^{-1} and 696 cm^{-1} (Only existing in H44 and RSN resin) after pyrolysis confirmed the conversion of the preceramic MK and H44 resin to SiOC ceramics. The formation of SiOC ceramics fibers is further proved by the appearance of the Si─O─Si peak at 1030 cm^{-1} and of the Si─C peak at 790 cm^{-1}. The mass loss, estimated by repetitive weight of a single piece cut from a fibrous mat, after the spinning process and once completed the ceramic transformation, is different among the three systems and are approximately:

- 30% for MK.
- 40% for H44.
- 25% for RSN.

The lower value displayed by RSN is imputable to the lower dwelling time of the final thermal treatment undergone by this material. The values calculated are in good agreement with those calculated via thermo-gravimetric analysis (TGA) and reported in [28]. The weight loss is due to the decomposition of PVP and polymer to ceramic transformation, involving the redistribution reactions between Si─O and Si─C bonds as well as the decomposition of organic moieties like methyl, ethyl, and phenyl groups.

4.2.2 Raman results

Raman spectroscopy of SiOC fibers was performed to further confirm the existence of the free carbon domains. Raman scattering is strongly sensitive to the electronic structure of the tested sample. Raman spectra of disordered carbonaceous materials are characterized by the presence of a disorder induced D-band and G-band corresponding to graphite like sp^2 carbons [40]. Figure 4.2.4 reports Raman spectra recorded for the three polymer-derived ceramic fibers pyrolyzed at 1000°C

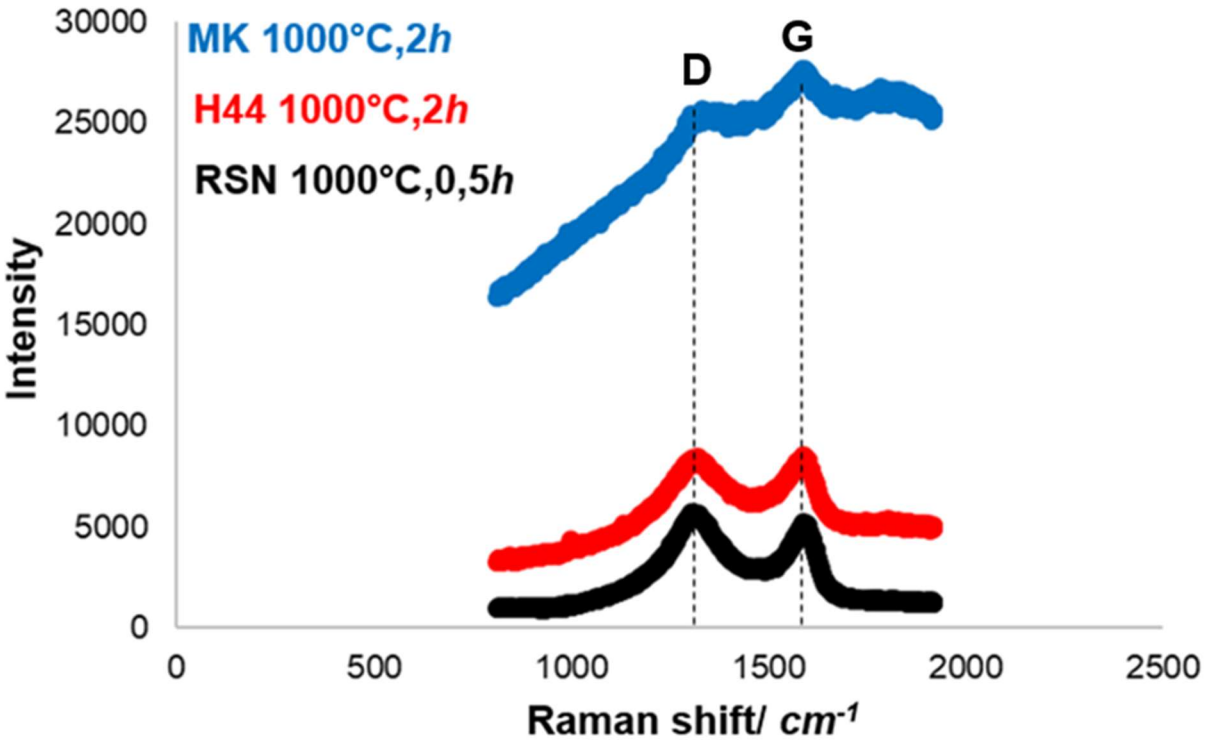

Fig. 4.2.4. The figure shows Raman spectra for the three different materials. (source: experimental figure)

Raman spectra exhibit D and G bands at around 1330 and 1590 cm^{-1}; pronounced for H44 and RSN samples, and less pronounced for MK one. Although the exact nature of the excess "free" carbon is not well studied, several reports have attributed the exceptional properties of these amorphous polymer-derived materials, such as high chemical durability and their resistance to crystallization, to the presence of this "free" carbon phase and its distribution within the network [25]. The development of a percolation network of turbostratic graphite, is fundamental for the electron conductivity of the fibers.

4.3 Electrochemical characterization results

A first screening electrochemical characterization has been conducted in a three-electrode cell for the three materials, MK, H44, RSN, at a voltage scan rate of 100 mVs^{-1} in 3.5 M Na_2SO_3 electrolyte using a Platinum plate as counter electrode and silver/silver-chloride electrode as the reference electrode, in a potential range from 0.0 to 1.0 V. Figure 4.3.1 show the CV curves obtained.

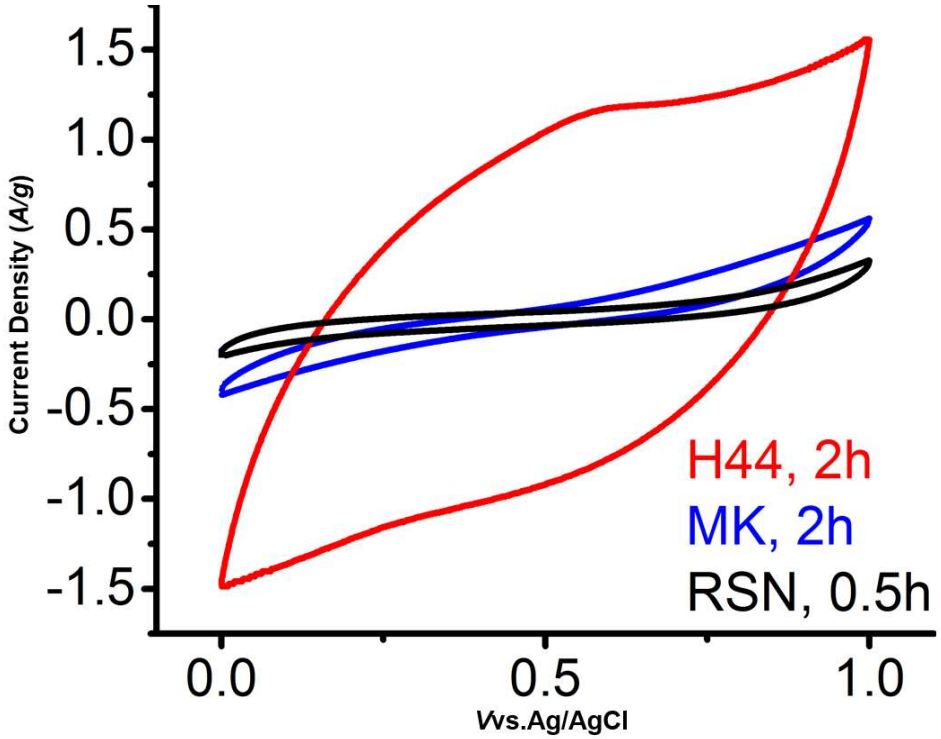

Fig. 4.3.1. The figure shows CV curves for MK, H44, RSN in three-electrode setup. (source: experimental figure)

Due to the particular preparation of three-electrode setup, from the reported test only qualitative information about the expected capacitance can be inferred. The specific capacitance, here referred to the total electrode's surface is proportional to the area circumscribed by the cyclic voltammetry curve, as expressed by equation 2.4.2. From the results obtained it looks like the ceramic fibers (grinded in the three-electrode setup) produced by H44 resin presents the higher capacitance. This fact, confirmed by further tests can be ascribed to the low fibers diameters, and so the high specific surface possessed by this material, and to the good quantity of C_{free} domains, that ensure a good (even if not optimum) conductivity.

4.3.1 Cyclic Voltammetry (CV) results

Two-electrode setup has been used in order to characterize the specific capacitance of the three types of ceramic fibers. Useful information can be obtained analyzing the resulting curves. The stand-alone binder-free electrodes made but MK, H44, RSN fibrous mats have been studied in a two-electrode cell, in a potential window from0 to 1 V at a voltage scan rate of 100, 200, 500 mVs^{-1} for the first and

the last system and 10, 20, 50, 100, 200, 500 mVs^{-1} for the H44 system; in 3.5 M Na_2SO_3 electrolyte. Figures from 4.3.2 to 4.3.4 report the CV curves for MK, H44, RSN materials, respectively.

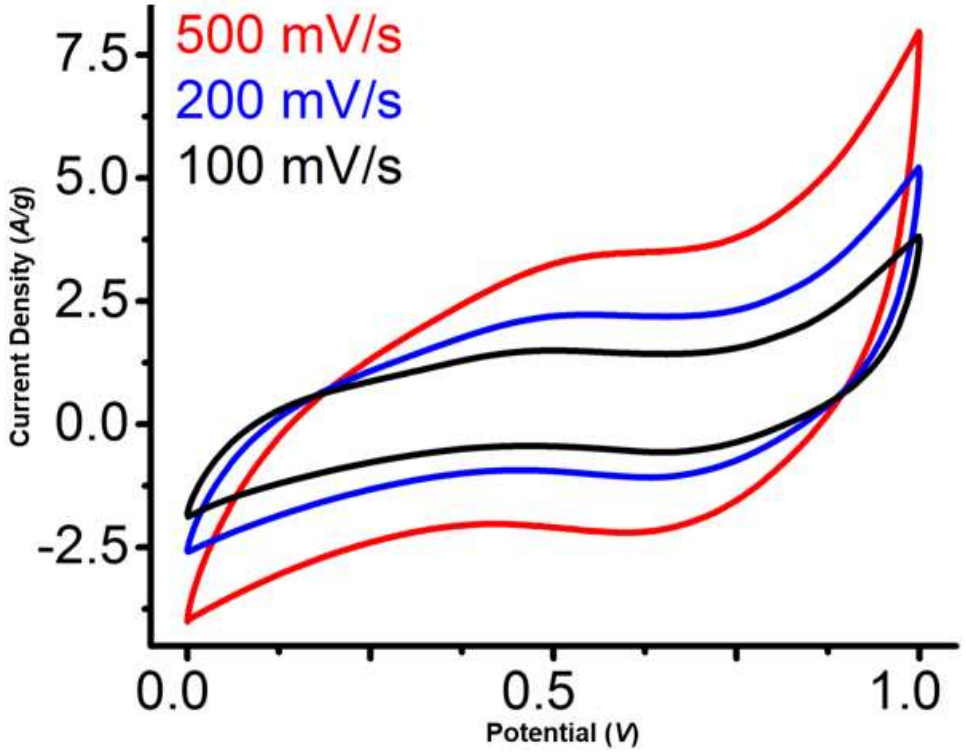

Fig. 4.3.2. The figure shows CV curve for MK material. (source: experimental figure)

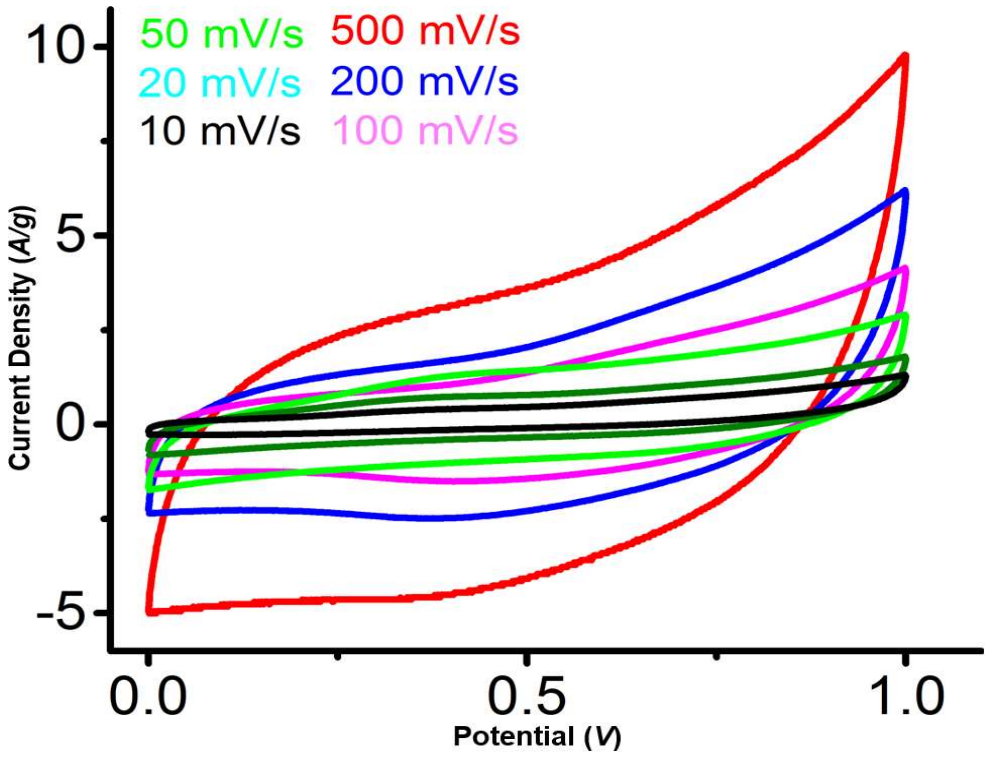

Fig. 4.3.3. The figure shows CV curve for H44 material. (source: experimental figure)

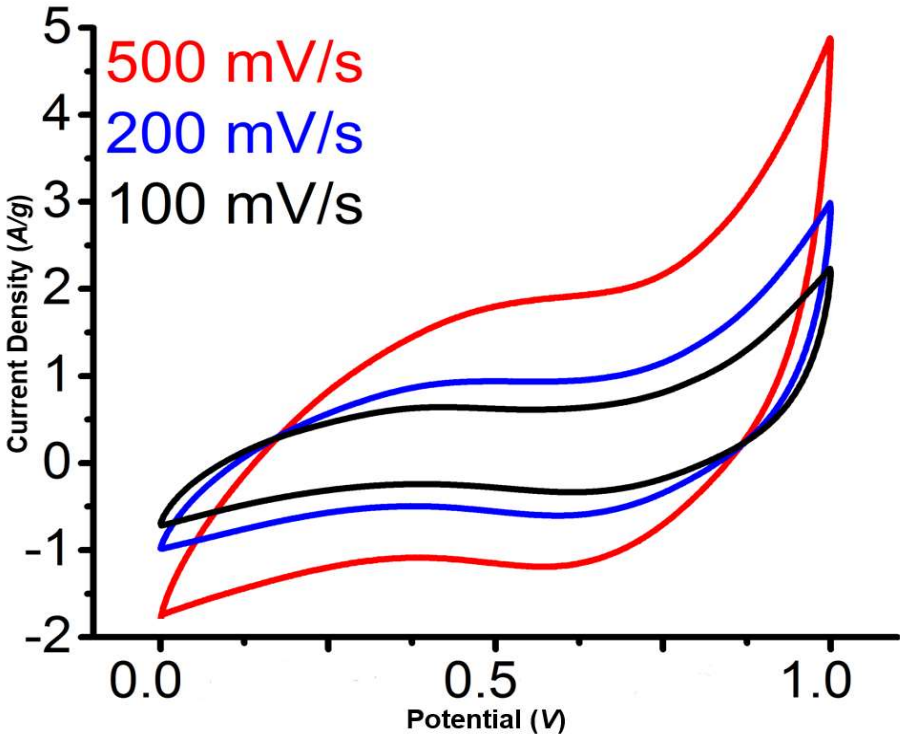

Fig. 4.3.4. The figure shows CV curve for RSN material. (source: experimental figure)

First of all, the three materials display a quasi-rectangular curve. This fact and the absence of reduction peaks related to the presence of electrochemical charge transfer process, are characteristic of double-layer capacitance and prove the chemical stability of the SiOC fibers [41, 42]. This shape is maintained also by the CV curves at higher scan rates (100, 200, 500 mVs^{-1}), which suggest that MK, H44, RSN fibrous mats have fast charge transfer and cation diffusion [42]. The area of the curves increases at higher scan rates, indicating good capacitive behavior and reversibility [43]. This fact is also confirmed by the unchanged curve' s shape when cycle number is increased till 50 (100 segments).

Figure 4.3.5 report a comparison between the CV curves collected at a scan rate of 100 mVs^{-1} for MK, H44 and RSN materials in red, blue and black color respectively.

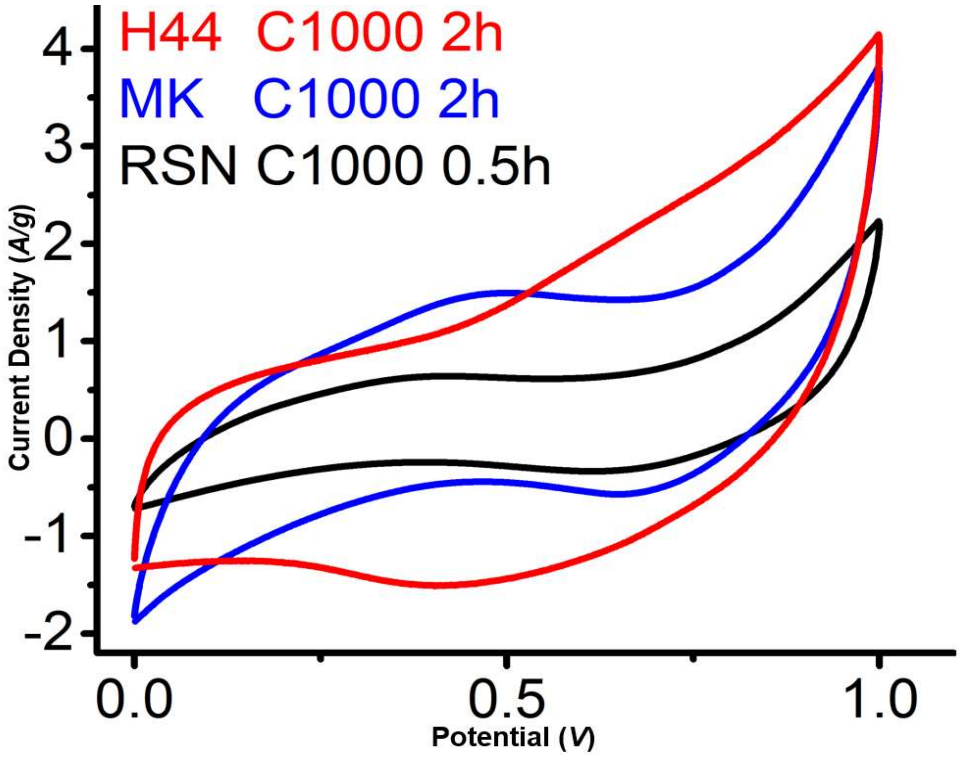

Fig. 4.3.5. The figure shows the comparison of the CV curves for the three systems. (source: experimental figure)

As already stated the specific capacitance of a material is related to the total area presented by the curve. It is clear that the best performing material resulting from the CV test is the mat formed by the ceramic fibers produced starting from H44 resin. The two main factors that can boots the capacitance of a EDL supercapacitor are the specific area and electron conductivity of the electrode's material (which for a symmetrical supercapacitor are the same for both the electrodes. Batteries and asymmetrical supercapacitors presents different material for different electrodes). Improving these two properties, results in improved electrochemical properties as high specific capacitance and low impedance. H44 ceramic fibers possess low fibers diameters, resulting from the electrospinning process and thermal treatment (seen through SEM analysis), coupled with a good electron conductivity given by the percolation of C_{free} domains (seen form Raman and EIS test). The MK polymer derived ceramic fibers produced in the present work possess an average diameter comparable to the H44 one. The higher area presented by the CV curves of the H44 fibers respect to these of MK ones, is imputable to the superior conductivity given buy the higher amount of carbon atoms, *sp2* hybridized and chemically bonded with other carbon atoms in the so called turbostratic graphite domains. This microstructural difference is ascribable to the different chemical composition between the two resin precursors, since that the pyrolysis treatment has been the same for both the two materials. H44 resin presenting some phenyl side groups instead of only methyl as the MK resin, possess higher carbon content. After the pyrolysis, the higher amount of graphitic carbon, notable

from Raman spectroscopy, give to H44 fibers a higher conductivity and thus a lower impedance, as can be seen from EIS. RSN fibers, as the MK ones, present a lower area and thus a lower specific capacitance respect to the H44 ones. RSN silsesquioxane, having only phenyl groups as side group, possess the higher carbon content among the three polymeric precursors. The poor electrochemical performance of RSN derived ceramics, which theoretically should be the best performing material for the application of the present work, is attributable to the worse spinning solution formulation and different pyrolysis treatment undergone by this material. With a dwelling time of only 30 minutes the high amount of carbon atoms, even if present in the material, don't have the time to completely form the graphite-like domains and remain in the amorphous network keeping a sp^3 hybridization. For this reason, the impedance of the RSN fibers will be high and the specific capacitance of this material will result restrained. An additional factor that influence the specific capacitance of the material is the higher, with respect to MK and H44, size of RSN fibers. The wider dimeter shown by the SEM images of RSN mats is imputable again to the contained temporal window set for the ceramization treatment of this material and to a non-optimum formulation of the solution for the electrospinning.

In table 4.3.1 the specific capacitance for each material calculated at the scan rate of 100 mVs^{-1} is reported. These values have been calculated using Origin for calculating the area of the CV curves and utilizing equation 2.4.2, the mass considered is the mass of a single electrode. These values confirm what stated previously and what shown form CV curves. H44 fibrous mat presents the wider integral area and so demonstrates the superior capacitive behavior.

Material	**Specific Capacitance (*F/g*)**
MK	30
H44	50
RSN	20

Tab. 4.3.1. The table reports the specific capacitance calculated for the three systems. (source: experimental data)

Specific capacitance depends by several factors. One among them is the scan rate. Table 4.3.2reports the specific capacitance of H44 at three different scan rates.

Scan Rate (mVs^{-1})	500	200	100	50
Specific Capacitance (*F/g*)	27	38	50	70

Tab. 4.3.2. The table reports the specific capacitance calculated for H44 system at different scan rates. (source: experimental data)

It could be observed that the capacitance values decrease with increasing the scan rate, as reported in [42]. In literature, some authors (see [38] and tables reported in [42], [43]) report the specific capacitance at lower scan rates than the one adopted in the present work (100 mVs^{-1}) for comparing the electrochemical performance of the materials studied. The medium value adopted in the present work expresses a more balanced capacitance; not boosted (by low scan rate values) nor penalized (by high scan rate values).

For a further confirmation of the pyrolysis's influence on the fibers size and on the development of carbon domains, which in turn affects the electrochemical performances of the electrode's material; CV test have been conducted selecting two materials (MK and RSN) and changing thermal treatment parameters. For MK polymer-derived ceramic fibers, the maximum treatment's temperature has been set 800°C instead of 1000°C. For RSN polymer-derived ceramic fibers the dwelling time has been set 3 minutes instead of 30. Figure 4.3.6 reports the comparison between the two CV curves obtained at the same testing conditions (potential window from 0 to 1 V and scan rate of 100 mVs^{-1}) for MK and RSN materials processed differently.

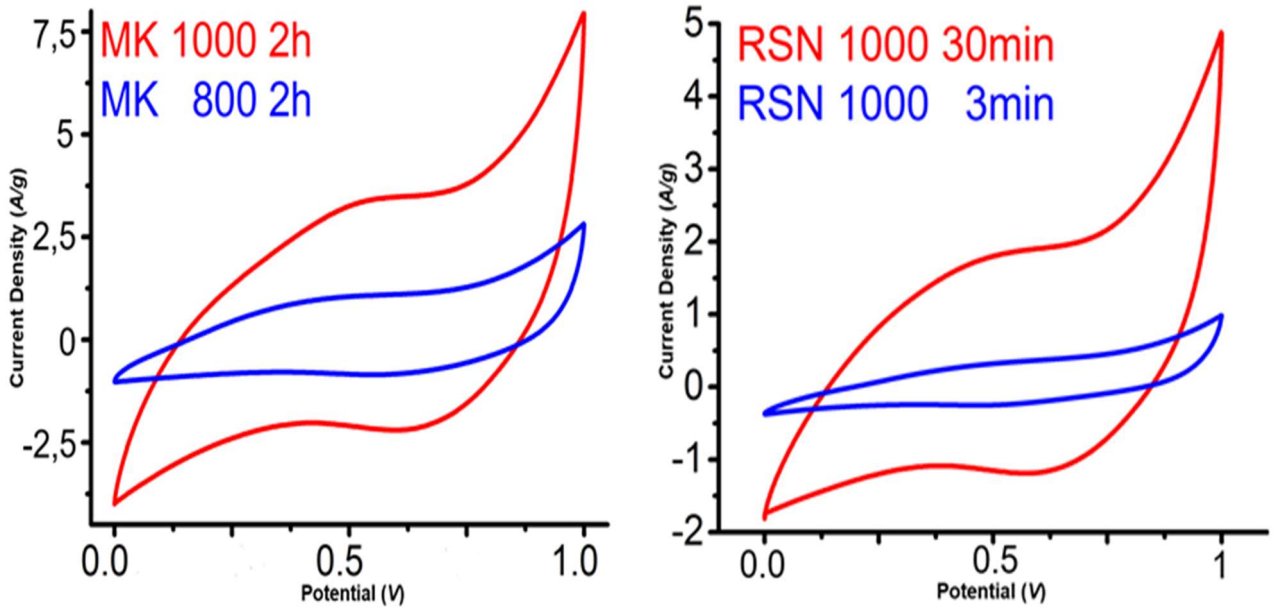

Fig. 4.3.5. The figure shows the comparison of the CV curves related to two materials treated differently for MK and RSN systems. (source: experimental figure)

The two comparisons reported in the figure above, confirm the theoretical conclusion already exposed. MK fibers which have been treated at a lower pyrolysis temperature, respect to original MK fiber, display smaller integral area and so worse electrochemical performance, due to limited microstructural evolution and sizes reduction. The same applies to RSN fibers which have been pyrolyzed for a lower time.

Although the specific capacitance of the best performing electrode's material (H44 fibers) produced in the present work is equal to the bottom limit value of the performance range for electrical double layer capacitors (50-150 *F/g* [33]); the reported specific capacitance is more realistic because of several reasons:

- Has been calculated for a balanced electrode mass (1 *mg)*.
- Has been calculated with a medium sweep rate (100 mVs^{-1}).
- Has been calculated for a free-standing electrode which does not require the use of current collectors which obscure its true capacitance value.
- No conducting agents have been added.

4.3.2 Galvanostatic charge discharge (GCD) results

The stand-alone binder-free electrodes made by MK, H44, RSN fibrous mats have been studied in a two-electrode cell in a potential window from 0 to 1 *V* at a current density of 1, 3, 5 *A/g* for the best performing material (H44), and 3 *A/g* for the other two PDCs (MK, H44), in 3.5 *M* Na_2SO_3 electrolyte. Figures from 4.3.8 to 4.3.10 report the GCD curves for MK, H44, RSN materials respectively.

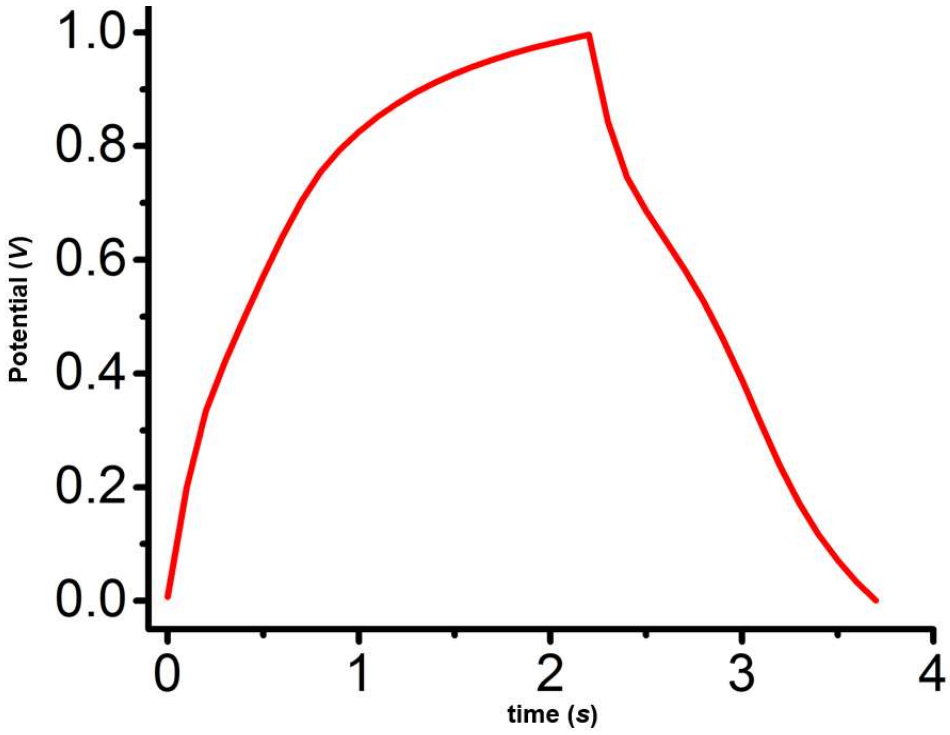

Fig. 4.3.8. The figure shows GCD curve for MK material. (source: experimental figure)

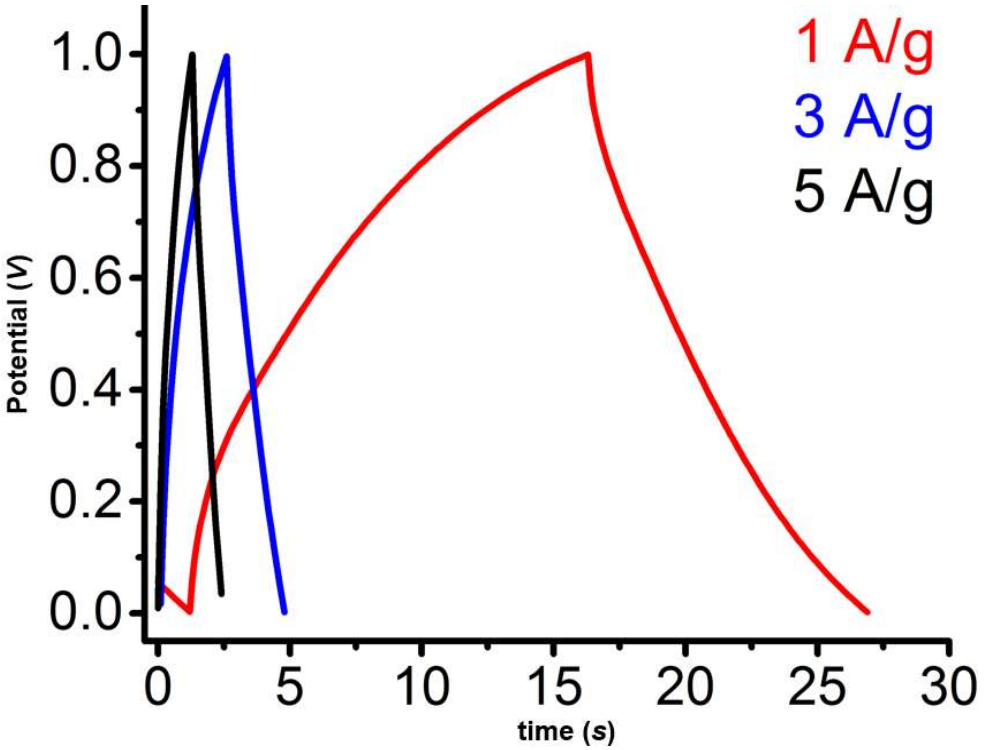

Fig. 4.3.9. The figure shows GCD curves for H44 material. (source: experimental figure)

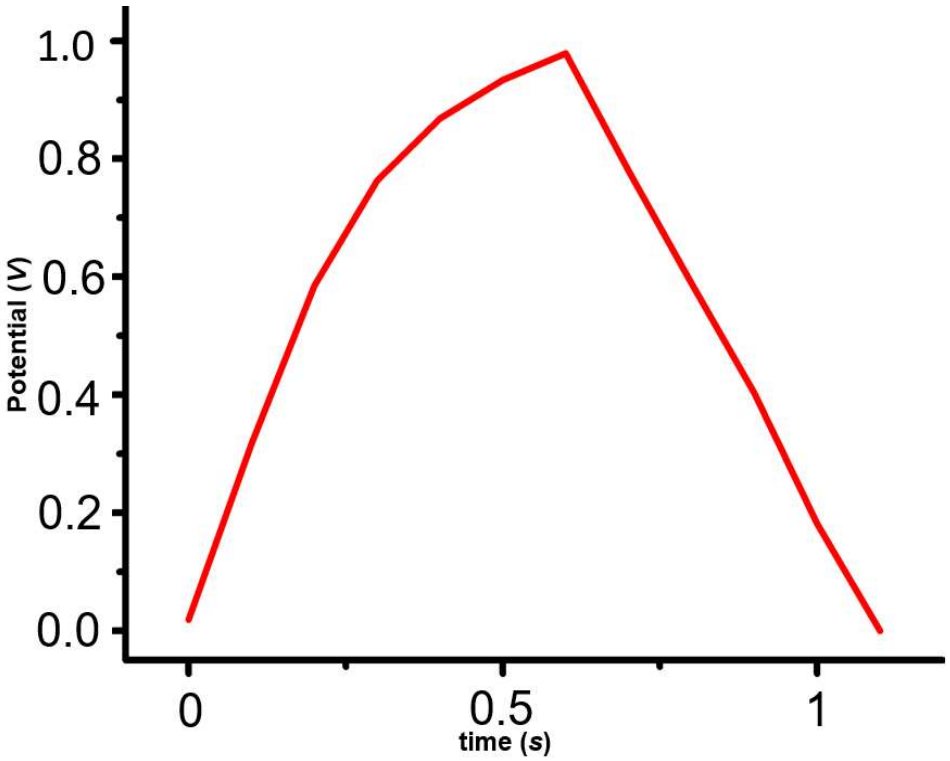

Fig. 4.3.10. The figure shows GCD curve for RSN material. (source: experimental figure)

Figure 4.3.11 report a comparison between the GCD curves collected at a current density of 3 *A/g* for MK, H44 and RSN materials in red, blue and black color respectively.

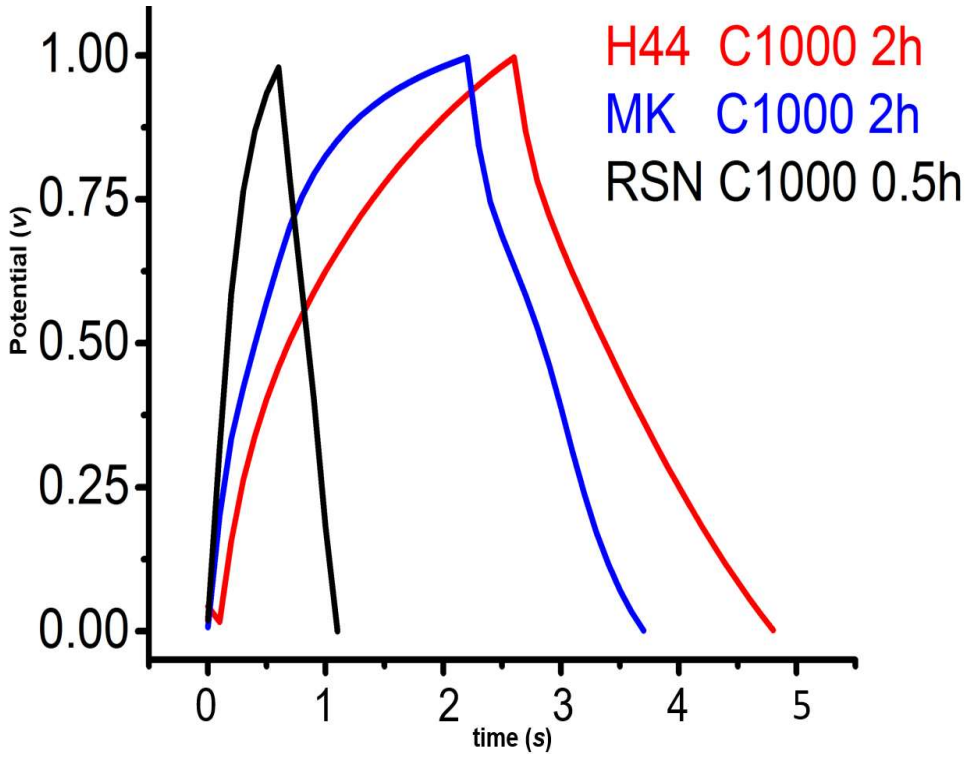

Fig. 4.3.11. The figure shows GCD curves for the three PDCs. (source: experimental figure)

GCD tests completely confirm the CV results. The best performing material is the H44 derived ceramic fibrous mat, followed by the MK and RSN ones. As already said H44 fibers possess high carbon atoms content that after the pyrolysis switch from sp^3 to sp^2 hybridization and form C_{free} clusters which ensure good electron conductivity to the material. Moreover, the proper formulation of the spinning solution ensures a low fibers diameter and so an elevated specific surface.

In table 4.3.3 the capacitance for each material calculated at constant current density of 3 *A/g* is reported. These values have been calculated utilizing equation 2.4.3, the mass considered is the mass of a single electrode. These values confirm what stated previously and what shown form GCD curves. H44 fibrous mat presents the higher discharge time so demonstrates the superior capacitive behavior.

Material	Specific Capacitance *F/g*
H44	5
MK	3
RSN	1

Tab. 4.3.3. The table reports the specific capacitance for the three PDCs. (source: experiment table)

The values reported in the table above seems to be very low compared to the ones obtained from CV curves. This is attributable to the high current density at which the DGC curves have been collected. For understanding the influence of the current density in table 4.3.4 the specific capacitances of the best performing material calculated for 1, 3, 5 *A/g* values are reported.

Current density *A/g*	Specific Capacitance *F/g*
1	25
3	5
5	0.5

Tab. 4.3.4. The table reports the specific capacitance for H44 calculated form GCD curves at different current density. (source: experiment table)

As already exposed specific capacitance depends by several factors. As we can see form the reported example the same material shows different values depending on the testing conditions, in this case the current density. It could be observed that the capacitance values decreased with the increasing the current density, as reported in [38]. In literature, some authors (see [38] and tables reported in [42], [43]) report the specific capacitance at lower current density than the one adopted here (1 and 3 *A/g*). The high value adopted in the present work, useful for understanding how markedly the testing conditions can affect the final result, is responsible for the low values of specific capacitance presented. With a lower current density, equal or lower to 0.5 *A/g* (current density commonly reported in literature) capacitances would be comparable or greater to the ones calculated form CV curves.

Long cycle life of supercapacitor is important for their practical application. For evaluating the capacitance retention of the best performing material (H44 ceramic fibers), the selected cell has been subjected to repetitive charge/discharge cycles, at the current density of 1 *A/g*, for 1000 seconds. Figure 4.3.12 reports the capacity retention against the charge/discharge cycles and in the right upper part shows the segments during the last seconds of testing.

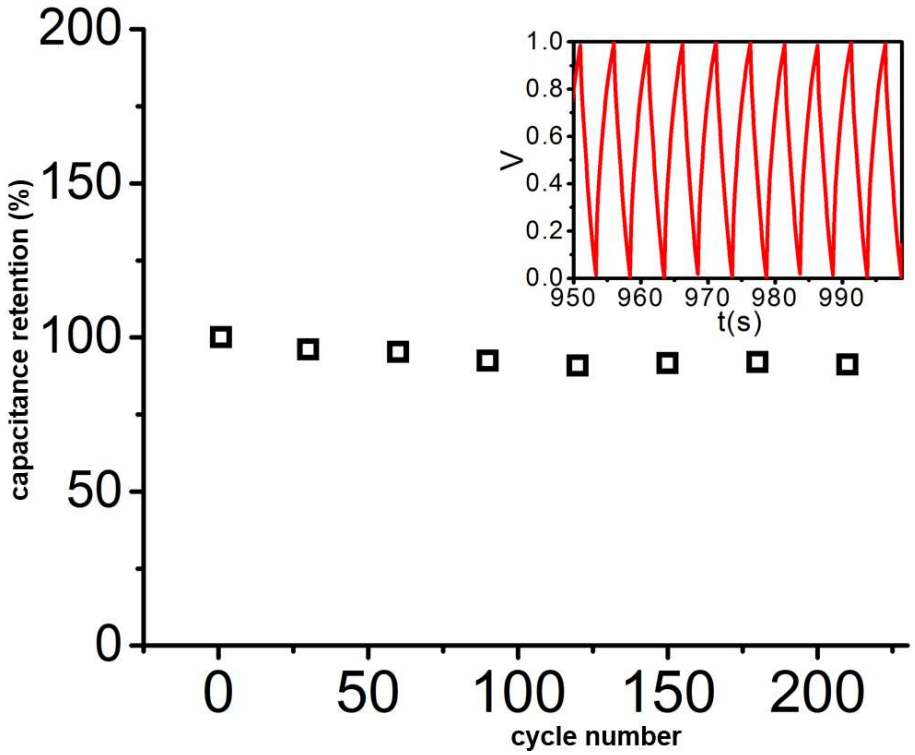

Fig. 4.3.12. The figure shows the cycling stability test of the best performing material (H44 PDC). (source: experimental figure)

A capacity retention percentage over 93% after 1000 seconds (250 cycles) has been evaluated, indicating the excellent electrochemical stability and cycling performance of H44 polymer-derived ceramic fibers.

4.3.3 Electrochemical Impedance Spectroscopy (EIS) results

Electrochemical impedance spectroscopy (EIS) has been employed for further understand the difference in the electrochemical performances of the three systems (MK, H44, RSN ceramic fibers) studied in the present work. Figure 4.3.16 displays a comparison between the three martials MK, H44, RSN in blue, red and black respectively.

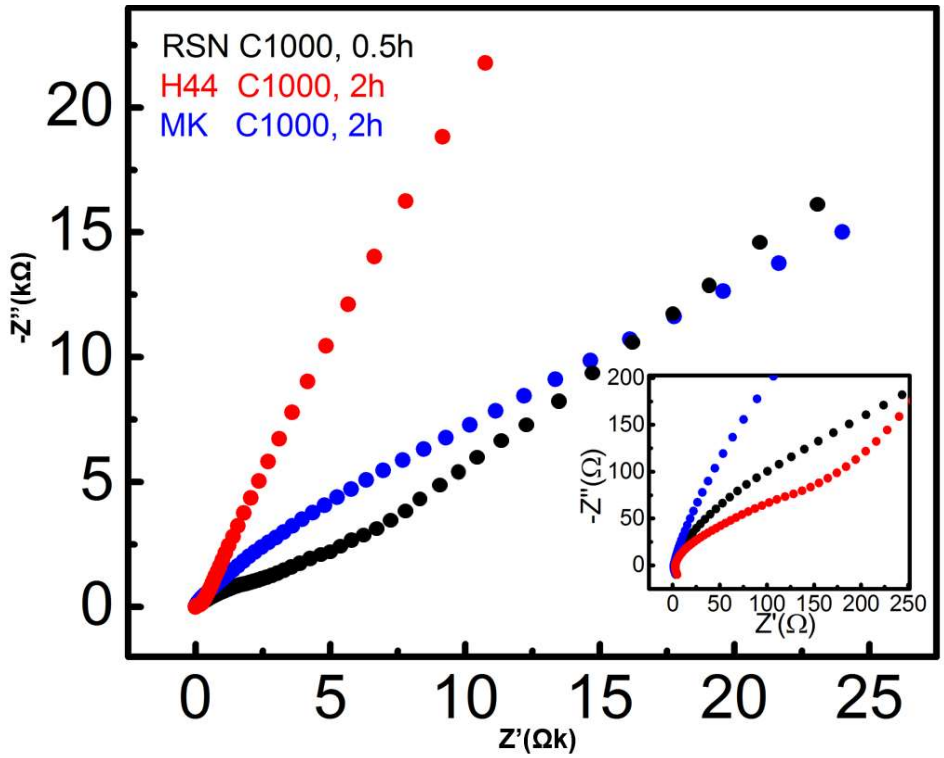

Fig. 4.3.16. The figure shows the Nyquist plots for the three systems studied. (source: experimental figure)

The higher frequency intercept of real impedance axis Z' is a measure of dominant resistive behavior due to the interface between the electrolyte, electrode and current collector, called interfacial resistance. All the three materials show high values between 1 and 3 Ω, consistent with the modest electrochemical performance valuated from CV and GCD tests. In the low-frequency region, the line related to the H44 fibers is the more perpendicular one, demonstrating the most marked proximity to an ideal capacitive behavior of the cell with rapid ion diffusion, of the best performing material (H44 system) [18]. A further confirmation of the superior electrochemical properties of the H44 system is the fact that his lane is the only one presenting a semicircular shape in the low-frequency region. The right intercept of the imaginary fitted semicircle with Z' axis represents the internal resistance of the electrode material. H44 without doubts present the lowest intercept value between the studied material (value between 50 and 60 Ω for H44 and far greater for MK and RSN), corresponding to the higher electron conductivity given by the C_{free} domains. Low internal resistance is of great importance in energy storing devices, as less energy is wasted to produce unwanted heat during charging /discharging processes [44]. EIS test confirms deductions made form CV and GCD results.

Conclusion

Supercapacitors are electrochemical storage device that store energy via charges separation in an electric double layer. These devices possess elevated power density and cycling stability due to the highly reversible physical storage mechanism. By contrast they present limited energy density. There is a strong interest in developing new electrodes materials with good energy/power densities, chemical stability and reasonable cost. The purpose of the present work was to study the usability of three different kind of polymer-derived SiOC fibers for making a self-standing electrode and to investigate how the production route, altering the material's structure, affect the electrochemical performances. Polymer-Derived Ceramics (PDCs) are an interesting ceramic materials which are produced by the pyrolysis of preceramic polymeric resins. These materials are interesting for different factors as their low cost, mechanical and chemical stability and the simple tunability of their properties. The three preceramic resins (MK, H44, RSN), which possess different carbon content, have been shaped in fibers via electrospinning. This process is attracting interest as versatile, cost-effective, reproducible and industrially suitable, fabrication method for one-dimensional materials. After the formation, polymeric fibers have been cross-lined in a hoven and pyrolyzed in a tube furnace under argon atmosphere. SEM and TEM techniques were used employed to characterize fibers dimension and morphology. FT-IR and Raman spectroscopy were used for following the evolution of material's nature and for confirming the presence of C_{free} domains, respectively. For testing the electrochemical performance of the materials, cyclic voltammetry (CV), galvanostatic charge discharge (GCD) and electrochemical impedance spectroscopy (EIS) test has been performed adopting a two-electrode setup. In the FT-IR spectra, the disappearance of peaks of the starting material (Si─CH_3, C─H) and the appearance of different peaks (Si─O─Si, Si─C), confirm the ceramization of the fibers. The presence of D and G band in Raman spectra confirm the presence of turbostratic graphitic domains. SEM images displays ceramic fibers with good morphology and homogeneity possessing average diameters approximately of 1 μm for H44 and MK system and 2 μm for RSN one. TEM images at higher magnification confirm the defect-less morphology of the fibers. From the cyclic voltammetry (CV) tests can be inferred that the best performing material quasi-rectangular curve, good capacitive behavior and reversibility, is the H44 fibrous mat. Lower fibers dimensions (high specific area) and more developed C_{free} percolation network (higher conductivity) ensure to this material the highest specific capacitance among the three tested materials (50 F/g, two electrode set-up, 100 mV/s, voltage from 0 to 1 V). Further tests confirm that lowering the pyrolysis temperature or dwelling time, produce a negative effect on electrochemical performance of the materials. Galvanostatic charge/discharge (GCD) completely confirm the CV's results. The best

performing material (H44 fibers) show a remarkable capacity retention of 91% after 1000 second of consecutive charge/discharge cycles. Electrochemical impedance spectroscopy confirms both the lower impedance of the H44 polymer-derived ceramic material and the overall modest electrochemical behavior of the materials tested. Self-standing, binder-free, cost-effective electrodes made by polymer-derived ceramic SiOC fibers have been successfully produced via electrospinning and following cross-link and pyrolysis. These electrodes, tested for supercapacitors in a two-electrode configuration, showed a well-developed capacitive behavior and electrochemical cyclability. The values for the specific capacitance of the material are modest but realistic due to the testing conditions and the unnecessity of supporting metallic plate for the studied electrodes. Basing on the promising results of the present work, in the optic of developing SiOC fibrous self-standing and cost-effective electrodes with excellent electrochemical performances; preceramic resin with high carbon content have to be chosen, electrospinning solution has to be carefully formulated and high pyrolysis temperature (1300°C) and dwelling time (3*h*) have to be adopted. Ceramic fibers discussed in the present work can be individually used as electrode material or as active support for pseudocapacitive particles.

Bibliography

[1] M.Armand, J.M.Tarascon, "*Review Article, Issues and Challenges Facing Rechargeable Lithium Batteries*", Nature, 414, 359. (2001)

[2] N. Nakicenovic, L. Gomez-Echeverri, T.B Johansson, A. Pathwardhan, "*Global Energy Assessment – Toward a Sustainable Future*", Cambridge University Press, Cambridge (UK). (2012)

[3] www.ec.europa.eu/transport themes.com.

[4] E.Musk, "*The missing piece*" Powerwall Presentation conference 1 May 2015.

[5] O.Ellabban, H.Abu-Rub, F.Blaabjerg, "*Renewable energy resources: Current status, future prospects and their enabling technology*", Elsevier, 10 1016. (2014)

[6] International Energy Agency, overview of "*Renewables Information 2017*". (2017)

[7] M.S.Dresselhaus, I.L.Thomas, "*Alternative energy technologies*", Nature 414 332-337. (2001)

[8] www.iter.org

[9] M.Armand, B.Dunn J.M.Tarascon, "*Electrical Energy Storage for the Grid: A Battery of Choices*", Science, 334, 928. (2011)

[10] www.expertreviews.co.uk

[11] C.H.Hamann, A.Hamnett, W.Vielstich, "*Electrochemistry, 2nd, Completely Revised and Updated Edition*", WILEY-VCH. (2007)

[12] P.G.Bruce, B.scrosati, J.M.Tarascon, "*Nanomaterials for rechargeable lithium batteries*", Angew Chem Int Ed Eng, 47 2930. (2008)

[13] A.S.Aricò, V.Baglio, V.Antonucci, in "*Nanotechnology for the Energy challenge*", ed. J. Garcia-Martinez, WILEY-VCH. (2010)

[14] P.Mazzoldi, M.Nigro, C.Voci, "*elementi di fisica, elettromagnetismo e onde*", 2nd edition, EdiSES. (2012)

[15] B.E.Conway, "*Electrochemical Supercapacitors: Scientific Fundamentals and Technological Applications*" Kluwer Academic/Plenum, New York. (1999)

[16] M.Chesneau, J.F.Fauvarque, J.Gamby, P.Simon, P.L.Taberna, "*Studies and characterizations of various activated carbons used for carbon/carbon supercapacitors*", J.Power Sources, 101 109-116. (2001)

[17] J.R.Miller, P.Simon, "*Electrochemical Capacitors for Energy Management*", Science, 321, 651-652. (2008)

[18] J.Chang, A.Ghosh, B.Li, Y.Hee-Lee, T.Hoon-Lee, D.H.Luong, V.T.Le, F.Yao, D.T.Pham, T.H.Kim , "*Carbon Nanotube-Bridged Graphene 3D Building Blocks for Ultrafast Compact Supercapacitors*", Am. Chem. Soc., 9 2018-2027. (2015)

[19] Y.Gogotsi, P.Simon, "*Materials for Electrochemical Capacitors*", Nature Materials, 7 845-854. (2008)

[20] C.Merlet, Y.Gogotsi, B.Rotenberg, M.Salanne, P.Simon, P.L.Taberna "*On the molecular origin of supercapacitance in nanoporous carbon electrodes*", Nature Materials, 11 306-310. (2012)

[21] J.Goodenough, "*Basic Research Needs for Electrical Energy Storage: Report of the Basic Energy Sciences Workshop on Electrical Energy Storage*", Office of Basic Energy Sciences, April 2-4. (2007)

[22] T. M. Serdyuk, Yu. M. Vol'fkovich, "*Electrochemical Capacitors*", Russ. J. Electrochem., 38 935-959. (2002)

[23] S. V. Litvinenko, S. N. Razumov, S.A.Kazaryan, G. G. Kharisov, V. I. Kogan, "*Mathematical Model of Heterogeneous Electrochemical Capacitors and Calculation of Their Parameters*", J. Electrochem. Soc., 153. (2006)

[24] P.Colombo, R.Riedel, G.D.Sorarù, and H.K.Kleebe, "*Historical Review of the Development of Polymer Derived ceramics (PDCs)*" pp. 1-12 in "*Polymer Dervied Ceramics: From Nanostructure to Apllications*", DEStech Publictions Inc., Lancaster, PA. (2009)

[25] P.Colombo, C.Mera, R.Riedel and G.D.Sorarù, "*Polymer-Derived Ceramics: 40 Years of Research and Innovation in Advanced Ceramics"*, J. Am. Ceram. Soc 93 1805-1837 (2010).

[26] F.I.Hurwitz, S.C.Farmer, F.M.Terepka, T.A.Leonhardt, "*Silsesquioxane-Derived Ceramic Fibers"*, J.Mater.Sci., 26, 1247-1252. (1991)

[27] L.A.Liew, R.A.Saravanan, V.M.Brigth, M.L.Dunn, J.W.Daily, R.Raj, "*Processing and Characterization of Silicon Carbon-Nitride Ceramics: Application of Electrical Properties Towards MEMS Thermal Actuators"*, Sens. Act. A: Phys., 103 171-18. (2003)

[28] P.Colombo, A.Guo, J.Liu, M.Modesti, M.Roso, "*Preceramic Polymer-Derived SiOC Fibers by Electrospinning"*, J. Appl. Polym. Sci.000, 39836, (2013).

[29] R. Pena-Alonso, G.D.Sorarù, R.Raji, "*Preparation of Ultrathin-Walled Carbon-Based Nanoporous Structures by Etching Pseudo-Amorphous Silicon Oxycarbide Ceramic*", J. Am. Ceram. Soc., 89 2473-2480 (2006).

[30] M.Takeda, J.Sakamoto, A.Saeki, Y.Imai, H.Ichikawa. "*High-Performance Silicon Carbide Fiber Hi-Nicalon for Ceramic-Matrix Composites*", ceram. Eng. Sci. Proc., 16 1349-1355 (1981).

[31] H.Li, W.Liu, R.Y.Tay, E.H.T.Teo, S.H.Tsang, "*Reduced Graphene Oxide/Boron Nitride Composite Film as a Novel Binder-Free Anode for Lithium Ion Batteries with Enhanced Performances*", Elect. Acta, 166 197-205. (2015)

[32] American Ceramic Society Bulletin, Vol. 96, No 3 42-49

[33] S.Cavaliere, S.subianto, I.Savych, D.J.Jones, J.Rozière, "*Electrospinning:designed architectures for energy conversion and storage devices*", Energy Environ. Sci., 4 4761-4785. (2011).

[34] D.H.Reneker, A.L.Yarin, H.Fong, S.Koombhongse. "*Bending Instability of Electrically Charged Liquid Jets of Polymer Solutions in Electrospinning*". J. of Applied Physics, 87, 4531-4547. (2000).

[35] Ramakrishna, K.Fujihara, W.Teo, T.Lim, Z.Ma, "*An Introduction to Electrospinning and Nanofibers*", World Scientific Publishing Co. Pte. Ltd., Singapore, p. 382. (2005).

[36] N.Pan, S.Zhang, "*Supercapacitors Performance Evaluation*", Adv. Energy Mater., 5,1401401 (2015).

[37] R.S.Ruoff, M.D.Stoller, "*Best practice methods for determining an electrode material's performance for ultracapacitors*", Energy Environ. Sci., 3, 1294-1301 (2010).

[38] M.A.Abass, L.david, G.Singh, M.S.Kolathodi, "*Polysiloxane-functionalized graphene oxide paper: pyrolysis and performance as a Li-ion Battery and supercapacitor electrode*", RSC Adv. 6 74323-74331. (2016)

[39] J. Adrien, P.Colombo, A.Guo, E.Maire, M.Modesti, M.Roso, "*Characterization of porosity, structure, and mechanical properties of electrospun SiOC fiber mats*" J. Mater. Sci., 50 4221-423. (2015)

[40] M.Graczyk-Zajac, V.S.Pradeep, R.Riedel, G.D.Sorarù, M.Wilamowska, "*Tailoring of SiOC composition as a wy to better performing anodes for Li-ion batteries*" Solid State Ionics 260 94-100. (2014)

[41] Y.Hsieh, Q.Huang, P.Lu, A.K.Mukherjee "*SiCO-doped Carbon Fibers with Unique Dual Superhydrophilicity/Superoleophilicity and Ductile and Capacitance properties*", ACS Applied Materials and Interfaces, 10.1021. (2010)

[42] B.Chen, Z.Guo, J.Mu, Y.Liu, C.Shao, M.Zhang, Z.Zhang, P.Zhang, "*Highly dispersed Fe_3O_4 nanosheets on one-dimensional carbon nanofibers: Synthesis, formation mechanism, and electrochemical performance as supercapacitor electrode materials*", Nanoscale 3 5034-5040. (2011)

[43] M.A.Abass, L.david, K.M.Shareef, G.Singh, "*Three-dimensional polymer-derived ceramic/graphene paper as a Li-ion battery and supercapacitor electrode*", RSC Adv. 6 53894-53902. (2016)

[44] A.Liu, G.Shi, Q.Wu ,Y. Xu, Z. Yao, "*Supercapacitors based on flexible graphene/polyaniline nanofiber composite films*." ACS Nano, 4 1963-1970. (2010)

Acknowledgement

I would like to thank Kansas State University (KS, USA), College of Engineering and department of Mechanical and Nuclear Engineering for the unique opportunity I have been given. Sincere thanks go to my supervisor, Professor Gurpreet Singh, whose kindness, understanding, and patience added considerably to my experience, and to Eng. M. A. Abass for his assistance and friendship.

I would like to express my sincere gratitude to Professor Paolo Colombo, for the assistance provided at all levels of the research project; to Professor M. Modesti and his research group for the helpfulness and to Eng. A. Conte for the precious support.

A thank form the depths of my heart and soul goes to my mother Renata, my father Federico and my siblings Davide and Giulia for the support and the unconditioned love provided me through my entire life. A special thank goes to my girlfriend Francesca for her love and complicity; and to all my friends.